THE CONVECTIVE DIFFUSION OF OXYGEN, CARBON DIOXIDE AND INERT GAS IN BLOOD

Thesis by

Edmund Eugene Spaeth

In Partial Fulfillment of the Requirements

For the Degree of

Doctor of Philosophy

California Institute of Technology

Pasadena, California

1967

(Submitted January 4, 1967)

ACKNOWLEDGMENTS

This study was performed under the direction of Professor Sheldon K. Friedlander. His guidance and continued encouragement during its accomplishment are very gratefully acknowledged.

Professors James J. Morgan and Andrew L. Gram are sincerely thanked for their assistance in the development of the oxygen and krypton analyses.

The efforts of Mr. Elton Daly and Mr. Robert Greenway in the design and construction of the rotating disk apparatus, and Mr. Fred Wild in the fabrication of the glassware, are greatly appreciated.

The author was supported during this work by a U.S. Public Health Service Training Grant. The experimental work was supported by funds from the U.S. Public Health Service and the National Science Foundation. This financial assistance is gratefully acknowledged.

The author will always be grateful to his wife for her constant support throughout the course of this study and her able typing of this manuscript.

ABSTRACT

In modern membrane-type artificial lungs, the major resistance to gas transfer is offered by the blood and not the membrane. Thus, a suitable theory for convective diffusion in blood must be available in order to design these devices. A general equation for the convective diffusion of gases in blood is presented in this work, and numerical solutions to this equation are compared with experimentally measured rates of oxygen, carbon dioxide, and krypton exchange with citrated blood in a boundary layer flow. The measurements were made in a new type of rotating disk apparatus which is especially suited to the study of gas transfer in complex fluids.

Solutions of the general equation based on velocities derived from the Navier-Stokes equations are shown to predict the measured transfer rates, even though blood is known to be non-Newtonian at low shear rates. The desorption rate of oxygen from blood at low oxygen partial pressures was found to be up to four times the corresponding transfer rate of inert gas. This effect is described somewhat conservatively by a simple local equilibrium form of the general convective diffusion equation. The carbon dioxide transfer rate in blood near venous conditions was found to be about twice that of inert gas. This great an augmentation is not predicted by any simple form of the general convective diffusion equation. The behavior of the membrane lung system was studied numerically using these results, and the practical implications of this study are discussed.

TABLE OF CONTENTS

PART	TITLE	PAGE
I.	INTRODUCTION	1
	A. Background.	1
	B. A General Convective Diffusion Equation for Gas Transfer in Blood.	6
	C. The Hydrodynamic Nature of Blood.	11
	D. The Carriage of O_2, CO_2 and Kr by Blood.	12
	E. The Nature of Diffusion in Blood.	20
	1. Heterogeneous Media Theory.	20
	2. Evaluation of $\mathscr{D}_{O_2,RC}$.	22
	F. The Displacement from Chemical Equilibrium in Blood.	24
	G. Previous Studies on Gas Transfer to Blood.	27
II.	EXPERIMENTAL APPARATUS AND PROCEDURE	31
	A. The Rotating Disk System.	31
	1. Theory.	31
	2. The Rotating Disk Apparatus.	36
	B. Experimental Procedure.	40
	1. General Procedures.	40
	2. Krypton Transfer Measurements.	44
	3. Oxygen Transfer Measurements.	44
	4. Carbon Dioxide Transfer Measurements.	45

PART	TITLE	PAGE
	C. Source and Treatment of the Blood.	46
III.	EXPERIMENTAL DATA AND ANALYSIS	49
	A. The Solubilities and Diffusivities of Kr, O_2, and CO_2 in Blood.	49
	B. Krypton Experiments.	55
	1. Results with Water and Freshly Drawn Blood.	55
	2. Results with Blood Used in Cardiac Surgery.	57
	C. Oxygen Experiments.	60
	1. Results with Water and Freshly Drawn Blood.	60
	2. Comparison of the Experimental Results with Three Theoretical Models.	65
	3. Test of the Local Equilibrium Hypothesis.	75
	4. Results with Hemoglobin Solution.	78
	D. Carbon Dioxide Experiments.	82
IV.	APPLICATIONS TO ARTIFICIAL LUNG DESIGN	89
	A. Local Equilibrium Oxygenation.	89
	B. The Relative Transfer Rates of O_2 and CO_2.	94
	C. Artificial Lung Design.	96
V.	SUMMARY AND CONCLUSIONS	100

PART	TITLE		PAGE
	A. Principal Results of this Research.		100
	B. Application of the Results.		103
	C. Further Studies.		103
	APPENDICES		106
	APPENDIX II-1	The γ Counting Technique Used to Measure Krypton Uptake Rates	107
	APPENDIX II-2	A Manganese Oxidation Method Used to Measure Deoxygenation Transfer Rates	115
	APPENDIX II-3	Blood Analysis Procedures	122
	APPENDIX III-1	Numerical Solution of the Convective Diffusion Equation	129
NOMENCLATURE			131
BIBLIOGRAPHY			134

LIST OF TABLES

NUMBER	TITLE	PAGE
II-1	Transfer Resistances of the G.E. one mil Silicone Rubber Membrane at 37.5°C for the Gases Used in This Study (65).	41
II-2	The Average Properties of the Blood Samples Taken from the Rotating Disk Apparatus.	48
III-1	Published Values of the Viscosity of Serum and Plasma.	51
III-2	Calculated and Reported Oxygen Diffusivities in Water, Plasma, and Concentrated Hemoglobin Solution.	52
III-3	Data from the Deoxygenation Experiments with Citrated, Freshly Drawn Blood.	73
III-4	Measured and Calculated Properties Used to Describe the Deoxygenation Experiment with Hemoglobin Solution.	79
IV-1	The Relative Rates of Oxygen Uptake and Carbon Dioxide Removal in Standard Blood at 37.5°C, Exposed to Wet Oxygen Gas Across a 1 mil Silicone Rubber Membrane.	95

LIST OF FIGURES

NUMBER	TITLE	PAGE
I-1	A Schematic Diagram of a Total Heart-Lung Bypass Circuit Incorporating a Stationary Screen Artificial Lung.	2
I-2	The Oxygen-Oxyhemoglobin Equilibrium Curve for Human Blood, Calculated Using Equation (9).	16
I-3	The Carbon Dioxide Equilibrium Curve for Blood (pH = 7.4, T = 37°C) Adjusted to $f = 0.6$, H = 0.4.	19
II-1	A Schematic Representation of the Concentration Profile in the Membrane Rotating Disk System, Illustrating the Nomenclature Used in the Text.	34
II-2	A Schematic Diagram of the Rotating Disk Apparatus.	38
II-3	A View of the Opened Rotating Disk Apparatus.	39
II-4	A Typical Rotating Disk Membrane Following Exposure to Blood.	42
III-1	The Non-Facilitated Effective Diffusivity of Oxygen in Whole Blood, Calculated From the Heterogeneous Media Theory Using the Data in Table III-2.	54
III-2	A Comparison of the Experimental Data for Krypton Uptake with Theoretical Curves.	56
III-3	A Krypton Experiment Performed with Blood Previously Used in a Non-Membrane Lung, Showing a Large Increase in Membrane Resistance with Time. The Data Points are Numbered Chronologically.	59
III-4	A Comparison of the Experimental Data for Oxygen Desorption from Water with the Theoretical Curve. Different Symbols Correspond to Different Membranes, and Include Data Taken Before and After Use of the Membrane in an Experiment with Freshly Drawn Blood. The Values of $P_{o_2,\infty}$ Range from 100-500 mm Hg.	61

NUMBER	TITLE	PAGE
III-5	A Comparison of the Experimental Data for the Deoxygenation of Citrated, Freshly Drawn Blood (P_{CO_2} = 25 - 59 mm Hg) with the Inert Theoretical Curve. Different Symbols Correspond to Different Blood Samples.	63
III-6	Deoxygenation Concentration Profiles at Low P_{O_2} Predicted by the Inert and Local Equilibrium Models for the Same Transfer Rate.	68
III-7	Deoxygenation Concentration Profiles at High P_{O_2} Predicted by the Inert and Local Equilibrium Models for the Same Transfer Rate.	69
III-8	The Effective Diffusivity of Oxygen in Standard Blood Calculated Using the Facilitated Local Equilibrium Model, with $\mathcal{D}_{Hb,RC} = 1.25 \times 10^{-7}$ cm^2/sec, $\alpha_{O_2,RC} = 2.2 \times 10^{-5}$ cc (STP)/cm^3 mm Hg, $\mathcal{D}_{O_2,RC} = 1 \times 10^{-5}$ cm^2/sec.	71
III-9	A Comparison of the Measured Deoxygenation Transfer Rates in Freshly Drawn, Citrated Blood (Corrected to Standard Conditions) with the Three Mathematical Models.	74
III-10	The Location of the Edge of the Chemically Reactive Region in the Concentration Boundary Layer Formed During the Deoxygenation of Standard Blood.	77
III-11	The Effective Diffusivity of Oxygen in the Hemoglobin Solution Described in Table III-4.	80
III-12	A Comparison of the Measured Deoxygenation Transfer Rates in Free Hemoglobin Solution with the Three Mathematical Models.	81
III-13	A Comparison of the Transfer Rate Data for CO_2 Extraction from Water, Taken Before and After Exposure of the Membrane to Freshly Drawn, Citrated Blood, with the Inert Theoretical Curve ($T = 37.5^{\circ}C$, $\mathcal{D}_{CO_2,H_2O} = 2.82 \times 10^{-5}$ cm^2/sec, $\alpha_{CO_2,H_2O} = 7.37 \times 10^{-4}$ cc (STP)/cm^3 mm Hg).	83
III-14	A Comparison of the Transfer Rate Data for CO_2 Extraction from Freshly Drawn, Citrated Blood	85

NUMBER	TITLE	PAGE
	(P_{O_2} = 40 mm Hg, pH = 7.22, ν = 0.026 cm^2/sec) with the Inert Theoretical Curve (T = 37.5°C, $\mathcal{D}_{CO_2,B}$ = 1.1 x 10^{-5} cm^2/sec, $\alpha_{CO_2,B}$ = 6.3 x 10^{-4} cc (STP)/cm^3 mm Hg).	
III-15	A Comparison of the Measured Carbon Dioxide Removal Rate from Blood with the Transfer Rates Predicted by the Inert and Local Equilibrium Models.	87
IV-1	The Rate of Oxygen Uptake by Standard Blood in the Rotating Disk Apparatus, Calculated Using the Local Equilibrium Model.	90
IV-2	A Schematic Comparison of the Flow Velocities in the Chemically Reactive Region (P_{O_2} < 100 mm Hg) for Deoxygenation and Oxygenation of the Concentration Boundary Layer.	92
II-1-1	The Rotating Disk System as Used During the Krypton Experiments.	108
II-1-2	The Experimental γ Spectrum Used to Tune the Counting Equipment.	109
II-1-3	A Typical Count-Rate History Obtained During a Krypton Experiment.	111
II-1-4	The Geometrical Factor Relating the Change in Dissolved Gas Concentration in the Apparatus to the Change in Count-Rate for Different Gas Activities.	114
II-2-1	A Schematic Diagram of the Gas Collection System Used During the Deoxygenation Experiments.	117
II-2-2	The o-Tolidine Standard Curve Obtained Using Aliquots of a Calibrated Dissolved Oxygen Solution.	119
II-2-3	The Development Time of the o-Tolidine Reaction in the Perchloric Acid - NaOH Environment (pH = 1.3).	120
II-3-1	The Calibration of the Hemoglobin Standard Solution Using the Connerty-Briggs Method for Total Iron.	124

NUMBER	TITLE	PAGE
II-3-2	The Cyanmethemoglobin Standard Curve Used in the Total Hemoglobin Determinations.	125
II-3-3	The Red Cell Size Distribution of a Typical Blood Sample, Adjusted to Normal Red Cell Volume.	126

CHAPTER I

INTRODUCTION

A. Background.

The use of extracorporeal circulation to restore venous blood to arterial conditions during heart-lung bypass is an established practice today, although less than two decades have elapsed since this procedure was first applied to human patients. During this time many publications have appeared in the literature, describing detailed mechanical designs for devices involved in the extracorporeal circuit.

A typical extracorporeal circuit used during heart-lung bypass is illustrated in Figure I-1 (26). Both the heart and lung are shunted, and their functions are taken over by the external circuit, allowing open heart surgery to be performed in a relatively quiet and dry surgical field. In the extracorporeal circuit, the venous blood first drains into a reservoir. This blood, and any blood collected by a suction device kept in the surgical field, is then pumped to the artificial lung, where the blood is oxygenated by an oxygen gas stream, carbon dioxide being simultaneously removed. The oxygenated blood is then brought to the desired temperature in a heat exchanger, raised to arterial

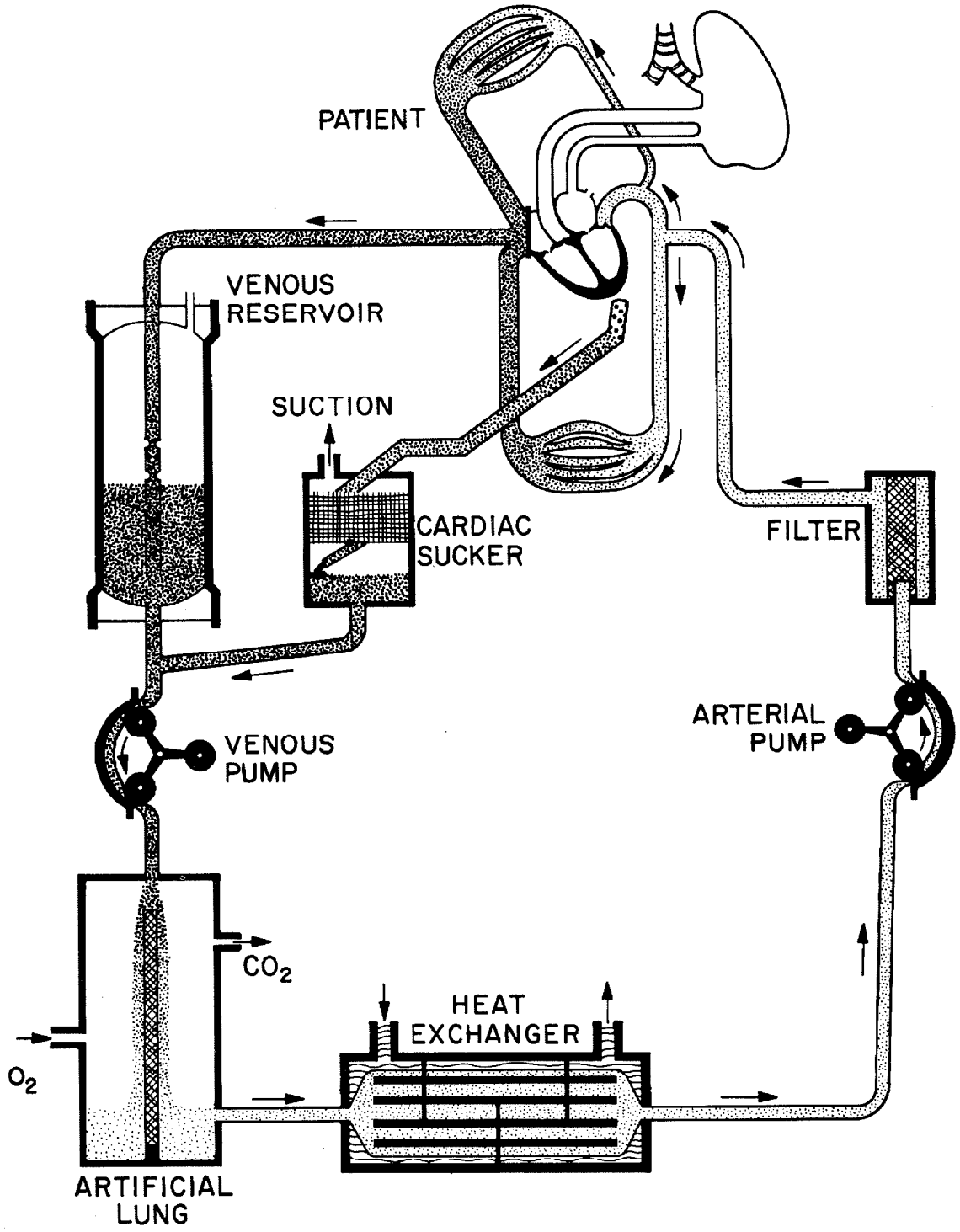

Figure I-1. A Schematic Diagram of a Total Heart-Lung Bypass Circuit Incorporating a Stationary Screen Artificial Lung

pressure by another pump, and returned to the patient through a filter, which removes any blood clots or other debris.

The many types of devices used in each phase of the extracorporeal circuit are well described by Galletti and Brecher (26). The particular combination used by a given surgical team varies widely, and apparently little standardization exists. Unfortunately the mortality rate is unusually high for procedures employing heart-lung bypass (79) and also varies widely from group to group. Many of the major causes of death following extracorporeal circulation, such as cerebral embolism, pulmonary edema, and renal insufficiency are felt to be the result of degradation of the blood during its passage through the artificial circuit. Lee, et al (50,51) have shown that the protein composition of blood is changed considerably by exposure to foreign surfaces, especially blood-gas interfaces. Dobell, et al (19) show further that the toxicity of blood circulated through artificial lungs is markedly increased by exposure to a blood-gas interface, and find that the effect appears to be contained in the plasma, most likely being the result of protein denaturation.

Several other damaging effects are also known to occur in extracorporeal circuits. Toxic materials, such as plasticizers, can be leached from the equipment surfaces, restricting the materials that can be used. The reverse can occur, when materials in the blood (e.g., platelets (73)) deposit onto the equipment

surfaces. Finally, it has been found that rough surfaces tend to cause hemolysis, or rupture of the red cells (26). These effects all reduce the time period over which an extracorporeal circuit can safely be used, regardless of its efficiency.

The gas transfer devices ("artificial lungs") used in an extracorporeal circuit are generally classified into three types: bubble, film, and membrane devices. In the bubble device oxygen gas is dispersed directly into the entering venous blood at the bottom of a chimney. The resulting foam swirls to the surface and spills over the chimney into a settling basin. Oxygen is added to the blood and carbon dioxide removed during this process. The foam is then allowed to coalesce, and any remaining bubbles are removed by the action of surface active substances, settling, trapping, filtration, centrifugation, or some combination of these. The major disadvantage of this type of device is the protein denaturation resulting from the large blood-gas interface. Another serious problem is the difficulty of removing small residual gas bubbles from the coalesced foam.

Film devices create the necessary large surface area by spreading the venous blood into a thin film. This film is produced either by flowing the blood over a stationary surface, such as a wire mesh or column packing material, or by forming the blood film on a moving surface, such as a partially submerged spinning disk or cylinder. This type of device is little better

than the bubbler since it also employs a large blood-gas interface. It does reduce the problem of residual bubbles.

In order to significantly reduce the amount of toxic, protein denaturation, it is necessary to employ a method similar to that used in living organisms -- namely, the introduction of a thin, semi-permeable membrane between the blood and gas phases. Indeed, this has been found to retard the deterioration of the blood (19,51), and this type of lung appears to be the only one capable of being used for extended periods of time. The problem with the membrane lung is the additional resistance to mass transfer presented by both the membrane and the slowly moving blood adjacent to it. Some types of membranes have been found to reduce the rate of carbon dioxide removal to the point where this removal rate becomes the limiting (slowest) process in restoring venous blood to arterial conditions, the reverse of the case in non-membrane lungs. The introduction of the highly permeable silicone rubber membrane has solved this problem, and the limiting resistance in a system using these membranes becomes that of the adjacent blood layer. In order to properly design this type of artificial lung, then, one must be able to estimate mass transfer rates in flowing blood. The development and evaluation of a suitable design theory for gas transfer to blood flowing through an artificial membrane lung is the subject of the work reported here.

B. A General Convective Diffusion Equation for Gas Transfer in Blood.

Blood is a suspension of various formed elements (the blood cells) in a complex solution of salts and non-electrolytes (the plasma). The most numerous cellular species by far is the erythrocyte, or red cell, comprising about 45% of the total volume of normal blood. The leukocyte, or white cell, although almost twice the size of the red cell, is very sparsely distributed among the red cells, outnumbered by more than 600 to 1. The platelets are about one-third the size of the red cell and are normally found to have 1/20 the population of the red cell. The average human red blood cell is a non-nucleated, biconcave disc-shaped cell 8.4 μ in diameter, 2.4 μ thick at the widest point near the edge, and about 1 μ thick near the center. Contained within the cell membrane is a concentrated hemoglobin solution (about 35 gm/100 ml.). Classically, the red cell has been considered to be simply a free hemoglobin solution retained by the cell membrane, but evidence has been found which suggests that the biconcave, discoidal shape is due to an ATP-dependent contractile protein within the cell (35). It is felt by many workers that the hemoglobin itself is an essential structural element.

The cell membrane is a patterned molecular structure of lipoprotein. Again, the structure is not fully understood, and perhaps the red cell can be best described as being highly struc-

tured and containing little or no hemoglobin near the cell surface, and becoming progressively less ordered, with higher hemoglobin concentrations near the center. It is difficult to draw absolute boundaries on the basis of present knowledge. Instead, the reader is referred to the detailed information concerning red cell structure presented in several excellent reviews (35,82).

Although blood is a highly heterogeneous fluid, it is reasonable to treat it as a homogeneous fluid if the scale of the system under consideration is large with respect to the dimensions of the red cell. A theory developed on this basis could not be expected to apply directly to the transport processes occurring in the capillaries, where the dimensions of the system are nearly equivalent to the red cell diameter, but could be expected to apply to the transport processes occurring in extracorporeal devices, such as artificial lungs and kidneys. Since the assumption of homogeneity is questionable even in this case, such a theory would have to be verified experimentally. Once established, a homogeneous-fluid transport theory would also be expected to apply to the transfer of materials in larger blood vessels - for instance, the deposition of materials during hardening of the arteries (66), or the deposition of fibrin on vessel walls (16). Even in the case of gas exchange in the capillaries, this theory would present an interesting limiting case. Its use would be similar to the use of Poiseuille's Law to describe

the hydrodynamic flow of blood through capillaries (11). Indeed, this simple continuum mechanics approach has been shown to successfully describe the flow of blood through capillary tubes with diameters as small as 72 μ (8).

The general equation describing the convective diffusion of a species k in a homogeneous, incompressible fluid can be written (17,3):

$$\underbrace{\frac{D}{Dt}(n_k)}_{\text{rate of change in a flowing element}} = \underbrace{-\nabla\cdot\vec{J}_k}_{\text{net diffusion from the element}} + \underbrace{\sum_j \xi_{kj} J_j}_{\text{net chemical reaction in the element}} \qquad (1)$$

where $\frac{D}{Dt}(\ )$ is the substantial derivative $\frac{\partial}{\partial t}(\ ) + \vec{v}\cdot\nabla(\ )$. If equation (1) is summed over the set of species k = 1, $\cdots$, r where k = 1 corresponds to a physically dissolved gas species i, and the remaining terms represent the concentration of i present in the various reacted forms in the system under consideration, then:

$$\frac{D}{Dt}\left(\sum_{k=1}^{r} n_k\right) = -\nabla\cdot\left(\sum_{k=1}^{r}\vec{J}_k\right) + \sum_{k=1}^{r}\sum_j \xi_{kj} J_j \qquad (2)$$

$\sum_{k=1}^{r} n_k$ is the total concentration of species i, $(n_T)_i$, including all of its chemically reacted forms. Since $(n_T)_i$ is not changed by the chemical reactions, the double summation term in equation (2) must vanish. $\sum_{k=1}^{r} \vec{J}_k$ is the total diffusional flux of i, $(J_T)_i$, which includes any flux due to the diffusion of species k containing i.

In the physiological literature it is customary to write the concentration of physically dissolved species i, n_i, separately. For the concentrations normally encountered in blood Henry's Law is obeyed, and we can write n_i as the product of a solubility coefficient, α_i, and the partial pressure or "tension" P_i of the blood. Then:

$$(n_T)_i = \alpha_i P_i + N_i \tag{3}$$

where:

$$N_i = \sum_{k=2}^{r} n_k \tag{4}$$

Using these relations, equation (2) can be written:

$$\frac{D}{Dt}\left(\alpha_i P_i + N_i\right) = -\nabla\cdot(\vec{J}_T)_i \tag{5}$$

The values of N_i corresponding to chemical equilibrium, N_i^*, are generally available in the literature as a function of P_i. Rearranging equation (5) in terms of this equilibrium value gives:

$$\underbrace{\frac{D}{Dt}\left(\alpha_i P_i + N_i^*\right)}_{\text{equilibrium rate of change in flowing element}} = \underbrace{-\nabla\cdot(\vec{J}_T)_i}_{\text{net diffusion from the element}} + \underbrace{\frac{D}{Dt}\left(N_i^* - N_i\right)}_{\text{rate of change of displacement from chemical equilibrium in the element}} \qquad (6)$$

Equation (6) is the completely general, convective diffusion equation describing the transfer of O_2, CO_2 or inert gas in blood flowing as a homogeneous fluid. To solve this equation the following parameters must be specified.

1. the velocity field $\vec{v}$
2. the solubility α_i
3. the equilibrium relationship $N_i^*(P_i)$
4. the form of the diffusive flux $(\vec{J}_T)_i$
5. the displacement from equilibrium $(N_i - N_i^*)$

C. The Hydrodynamic Nature of Blood.

The rheological properties of blood have been studied in considerable detail, using conventional systems such as coaxial cylinder and capillary viscometers. Since these viscometers are large-scale devices, the measurements can be applied to a homogeneous fluid theory. The viscosity of blood has been found to be non-Newtonian at very low shear rates (57,58), presumably due to the break-up of red cell clusters. In a strongly sheared system ($\dot{\gamma} > 100$ sec^{-1}) the viscosity of blood approaches a constant, "Newtonian" value. Plasma has been found to always exhibit a Newtonian viscosity (10).

Velocity distributions of homogeneous, Newtonian fluids flowing in a multitude of complex systems are available from solutions of the Navier-Stokes equations (70,46,29). It is not intuitively clear to what extent these solutions would describe the flow of blood in these systems, since blood is not really homogeneous, and can behave, depending on conditions, as either a Newtonian or non-Newtonian fluid. An important consideration is that the velocity distribution will be used to estimate a mass transfer rate across a membrane surface. Mass transfer rates in systems of this type are generally controlled by the velocity near the surface, and in this region the shear is greatest and the non-Newtonian effects least important.

Experimental confirmation of the applicability of the homogeneous fluid theory to the flow of blood has been obtained only in simple shear systems (57,58). Since complex shear systems are difficult to treat analytically, it is necessary to perform experimental mass transfer studies with blood in such systems to establish whether or not the homogeneous, Newtonian velocity distributions can indeed be used to predict rates of convective diffusion. In the study to be presented here, the use of the homogeneous, Newtonian equation describing the rotating disk flow system is tested experimentally over a considerable range of fluid velocities.

D. The Carriage of O_2, CO_2 and Kr by Blood.

Oxygen dissolves physically in the various constituents of blood, but over 98% of the available oxygen in blood has formed a reversible combination with the protein hemoglobin, contained within the red cell. Of the total O_2 exchange occurring in the body, about 3% is due to changes in dissolved O_2, and the remainder due to changes in oxyhemoglobin concentration. About 5% of the total CO_2 in blood is physically dissolved. Almost 90% of the total CO_2 is in the form of HCO_3^- ion, and the remaining 5% has reacted with $-NH_2$ groups on protein molecules (primarily hemoglobin), to form carbamino groups (-NHCOOH). Of the total CO_2 exchange normally occurring in the body, about 8% is due to

changes in dissolved CO_2, 63% due to changes in HCO_3^-, and 29% due to changes in carbamino-bound CO_2. Krypton, on the other hand, is an inert gas, and is present solely in the physically dissolved form (15,34). Since for both carbon dioxide and oxygen transfer through whole blood, most of the changes occur within the red cell, it is worthwhile to consider the processes occurring there in greater detail.

Almost all of the oxygen in blood is carried in reversible combination with hemoglobin. The hemoglobin molecule is a spheroidal-shaped protein 64 x 55 x 50 Å large, with a molecular weight of approximately 66,700. It contains four iron atoms in the centers of four protoporphyrin rings termed "heme groups," which are physically located within crevices on the surface of the protein body. The iron molecule in each heme group can bond with six atom groups. In the plane of the porphyrin ring four of these bonds are made with the nitrogen atoms of the adjacent pyrrole rings. Apparently, only when the fifth bond is attached to the proper site in the globin chain, and the heme group is properly positioned, does the remaining covalent bond become able to combine reversibly with oxygen molecules. The unique feature of this combination is that a stable oxygen complex is formed in which the iron remains in the ferrous state, rather than being oxidized to the ferric state. Many similar heme-bearing proteins combine with oxygen, but in these cases, the

iron is rapidly oxidized to the ferric state. The unique behavior of hemoglobin is felt to be at least partially due to the location of the heme group within a crevice formed by hydrophobic groups of the globin chain, providing an environment with low dielectric properties.

The oxygen-oxyhemoglobin equilibrium curve for human blood exhibits a sigmoidal shape rather than the hyperbolic shape normal for an equilibrium of the form

$$Hb + O_2 \rightleftharpoons HbO_2 \qquad (7)$$

The sigmoidal shape is usually interpreted as being the result of the presence of oxygen molecules on one heme group affecting the dissociation constants of the other heme groups on the molecule. However, the heme groups are quite remote from one another, and many workers consider direct heme-heme interactions unlikely. The mechanism substituted by them is an increased affinity due to the profound conformational changes observed upon oxygenation of hemoglobin. In any case, the dissociation curve of human hemoglobin is usually described by the set of equations comprising the Adair Theory (1):

$$Hb_4 + O_2 \rightleftharpoons Hb_4O_2 \; ; \quad K_1 = \frac{[Hb_4O_2]}{[Hb_4][O_2]} \qquad (8)$$

$$Hb_4O_2 + O_2 \rightleftharpoons Hb_4O_4 \; ; \quad K_2 = \frac{[Hb_4O_4]}{[Hb_4O_2][O_2]}$$

$$Hb_4O_4 + O_2 \rightleftharpoons Hb_4O_6 \quad ; \quad K_3 = \frac{[Hb_4O_6]}{[Hb_4O_4][O_2]} \qquad (8)$$

$$Hb_4O_6 + O_2 \rightleftharpoons Hb_4O_8 \quad ; \quad K_4 = \frac{[Hb_4O_8]}{[Hb_4O_6][O_2]}$$

If the heme groups are assumed to be equivalent, the fractional saturation of the blood is given in terms of the oxygen tension P_{O_2} by:

$$f(P_{O_2}) = \frac{K_1'P_{O_2} + 2K_1'K_2'P_{O_2}^2 + 3K_1'K_2'K_3'P_{O_2}^3 + 4K_1'K_2'K_3'K_4'P_{O_2}^4}{4(1 + K_1'P_{O_2} + K_1'K_2'P_{O_2}^2 + K_1'K_2'K_3'P_{O_2}^3 + K_1'K_2'K_3'K_4'P_{O_2}^4)} \qquad (9)$$

Roughton (67) has recently fitted this equation to the best data available for whole human blood at normal physiological conditions (37° C, pH = 7.4, P_{CO_2} = 40 mm Hg) obtaining:

$$K_1' \equiv 0.0219$$
$$K_4' \equiv 0.31$$
$$K_2' = 0.0427 \pm 0.019$$
$$K_3' = 0.00842 \pm 0.002$$

The dissociation curve is a function of pH and P_{CO_2} (the Bohr effect), as well as temperature. The effects of pH, and temperature have been empirically evaluated by Sveringhaus (78), and examples of corrected dissociation curves used in this study are shown in Figure I-2. These corrections do not allow for dis-

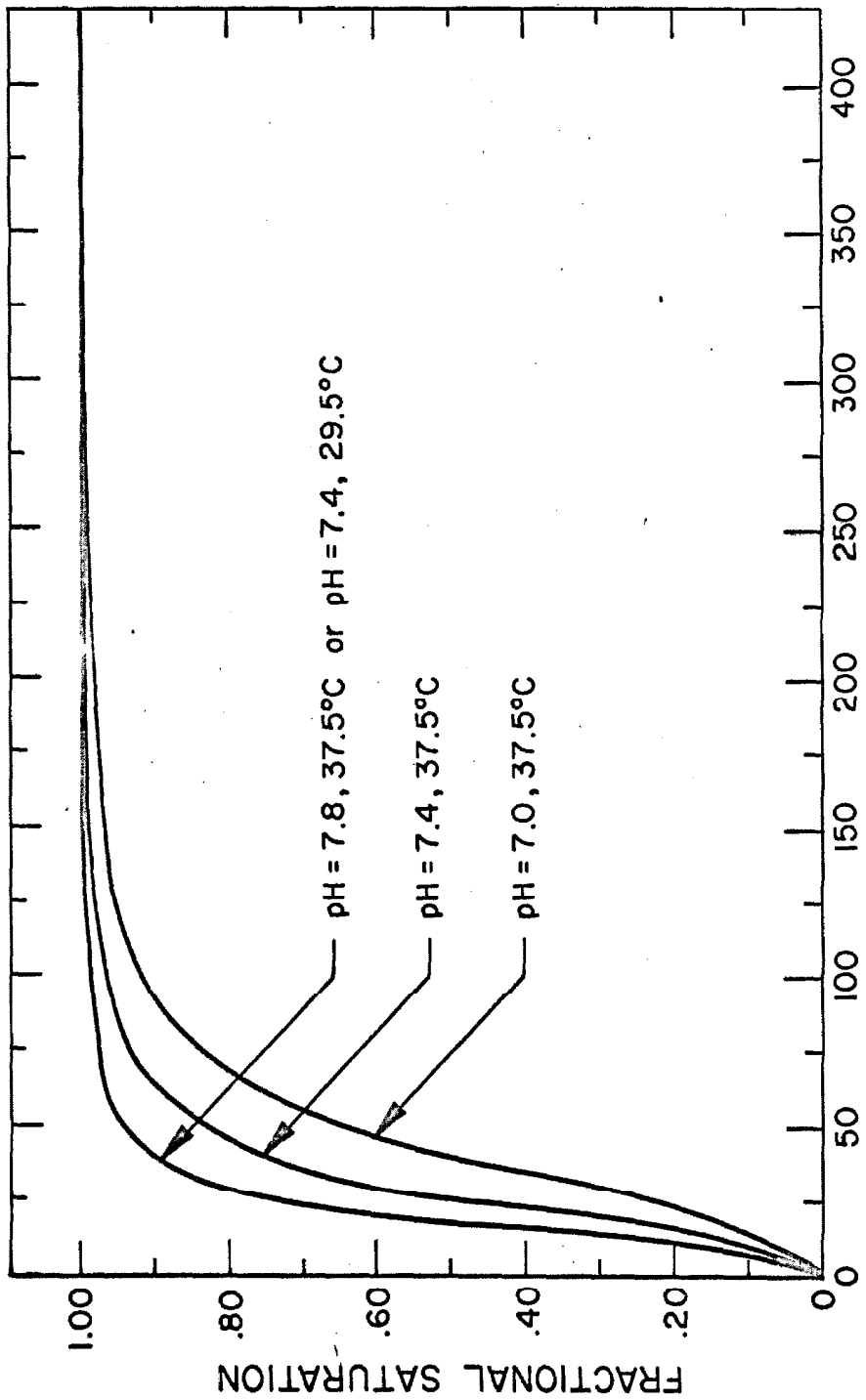

Figure I-2. The Oxygen-Oxyhemoglobin Equilibrium Curve for Human Blood, Calculated Using Equation (9).

tortion of the shape of the dissociation curve, which has been shown to occur at high saturations (54,28), and therefore are only approximate. From the purely theoretical viewpoint this is unpleasant, but it is necessary to retain the proper perspective. The use of an equilibrium curve for a fixed set of conditions is in itself only an approximation, since both P_{CO_2} and pH can vary across the boundary layer for blood being treated in an artificial lung. Furthermore, it must be established to what degree local chemical equilibrium exists. Part of the problem of developing a design theory for artificial lungs is to determine whether the approximation of using the equilibrium dissociation curve corresponding to the ambient conditions outside the blood boundary layer results in an adequate description of the actual process occurring within the boundary layer.

The oxygen-oxyhemoglobin dissociation curve can be used to evaluate $N_{O_2}^*$, since one gram of hemoglobin carries 1.34 cc of oxygen when fully saturated, giving:

$$N_{O_2}^* = 1.34\, C_{Hb}\, f(P_{O_2}) \tag{10}$$

Carbon dioxide, like oxygen, is carried by blood mostly in reversible chemical combination. Unlike oxygen, however, carbon dioxide is involved in more than one chemical reaction. The study of the equilibrium between carbon dioxide and blood has

has been mainly concerned with identifying the particular reactions and their relative importance, rather than with analyzing them in detail, as was done with the oxygen-hemoglobin reaction.

Carbon dioxide exists in three forms in blood - physically dissolved CO_2, HCO_3^-, and carbamino compound. In the plasma, neither of the last two forms is able to react rapidly enough to affect CO_2 transport. Within the red cell both become important. The bicarbonate is able to react reversibly to form CO_2 within the red cell due to the presence of a catalytic agent, carbonic anhydrase, which catalyzes both the hydration of CO_2 and the dehydration of H_2CO_3. The changes in carbamino CO_2 (carbhemoglobin) due to changes in P_{CO_2} within the red cell are small, as in the plasma, but a major change in carbhemoglobin content occurs when the hemoglobin is oxygenated, since oxyhemoglobin has a lower capacity for CO_2 than reduced hemoglobin. Thus, the carriage of carbon dioxide by blood is a complex process, mechanistically coupled with the transport of oxygen.

A typical carbon dioxide dissociation curve for blood is given in Figure I-3. In this case the total carbon dioxide content, $(n_T)_{CO_2}$, is related to the gas tension, where:

$$(n_T)_{CO_2} = \alpha_{CO_2} P_{CO_2} + N^*_{CO_2} \qquad (11)$$

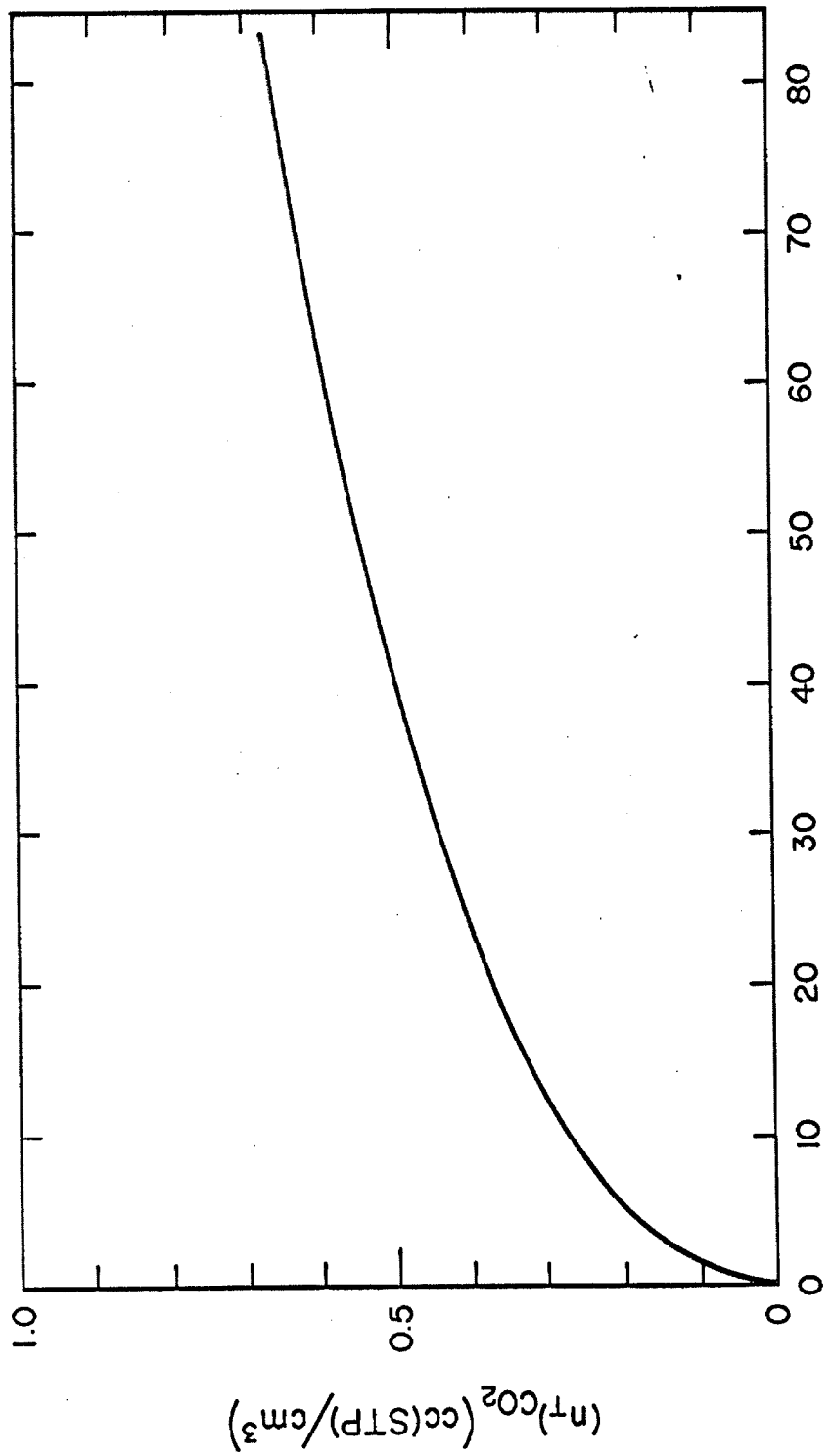

Figure I-3. The Carbon Dioxide Equilibrium Curve for Blood (pH = 7.4, T = 37°C) Adjusted to β = 0.6, H = 0.4.

E. The Nature of Diffusion in Blood.

1. Heterogeneous Media Theory.

Perhaps the most difficult term to evaluate in equation (6) is the diffusive flux $(\vec{J}_T)_i$. In a homogeneous fluid a diffusional flux $\vec{J}_i$ is normally written as Fick's Law:

$$\vec{J}_i = -\mathcal{D}_i \nabla n_i \tag{12}$$

where $\mathcal{D}_i$ is the molecular diffusivity of species i in the fluid. Since blood is a highly heterogeneous fluid, this simple formulation cannot be used, unless the permeability of the suspended phase (red cell) is identical to that of the continuous phase (plasma). This is not the case (30). The established procedure for treating diffusion in a heterogeneous medium is to define an effective diffusivity which, for the case of dissolved gases diffusing through blood, is given by:

$$\vec{J}_{i,\beta} = -(\mathcal{D}_{eff})_i \nabla(\alpha_{i,\beta} P_i) \tag{13}$$

The effective diffusivity $(\mathcal{D}_{eff})_i$ is a function of both the volume fraction of suspended phase (hematocrit) and the relative permeability of the suspended phase to that of the con-

tinuous phase, as well as a function of temperature and viscosity.

Effective diffusivities can be evaluated using Maxwell's treatment of the analogous case of conduction in a suspension of non-interacting spheres (7). Fricke (23) has derived a set of equations within this framework, which describe conduction in a suspension of spheroids, and has empirically determined the proper axial ratio for dog red cells. He found that the measured conductivity was predicted to within 2% for hematocrits up to 0.75, by the equation:

$$(\mathcal{D}_{eff})_i \equiv \mathcal{D}_{i,B} = \mathcal{D}_{i,P}\left[\frac{1+\chi R_i}{1-R_i}\right] \qquad (14)$$

where

$$R_i = H \cdot \left[\frac{\left(\mathcal{D}_{i,RC}/\mathcal{D}_{i,P}\right) - 1}{\left(\mathcal{D}_{i,RC}/\mathcal{D}_{i,P}\right) + \chi}\right] \qquad (15)$$

and x is a shape factor dependent on both the axial ratio and the diffusivity ratio $\left(\mathcal{D}_{i,RC}/\mathcal{D}_{i,P}\right)$. The value of x reduces to 2.0 for spheres. It is necessary to know the value of $\mathcal{D}_{i,RC}$ in order to make these calculations, and since this property is not available, it is usually assumed

that $\mathcal{D}_{i,RC}$ is identical to the diffusivity in a concentrated hemoglobin solution. This assumption neglects any resistance due to the red cell membrane. Roughton (68) attributes a considerable portion of the total red cell transfer resistance to the membrane, but direct experimental comparison of diffusion through packed red cells and through hemolysate from the same cells (44) indicates no significant membrane resistance. Thus, the use of the diffusivity in a concentrated hemoglobin solution appears to be reasonable.

2. Evaluation of $\mathcal{D}_{O_2,RC}$.

The diffusivity of oxygen through hemoglobin solutions has recently been the subject of extensive experimental study. Scholander first reported observing augmented diffusion of oxygen through hemoglobin solutions in 1960 (71). He found that the ratio of oxygen transfer to nitrogen transfer through a Millipore filter soaked with hemoglobin solution, for identical pressure differences across the filter, was markedly increased at low oxygen tensions, where the hemoglobin was not fully saturated. The phenomenon has since been widely studied (38,12,77,84,83,42) , and there is general agreement that the facilitation is due to the simultaneous diffusion of oxyhemoglobin along with the dissolved oxygen, under conditions of near chemical equili-

brium. However, considerable controversy remains regarding oxygen diffusion through intact red cells. Scholander reported in the same paper that the diffusion of oxygen through a red cell paste smeared on filter paper was also facilitated, but some workers suspect that this effect was due to significant hemolysis of the red cells. Roughton (68), in particular, discounts the facilitation of oxygen diffusion in intact red cells, arguing that the diffusivity of the hemoglobin molecules would be too low. Keller and Friedlander (43) measured the hemoglobin diffusivity at concentrations approaching that of the red cell interior and found the diffusivity to be higher than Roughton's estimate. But their measurements were made in free hemoglobin solution, and would not include any effects due to the internal structure of the red cell. Thus, the question of the mobility of the hemoglobin molecule within the red cell is still unsettled.

The use of the facilitation theory to describe oxygen diffusion in intact red cells is also questionable on the basis of the theoretical analysis presented by Friedlander and Keller (24,42). They show that the near-equilibrium behavior necessary for facilitation to occur might not be completely established in hemoglobin layers on the order of the thickness of the red cell. If this is the case, then even when the mobility of the hemoglobin molecule within the

the red cell is unhindered, the amount of facilitation that could occur remains questionable.

If facilitation does occur within the red cell, $\mathcal{D}_{O_2,RC}$ and therefore $\mathcal{D}_{O_2,B}$ will be a function of the oxygen tension. Fatt and La Force (21) have qualitatively compared the facilitated $\mathcal{D}_{O_2,B}$ to Scholander's data with some success, but no quantitative conclusions could be drawn. Both the inert and facilitated values for $\mathcal{D}_{O_2,B}$ are compared with the quantitative experimental results to be presented here.

F. The Displacement From Chemical Equilibrium in Blood.

The last term on the right in equation (6) describes the departure of the system from local chemical equilibrium. The importance of this term can be estimated using measurements of the equilibration rate of red cells, for as indicated above, the changes in CO_2 and O_2 content occur primarily within the cells. This equilibration involves both chemical reaction and diffusional processes, since the reacting materials must diffuse from the reaction site to the surface of the cell, and vice-versa. The results of many such equilibration rate studies are available for the case of oxygen transfer both to and from the red cell (68,22,76,49), but unfortunately few studies of this type have been made on CO_2 transfer. The equilibration rates of red cells with both oxygen and carbon dioxide are an

order of magnitude smaller than the pure chemical reaction rate in free solution, indicating the importance of the diffusional aspects of the process.

The most widely used experimental system for measuring the equilibration rates of red cells is the Hartridge-Roughton rapid-reaction apparatus (36). In this experiment, a suspension of red cells at one gas tension is rapidly mixed with a saline solution at another tension, in a carefully designed mixing chamber. The mixture then flows turbulently down an observation tube. In the continuous flow form of this device (22), the concentration is monitored at fixed locations along the observation tube, corresponding to fixed residence times of the cells in the mixture. Alternatively, either the measuring instrument can be located at a single position and the flow velocity varied, or the change with time can be measured when the flow is suddenly stopped (76).

The equilibration of red cells with oxygen has been found to be approximately a first order process, and is described by the equation:

$$\frac{d}{dt}[O_2Hb] = k'_{Rc}[O_2][Hb]_T \qquad (16)$$

for oxygenation (68), and by the equation:

$$-\frac{d}{dt}[O_2Hb] = k_{Rc}\left([O_2Hb] - [O_2Hb]_{t=\infty}\right) \qquad (17)$$

for deoxygenation (49). Since these relations are convenient to use, it is possible to analyze the displacement from chemical equilibrium during oxygen transfer in flowing blood, in a quantitative manner. For a complex flow system, it is important to determine this displacement from equilibrium "locally" in the flow field since the velocity of the blood, and therefore the effective "residence" of the red cells as they travel through the concentration gradient, can vary widely with position. Such an analysis is presented in the work to be described here, for the case of oxygen transfer.

A similar analysis cannot be made as easily for carbon dioxide transfer. The equilibration in this case involves several simultaneous chemical processes. The rates of some of the individual processes have been studied (18,80), but only one study on the overall equilibration rate is known (14), and it treats CO_2 uptake rather than removal. The process was found to be only approximately exponential and appeared to occur in two stages - a fast initial rate followed by a slower rate. The exchange of HCO_3^- and Cl^- between the red cell and the plasma appears to be a relatively slow process, and perhaps is respon-

sible for the secondary, slow equilibration rate. Because the overall equilibration rate of red cells with carbon dioxide is so poorly understood, it is difficult to estimate the displacement from chemical equilibrium in a quantitative manner, and this point will not be stressed in the work to be presented here.

G. Previous Studies on Gas Transfer to Blood.

It is interesting to look at the previously published studies concerning gas transport in blood from the point of view of equation (6). The only experimental study on mass transfer in whole blood published to date is the work of Marx et al (56). They employed a simplified form of equation (6), obtained by assuming local chemical equilibrium $(N_{O_2} = N_{O_2}^*)$ and a constant value for $\mathcal{D}_{O_2,B}$. The experimental system was a stationary horizontal blood film separated from a flowing oxygen gas stream by a silicone rubber membrane. Since this was a non-convective, unsteady state system, equation (6) reduces to:

$$\frac{\partial}{\partial t}\left(\alpha_{O_2,B} P_{O_2} + N_{O_2}^*\right) = \mathcal{D}_{O_2,B}\,\alpha_{O_2,B}\,\nabla^2 P_{O_2} \qquad (18)$$

or, in their nomenclature:

$$\frac{\partial S}{\partial t} = D \frac{\partial^2 C}{\partial x^2} \qquad (19)$$

Since oxygen was diffusing from a pure gas stream into the blood, the diffusion occurred mostly through saturated blood ($f = 1.0$), with the unsaturated region confined to a thin "advancing front." The experimental value obtained for $\mathcal{D}_{O_2,B}$, 1.3×10^{-5} cm^2/sec at 27° C, would therefore be close to the effective diffusivity of oxygen through saturated blood. The times required for the experimental measurements ranged from less than one minute to more than twenty minutes, easily enough time for significant red cell sedimentation to occur, but this effect was neglected in their analysis of the data. Since the gas stream was below the blood layer, settling of the red cells would tend to shorten the diffusion path, causing an artificially high value for the effective diffusivity to be measured. Additional measurements of this diffusivity are clearly called for. Landino et al (47) present a study on transfer to flowing blood employing the same assumptions as Marx et al, but they do not provide experimental verification of their results.

An experimental study on steady state oxygen transfer from an oxygen gas stream (P_{O_2} = 686 mm Hg) to reduced blood flowing through a hollow silicone rubber fiber has recently been completed (6). The gas stream and the blood were both at P_{CO_2} = 36 mm Hg. The theoretical analysis employed in this work also assumes local chemical equilibrium and constant

$\mathcal{D}_{O_2,B}$. The velocity profiles used are those predicted by Benis' integration of the Casson equation (58), and include any non-Newtonian effect. The form of equation (6) corresponding to these conditions is:

$$\vec{v} \cdot \nabla (\alpha_{O_2,B} P_{O_2} + N^*_{O_2}) = \mathcal{D}_{O_2,B} \alpha_{O_2,B} \nabla^2 P_{O_2} \qquad (20)$$

or, neglecting axial diffusion,

$$v(r) \frac{\partial}{\partial z} \left[\alpha_{O_2,B} P_{O_2} + N^*_{O_2} \right] = \mathcal{D}_{O_2,B} \alpha_{O_2,B} \left[\frac{1}{r} \frac{\partial}{\partial r} \left(r \frac{\partial P_{O_2}}{\partial r} \right) \right] \qquad (21)$$

Experimental verification of the behavior predicted by this equation was sparse. One disadvantage of the fiber system is that the measurement obtained represents the local transfer rate integrated over the entire length of the tube. Deviations in the local transfer rate with axial position are difficult to detect, since they are averaged into the measured integral rate. A one-dimensional mass transfer system, on the other hand, does provide the local transfer rate. Such a system was used in the study presented here and is described in the next chapter.

A fundamental difference between the fiber study and the work on oxygen transfer to be presented here is the operation

of the fiber system without simultaneous carbon dioxide transfer reducing it to a simple oxygenator rather than a true artificial lung. The application of the results for a simple oxygenator to the design of an artificial lung is not necessarily valid, because the P_{CO_2} gradient in an artificial lung can affect the dissociation curve (Bohr effect), and thereby affect the oxygen transfer rate.

In another sense, the work to be presented here complements the fiber study, in that each study represents a different type of mass transfer situation. Flow through a hollow tube is an example of the class of internal flows termed "parallel flow" (i.e., there is only one velocity component), while the system used in the work presented here involves an external "boundary layer flow," which is multi-dimensional. Since there are advantages associated with both types of flows, it is important to develop a design theory applicable to each of them in order to be able to select the best system for a given situation.

CHAPTER II

EXPERIMENTAL APPARATUS AND PROCEDURE

A. The Rotating Disk System.

1. Theory.

Von Karman (81) and later Cochran (9) solved the Navier-Stokes equations describing the laminar flow of a liquid entrained by a flat disk rotating at constant velocity about an axis perpendicular to its surface. The fluid near the disk is given an angular velocity by the motion of the disk surface, this velocity approaching the angular velocity of the disk as the distance from the surface decreases. Centrifugal forces simultaneously impart a radial velocity to the fluid, and to replace the fluid thrown outwards by centrifugal force, additional fluid is drawn towards the disk, creating an axial velocity. Thus, a steady state condition is reached where the fluid flow is fully three-dimensional. Despite this complex flow scheme, the rotating disk is one of the few hydrodynamic systems for which the Navier-Stokes equations can be solved exactly.

Levich (52) simplified the convective diffusion equation for the rotating disk system by assuming the concentration

profile to be independent of radial and angular position - that is:

$$n_i = n_i(y) \tag{22}$$

The resulting simple form of the convective diffusion equation for a system without chemical reaction:

$$v_y \frac{dn_i}{dy} = \mathcal{D}_i \frac{d^2 n_i}{dy^2} \tag{23}$$

could then be solved for the case of a thin concentration boundary layer (i.e., when $\mathcal{D}_i << \nu$), to obtain the transfer rate:

$$(J_i)_{\text{inert}} = 0.62\, \mathcal{D}_i^{2/3} \nu^{-1/6} \omega^{1/2} \alpha_i \Delta P_i \tag{24}$$

This relation applies to most liquids, and has been shown to predict the behavior of a variety of actual rotating disk systems (64,25,53).

The two key features of the rotating disk system are:

1. The equations have exact, steady state solutions.

2. The diffusion boundary layer thickness, and therefore the transfer rate to the disk, is not a function of radial position, making the surface "uniformly accessible."

The only qualification on the second condition is an edge effect which will extend radially inward over a distance of the order of the hydrodynamic boundary layer thickness, δ_f (i.e., the region where the angular velocity component is greater than $0.05\,\omega$). For large disks ($R >> \delta_f$) this effect becomes negligible. As mentioned earlier, this type of one-dimensional mass transfer system is particularly advantageous since the measured transfer rate is a "local" rate, rather than an "integrated" rate.

In the experiments to be described here, the surface of the rotating disk was composed of a semi-permeable membrane. Since this membrane introduces an additional mass transfer resistance into the system, Levich's simple expresion for the transfer rate of an inert material must be modified. Using the nomenclature illustrated in Figure II-1, we can write the transfer rate as:

$$J_{inert} = \mathcal{D}_m \left[\frac{\alpha_m (P_g - P_m)}{\delta_m}\right] = \mathcal{D}_f \left[\frac{\alpha_f (P_m - P_\infty)}{\delta_c'}\right] \qquad (25)$$

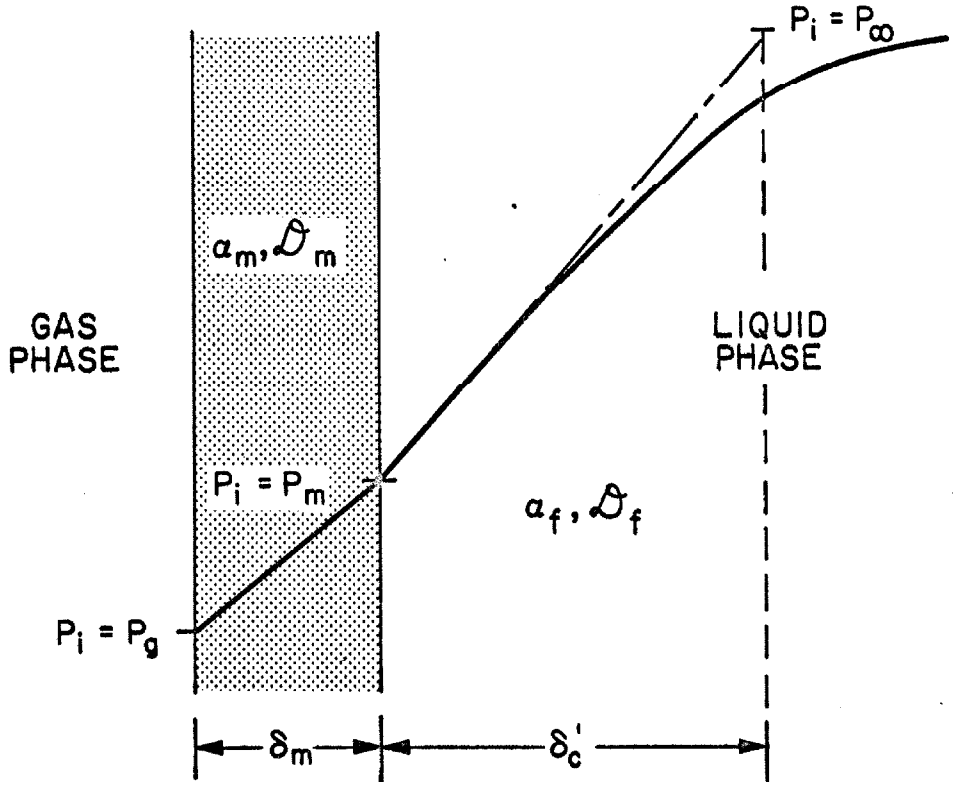

Figure II-1. A Schematic Representation of the Concentration Profile in the Membrane Rotating Disk System, Illustrating the Nomenclature Used in the Text.

where δ_c' is defined by this expression and corresponds to the diffusion boundary layer thickness for a linear concentration gradient. Membrane properties are available for a wide variety of gases, in terms of the permeability:

$$\Phi_m = \mathcal{D}_m \alpha_m \tag{26}$$

Substituting in equation (25) and rearranging:

$$J_{\text{inert}} = \left[\frac{1}{\left(\frac{\delta_c'}{\mathcal{D}_f \alpha_f}\right) + \left(\frac{\delta_m}{\Phi_m}\right)} \right] (P_g - P_\infty) \tag{27}$$

From Levich's analysis:

$$\frac{\delta_c'}{\mathcal{D}_f} = \frac{\alpha_f (P_m - P_\infty)}{J_{\text{inert}}} = 1.61\, \mathcal{D}_f^{-2/3} \nu^{1/6} \omega^{-1/2} \tag{28}$$

so equation (27) can be written:

$$\frac{\Delta P}{J} = \left[1.61 \mathcal{D}_f^{-2/3} \nu^{1/6} \alpha_f^{-1} \right] \omega^{-1/2} + \frac{\delta_m}{\Phi_m} \tag{29}$$

where $\Delta P = P_g - P_\infty$. Thus a plot of $\Delta P/J$ versus $\omega^{-1/2}$ will give a straight line of slope:

$$m = 1.61\, \mathcal{D}_f^{-2/3} \nu^{1/6} \alpha_s^{-1} \qquad (30)$$

and an intercept at $\omega^{-1/2} = 0$ equal to $\left(\delta_m / \Phi_m\right)$. Conversely, if the difference:

$$\alpha_f \left[\frac{\Delta P}{J} - \frac{\delta_m}{\Phi_m} \right] \qquad (31)$$

is plotted against $\omega^{-1/2}$, a straight line through the origin is obtained, with a slope:

$$m' = 1.61\, \mathcal{D}_f^{-2/3} \nu^{1/6} \qquad (32)$$

involving only the diffusivity of the gas in the liquid and the kinematic viscosity of the liquid.

Both these types of plots will be used to illustrate the characteristics of inert gas transfer in the rotating disk system. For the case of transfer of a chemically active species these simple relations do not hold, and it is necessary to solve the original differential equation.

2. The Rotating Disk Apparatus.

The use of a rotating disk system to study gas transport in whole blood presents two design problems.

First, a semi-permeable membrane must be used as the surface of the rotating disk, and second, a rotating bearing must be exposed to the blood. These features must be provided without altering the performance characteristics of the rotating disk system. The rotating disk apparatus used in these studies is shown schematically in Figure II-2. The external housing is constructed of Lucite and all internal surfaces which contact the experimental fluid are made of Teflon, with the exception of the rotating disk and shaft (stainless steel), and the bearing assembly (nylon). It is important to pack the bearing carefully with silicone paste (Dow Corning) before each experiment. The apparatus is maintained at constant temperature by a circulating water bath. The rotating portion of the apparatus is drawn-in solid in Figure II-2, the remaining pieces of the disk assembly being held stationary by associated equipment. The disk is rotated by a PIC geared-pulley system driven by a Minarek-Bodine SH-52 variable speed DC motor. The angular velocity of the disk is directly related to that of the slower moving pulley on the motor, and this latter speed can be measured visually. A teflon-coated magnetic stirrer is placed in the teflon pot to provide complete mixing of the fluid when desired.

The opened apparatus is shown in Figure II-3. The surface of the disk is a dacron-backed silicone rubber membrane

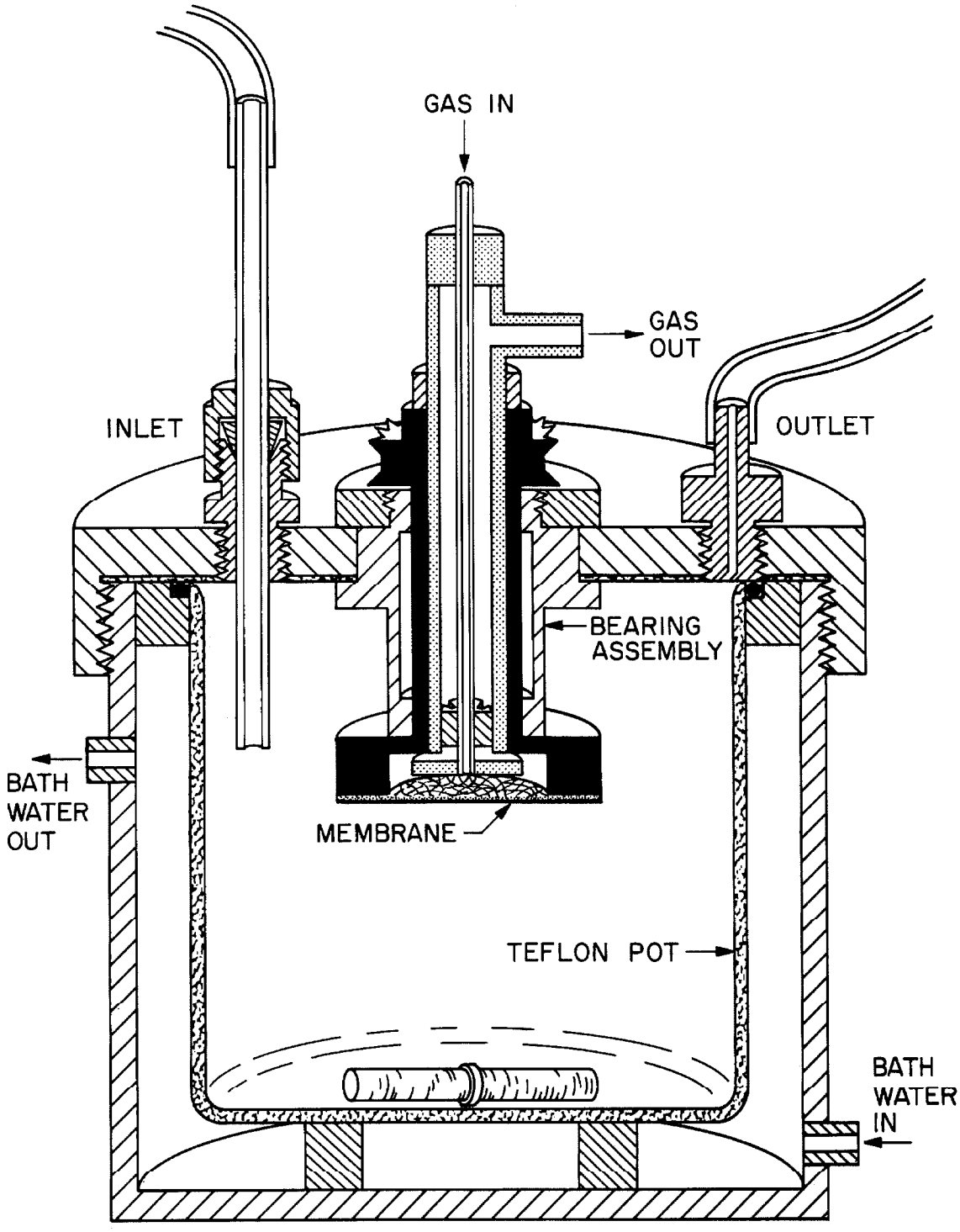

Figure II-2. A Schematic Diagram of the Rotating Disk Apparatus

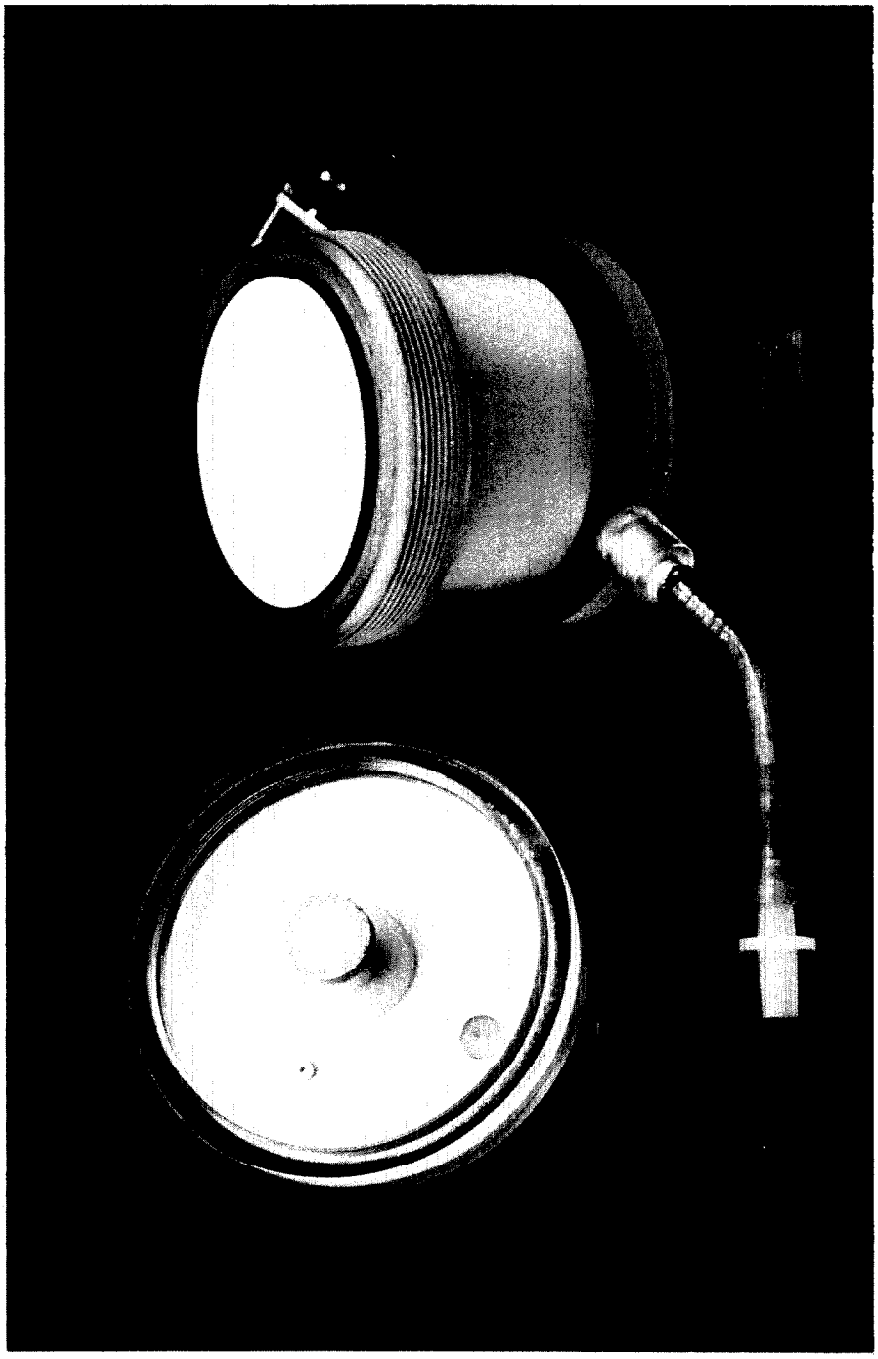

Figure II-3. A View of the Opened Rotating Disk Apparatus

(General Electric Co.), cemented onto the stainless steel disk body with G.E. RTV 102 cement. This membrane is composed of two half-mil silicone rubber sheets laminated together to eliminate pin holes, and attached on one side to a loosely woven mat of 25μ dacron fibers to provide mechanical strength. The diffusional resistances of this membrane to the gases used in this study are listed in Table II-1. The appearance of a typical disk surface following exposure of the disk to whole blood for several hours is shown in Figure II-4. The only visible change is the slight seepage into the edge of the cemented region, the blood being between the membrane and the steel, and not on the membrane surface. This seepage was always confined to the edge of the disk, and never reached the central region of the membrane where the transfer occurred. The gas inlet hole and circular baffle are barely distinguishable behind the membrane. The loosely woven mat of the dacron backing is clearly visible through the relatively transparent membrane.

B. Experimental Procedure.

1. General Procedures.

In a typical experiment, the fluid to be studied is preheated and adjusted to the desired gas concentration in a separate system, and then introduced into the apparatus

Table II-1. Transfer Resistances of the G.E. one mil Silicone Rubber Membrane at 37.5° C for the Gases Used in This Study (65).

$$\left(\delta_m / \Phi_m\right)_{Kr} = 0.24 \times 10^6 \quad \left(\frac{cm^2 \text{ sec mm Hg}}{cc \text{ (STP)}}\right)$$

$$\left(\delta_m / \Phi_m\right)_{O_2} = 0.36 \times 10^6 \quad \left(\frac{cm^2 \text{ sec mm Hg}}{cc \text{ (STP)}}\right)$$

$$\left(\delta_m / \Phi_m\right)_{CO_2} = 0.08 \times 10^6 \quad \left(\frac{cm^2 \text{ sec mm Hg}}{cc \text{ (STP)}}\right)$$

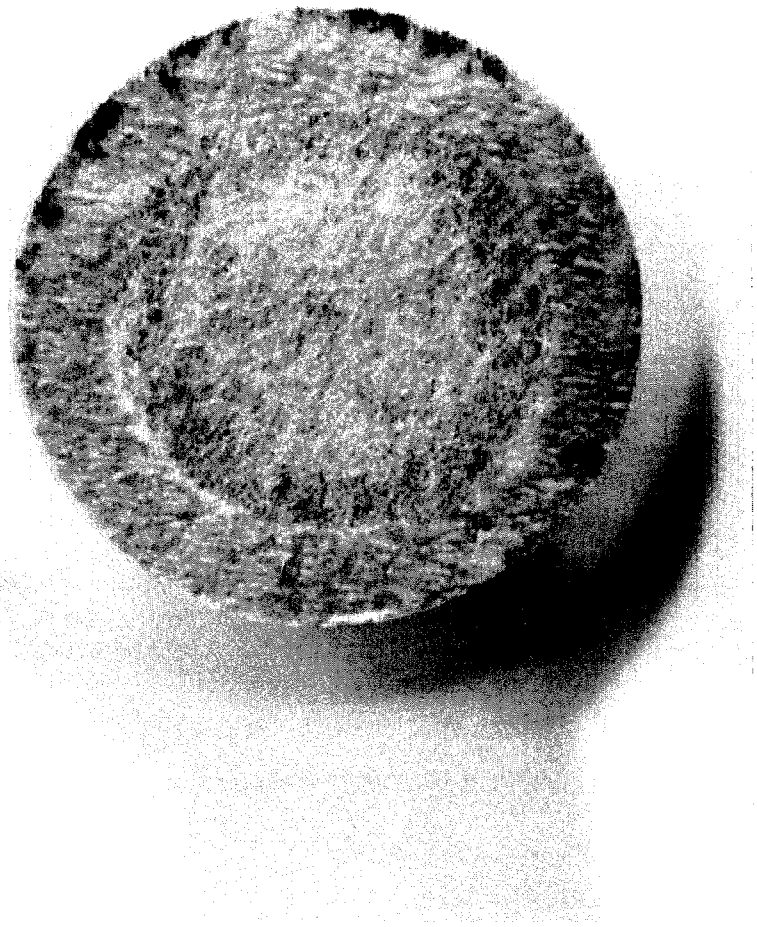

Figure II-4. A Typical Rotating Disk Membrane Following Exposure to Blood

via the movable teflon inlet tube. Initially the tube extends to the bottom of the teflon pot, so that no bubbles will be formed during the filling. During the final stages of filling, the tube is raised above the level of the disk surface, and any remaining gas phase is displaced from the apparatus by tilting it so that the outlet tube becomes the highest point in the pot. The system is then allowed to come to thermal equilibrium before the experiment is begun.

During an experimental measurement, wet gas enters the apparatus through the stainless steel inlet tube and flows between the stationary stainless steel baffle and the rotating back-surface of the silicone rubber membrane. The gas flow rate is set high enough to insure that the gas tension at the back-surface of the membrane is that of the gas entering the apparatus. The gas stream leaves the apparatus via the annular space between the inlet tube and the wall of the stationary core of the rotating disk shaft.

Fluid samples can be withdrawn from the apparatus with a syringe, through a syringe stopper not shown in Figure II-2. To supply the fluid to replace this withdrawn sample, and to provide a constant hydrostatic pressure at the membrane surface, a reservoir (see Figure II-1-1) is connected to the outlet tube of the apparatus and is filled with fluid from the apparatus immediately after displacement of the gas phase.

The surface level of this second reservoir can be adjusted to eliminate any pressure difference across the disk membrane. All fluid connections were made with plastic tubing, and all gas connections were made with glass tubing.

Three types of gas transfer measurements were made, and since each involved a different assemblage of auxiliary equipment, each will be discussed separately.

2. Krypton Transfer Measurements.

In these experiments the uptake of radioactive Kr-85 gas was measured using a NaI (Tl) scintillation detector mounted against the side of the disk apparatus. The transfer was measured as an increase in total activity of the system over a fixed time of rotation at constant speed. This total activity includes the radiation from the gas in the core of the rotating disk. The system was calibrated by comparing the activity of samples of krypton-saturated water with that of water taken directly from the apparatus. The details of these procedures are presented in Appendix II-1.

3. Oxygen Transfer Measurements.

Two types of oxygen transfer experiments were performed. In the oxygenation experiments, wet oxygen gas was flushed

over the back surface of the membrane, and oxygen was transferred to the fluid in the apparatus. The transfer rate was determined by measuring the increase in mixed P_{O_2} of the fluid over a known period of rotation at constant rotational speed.

In the deoxygenation experiments, wet nitrogen gas was flushed through the apparatus, stripping oxygen from the fluid. This trace oxygen gas stream was collected for a measured period of time at each rotational speed, by displacement of an oxygen-free $MnSO_4$ solution from specially designed flasks. The contents of the flasks were then treated chemically to react all of the oxygen with an organic indicator and the total amount of oxygen in each flask was determined spectrophotometrically. The details of this procedure are given in Appendix II-2.

4. Carbon Dioxide Transfer Measurements.

In these experiments carbon dioxide was stripped from the fluid in the apparatus by a wet nitrogen gas stream. The resulting trace concentration of CO_2 in the stream was measured using a Beckman L/B Infrared Analyzer (Model 15A). For a fixed flow rate of gas, the concentration of the stream was directly proportional to the transfer rate. This measurement is not a time average, but rather an instantaneous

measurement of the transfer rate, providing an excellent check on the time required to establish steady state. This time was assumed to be negligible in the preceding types of experiments. Indeed, these CO_2 measurements showed that the transient behavior of the rotating disk system was limited to less than the first 2% of the time period required to measure an oxygen or krypton transfer rate.

C. Source and Treatment of the Blood.

The blood used during the exploratory phase of this study was obtained from St. Vincent's Hospital (Los Angeles). It was the residual blood from an artificial lung (non-membrane type) that had been used in surgery. The blood was citrated, as well as heparinized. This blood was found unsuitable for quantitative studies because it had deteriorated during the course of surgery (see Chapter III). In order to insure that the condition of the blood used in the quantitative experiments was more normal and reproducible, it was decided to use freshly drawn blood. This blood was drawn at the Los Angeles County Blood Bank and contained 50 ml. of 4 % (w/v) sodium citrate in 500 ml. of whole blood. Within several hours of the time it was drawn, the blood was prepared for the experiment by bringing it to body temperature and adjusting it to the desired gas tension by gently bubbling gas through it. Only large bubbles ($d > 0.5$ cm) were

used to minimize protein denaturation and the formation of residual bubbles. When the blood reached the desired conditions, it was introduced into the rotating disk apparatus as described above. The blood was stirred between experimental measurements to eliminate sedimentation effects. Samples were taken from disk height within the apparatus both before and after the series of measurements, and total hemoglobin, methemoglobin, plasma hemoglobin, hematocrit, and viscosity were measured, using the procedures described in Appendix II-3. The average properties of the blood samples obtained in this way are listed in Table II-2. The experimental results for oxygen transfer in different blood samples were adjusted to these "standard" conditions (with pH = 7.4) so that all the data could be presented on the same plot.

Table II-2. The Average Properties of the Blood Samples Taken from the Rotating Disk Apparatus.

Property	Average Value
Total Hemoglobin	$0.136 \pm .01$ (gm/ml)
Plasma Hemoglobin (Initial)	$0.0003 \pm .0001$ (gm/ml)
Plasma Hemoglobin (Final)	$0.0013 \pm .0004$ (gm/ml)
Viscosity	$0.030 \pm .004$ (cm^2/sec)
Hematocrit	$0.41 \pm .04$
Methemoglobin	$0.002 \pm .002$ (gm/ml)

CHAPTER III

EXPERIMENTAL DATA AND ANALYSIS

A. The Solubilities and Diffusivities of Kr, O_2, and CO_2 in Blood.

In order to compare the transfer rates measured in the rotating disk apparatus with transfer rates predicted by various mathematical models, it is necessary to have values for the diffusivity and solubility of Kr, O_2, and CO_2 in blood.

The solubility of krypton in water is readily available (15,33), and the solubility of krypton in blood has been thoroughly studied by Hardewig et al (34). But no values could be found for the diffusivity of krypton in either blood or water, and it was necessary to approximate these values by applying corrections based on molecular diameter differences (74) to available information on oxygen diffusivities. Since the molecular diameters of oxygen and krypton are nearly the same, this correction was always small.

The solubility of oxygen in water is a well-reported property (33), and its solubility in saturated blood ($f = 1.0$) has been shown to obey Henry's Law (37) with reasonable

agreement between measured values (72,20). The diffusivity of oxygen in water has been accurately measured at room temperature (30), but few data are available at body temperature. The simple Stokes-Einstein relation, however, brings the room temperature data into good agreement with the data available at body temperature, as shown in Table III-2. The diffusivity of oxygen in whole blood can be estimated using the heterogeneous media theory discussed earlier. This, in turn, requires values for the diffusivity of oxygen in both concentrated hemoglobin solution and plasma. Yoshida et al (85) measured the diffusivity of oxygen in ox serum at 37° C, but not in plasma. Their results can be adjusted to values for plasma with the Stokes-Einstein relation, using the data of Cokelet (10) for the ratio $(\nu_{plasma}/\nu_{serum})_{37^\circ C}$ in human serum. The viscosity of ox serum is within 10% of the value for human serum (Table III-1) so using the human plasma-serum viscosity ratio seems justified. Buckles (6) has shown that the diffusivity of oxygen in plasma can also be estimated from the diffusivity in water, using the Stokes-Einstein relation. Values obtained for the oxygen diffusivity in plasma by both these procedures are given in Table III-2. Goldstick (30) has carefully measured the non-facilitated diffusivity of oxygen in concentrated hemoglobin solutions at 25° C. In order to use this information at body temperature, it is necessary to assume that the temperature dependence of the viscosity of these hemoglobin solutions is the same as that

Table III-1. Published Values of the Viscosity of Serum and Plasma.

	$T = 25^{\circ}C$	$T = 37^{\circ}C$	ν_{25}/ν_{37}
$\nu_{ox\ serum}$ (85)	1.29 cp *	1.00 cp	1.29
$\nu_{human\ serum}$ (10)	1.39 cp *	1.08 cp	1.29
$\nu_{human\ plasma}$ (10)	1.52 cp	1.21 cp	1.26

* based on temperature dependence of water

	Human	Ox
$\frac{\nu_{serum}}{\nu_{water}}$	1.57	1.46
$\frac{\nu_{plasma}}{\nu_{serum}}$	1.12	----

Table III-2. Calculated and Reported Oxygen Diffusivities in Water, Plasma, and Concentrated Hemoglobin Solution.

Experimenter	$\mathcal{D}_{O_2,H_2O}$		$\mathcal{D}_{O_2,P}$		$\frac{\mathcal{D}_{O_2,P}}{\mathcal{D}_{O_2,H_2O}}$	$\frac{\mathcal{D}_{O_2,RC}}{\mathcal{D}_{O_2,P}}$
	25°C	37°C	25°C	37°C		
Goldstick (30) (human blood)	2.13×10^{-5}	[1] 2.89×10^{-5}	[2] 1.21×10^{-5}	[2] 1.63×10^{-5}	0.58	0.63
Yoshida et al (85) (ox blood)	-	2.76×10^{-5}	[3] 1.24×10^{-5}	[3] 1.66×10^{-5}	0.60	0.61

$$\mathcal{D}_{O_2,RC} = 0.76 \times 10^{-5} \text{ cm}^2/\text{sec} \text{ at } 25^\circ\text{C (30)}.$$

[1] Stokes-Einstein correction from measured value at another temperature.

[2] Stokes-Einstein correction of $\mathcal{D}_{O_2,H_2O}$.

[3] Stokes-Einstein correction of $\mathcal{D}_{O_2,S}$.

of water. Cokelet has shown this to be true for serum and plasma, but it is not clear whether this should be true for more highly concentrated protein solutions. If this assumption is made, then the diffusivity ratio $\left(\mathscr{D}_{O_2,RC}/\mathscr{D}_{O_2,P}\right)$ is independent of temperature and can be calculated at 25° C. Values obtained in this way are given in Table III-2.

The non-facilitated diffusivity of oxygen in blood, calculated from the heterogeneous media theory using a value of 0.62 for the ratio $\left(\mathscr{D}_{O_2,RC}/\mathscr{D}_{O_2,P}\right)$, is given in Figure III-1. Fatt and La Force (45) present a method for calculating the effective diffusivity of oxygen in a system composed of alternating layers of plasma and concentrated hemoglobin solution, arranged either in parallel or in series. These values are included in Figure III-1 since they represent two limiting cases.

Values for the diffusivity and solubility of carbon dioxide in water are available in the literature (74), the diffusivity requiring correction to 37.5° C using the Stokes-Einstein relation. The solubility of carbon dioxide in blood is also known (78). The diffusivity of carbon dioxide in plasma can be estimated using the Stokes-Einstein correction, as discussed earlier, but no values are available for the diffusivity of carbon dioxide in concentrated hemoglobin solution. Thus, in order to use the conductivity equations to calculate $\mathscr{D}_{CO_2,B}$ it is necessary to assume the ratio $\left(\mathscr{D}_{RC}/\mathscr{D}_{P}\right)$ to be the same

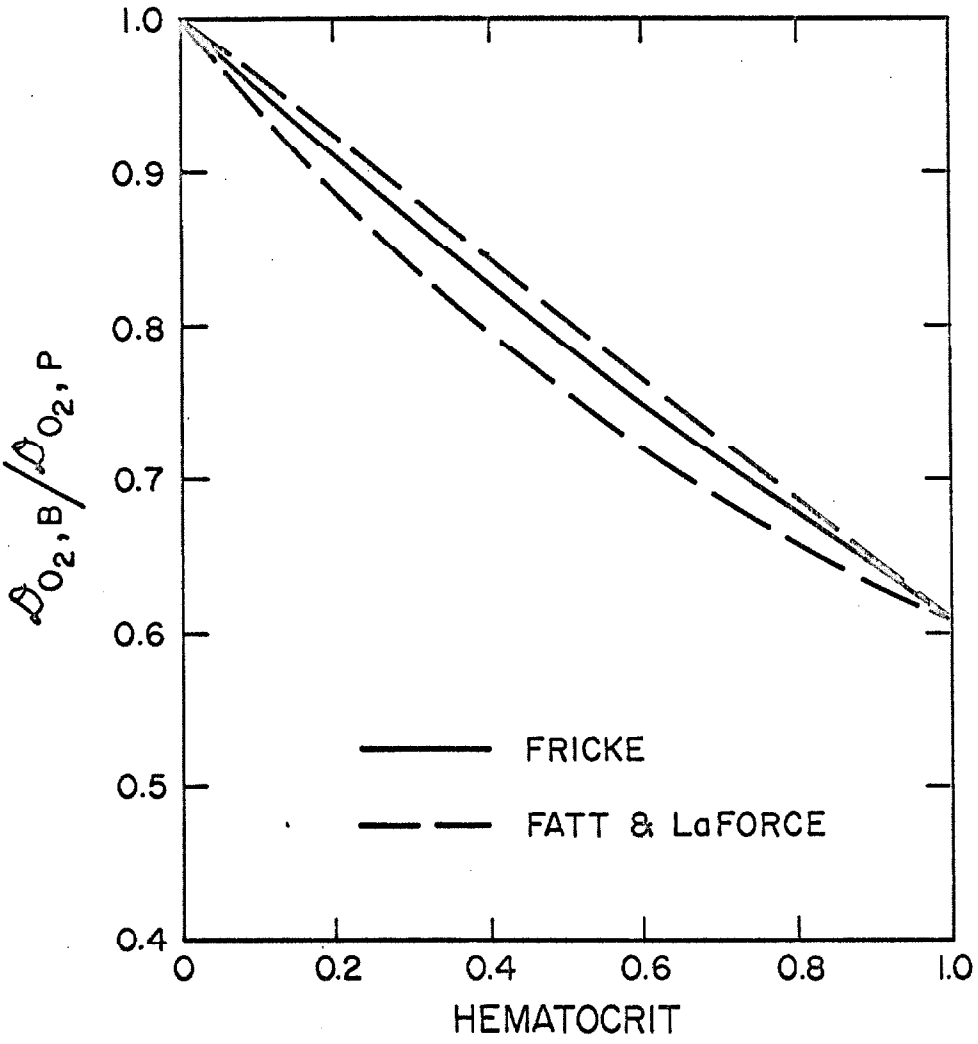

Figure III-1. The Non-Facilitated Effective Diffusivity of Oxygen in Whole Blood, Calculated From the Heterogeneous Media Theory Using the Data in Table III-2.

for carbon dioxide as for oxygen.

B. Krypton Experiments.

1. Results with Water and Freshly Drawn Blood.

The results of the krypton-water experiments are shown in Figure III-2. Each data symbol represents a different membrane, and data points for several of the membranes include values before and after exposure for several hours to freshly drawn blood. No significant increase in membrane resistance occurred in any of the experiments, and the transfer rates are shown to be reproducible from one experiment to another.

Theoretical transfer rates were calculated using the reported solubility and estimated diffusivity of krypton in water. The diffusivity was estimated by correcting the diffusivity of oxygen in water, using both molecular diameter differences obtained from data on properties such as virial coefficients, viscosity, and thermal conductivity (15,39), and differences in the molal volumes at the normal boiling point (15). The ratio of the krypton diffusivity to the oxygen diffusivity was found to be 0.94 using an average of the various values in the literature for the molecular diameters, and 0.88 using the molal volumes at the normal

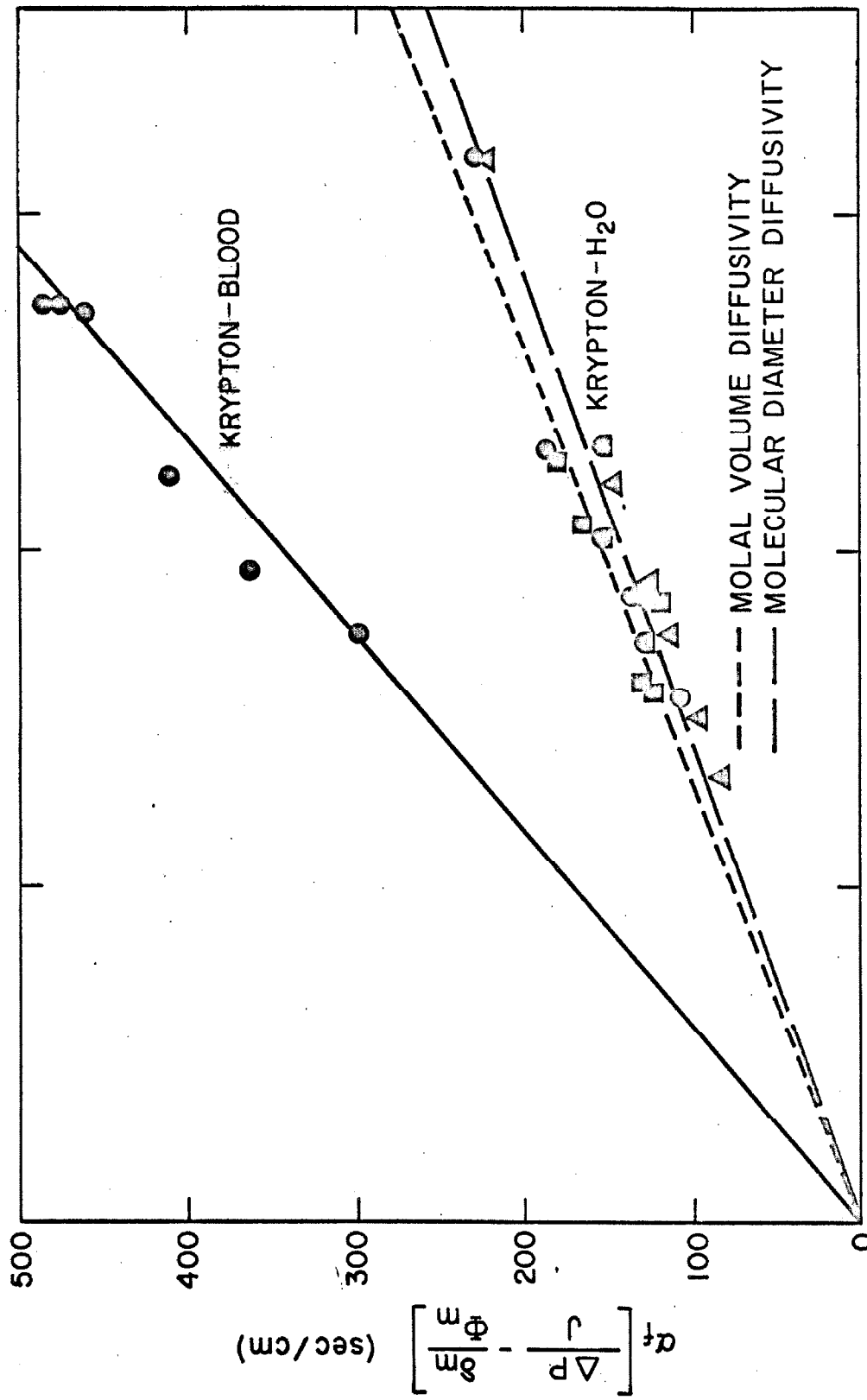

Figure III-2. A Comparison of the Experimental Data for Krypton Uptake with Theoretical Curves.

boiling point. Theoretical lines corresponding to each of these values are drawn on Figure III-2, and both lines are within the experimental error of the data.

The experimental results for krypton transfer to freshly drawn blood are also shown on Figure III-2. The data exhibit, within reasonable experimental error, a linear relationship with $\omega^{-1/2}$, indicating that non-Newtonian effects on the fluid mechanical behavior of the system do not profoundly affect the mass transfer rate over the range of rotational speeds studied. Moreover, if the effective diffusivity of krypton in blood is estimated by correcting the inert effective diffusivity of oxygen in blood, a theoretical line can be calculated for whole blood. This line is the one shown in Figure III-2, and falls close to the measured values. Thus, the convective diffusion of an inert material in flowing blood appears to be reasonably well described by the equation of convective diffusion using the velocity distribution calculated from the Navier-Stokes equations for a Newtonian fluid, and using an effective diffusivity obtained from the theory for diffusion in a heterogeneous media.

2. Results with Blood Used in Cardiac Surgery.

An exception to the conclusions concerning the membrane resistance occurred in an early, exploratory krypton experiment

performed with blood taken from a screen-type oxygenator following use in surgery for several hours. This blood had been exposed to the trauma associated with gas-liquid interface oxygenators and with the suction device used to clear the surgical field. Since quantitative characterization of the blood was not made, only qualitative information can be drawn from the results. The data, shown in Figure III-3, are numbered in chronological order, each point representing an increase in elapsed time of ten to fifteen minutes. The first four points lie on a straight line drawn through the membrane resistance, as theory predicts. Succeeding points then show an ordered increase in total resistance $\Delta P/J$. Following the experiment, the membrane was observed to have a gramular, reddish-brown film deposited on it. The membrane was kept submerged in distilled water while the apparatus was cleaned, and an experiment was then performed with krypton and water, using the fouled membrane. Extrapolation of this water data gave a new, five-fold higher value for the membrane resistance, as shown, and a line originating at this value of the resistance and drawn parallel to the original blood line passes near the final data point. Thus, the observed increase in transfer resistance resulted from the deposit on the membrane. This effect was never observed in experiments with freshly drawn blood. The magnitude of this increase in membrane resistance, and its growth rate indicate that it

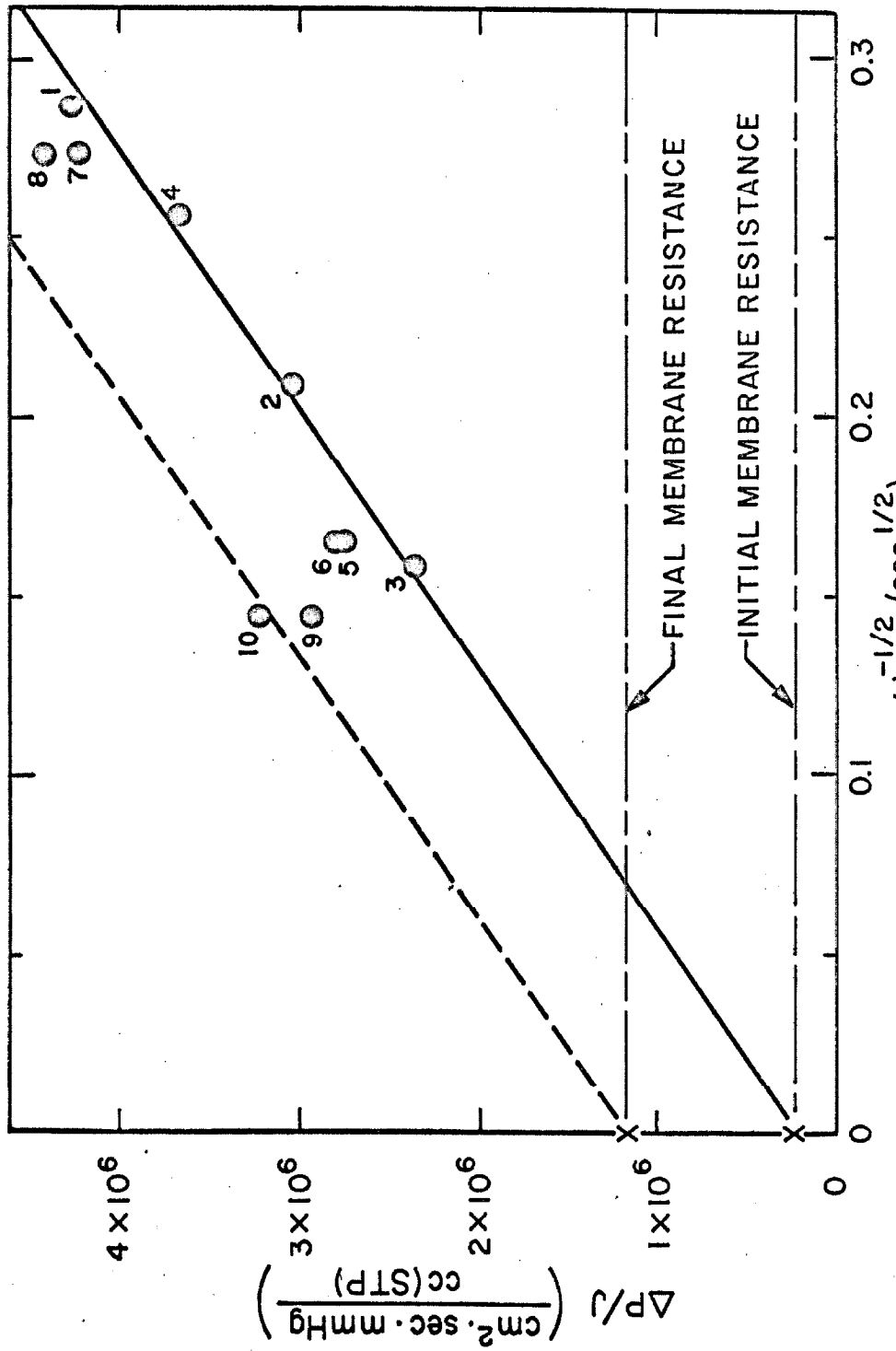

Figure III-3. A Krypton Experiment Performed with Blood Previously Used in a Non-Membrane Lung, Showing a Large Increase in Membrane Resistance with Time. The Data Points are Numbered Chronologically.

would limit the useful life of a membrane oxygenator. How important this effect is in the operation of membrane oxygenators is an important unanswered question; this effect would completely change the nature of the transfer process from a boundary layer limited process to a membrane limited one.

C. Oxygen Experiments.

1. Results with Water and Freshly Drawn Blood.

The measured oxygen transfer rates in water at 37.5° C were found to be within experimental error of the theoretical transfer rate, for both oxygenation and deoxygenation of the water. Deoxygenation data obtained from water experiments before and after use of the disk membranes in fresh blood experiments are shown in Figure III-4. Again, the membrane permeabilities and transfer rates are reproducible to within a few percent of theoretical behavior, so no significant, ordered change in the permeability of silicone rubber membranes to oxygen occurs during exposure of the membranes to fresh blood for periods up to four hours.

Some preliminary experiments were made to study the uptake of oxygen by partially saturated blood, but the technique was found unsuitable for several reasons. The uptake measurements with blood required an accurate knowledge

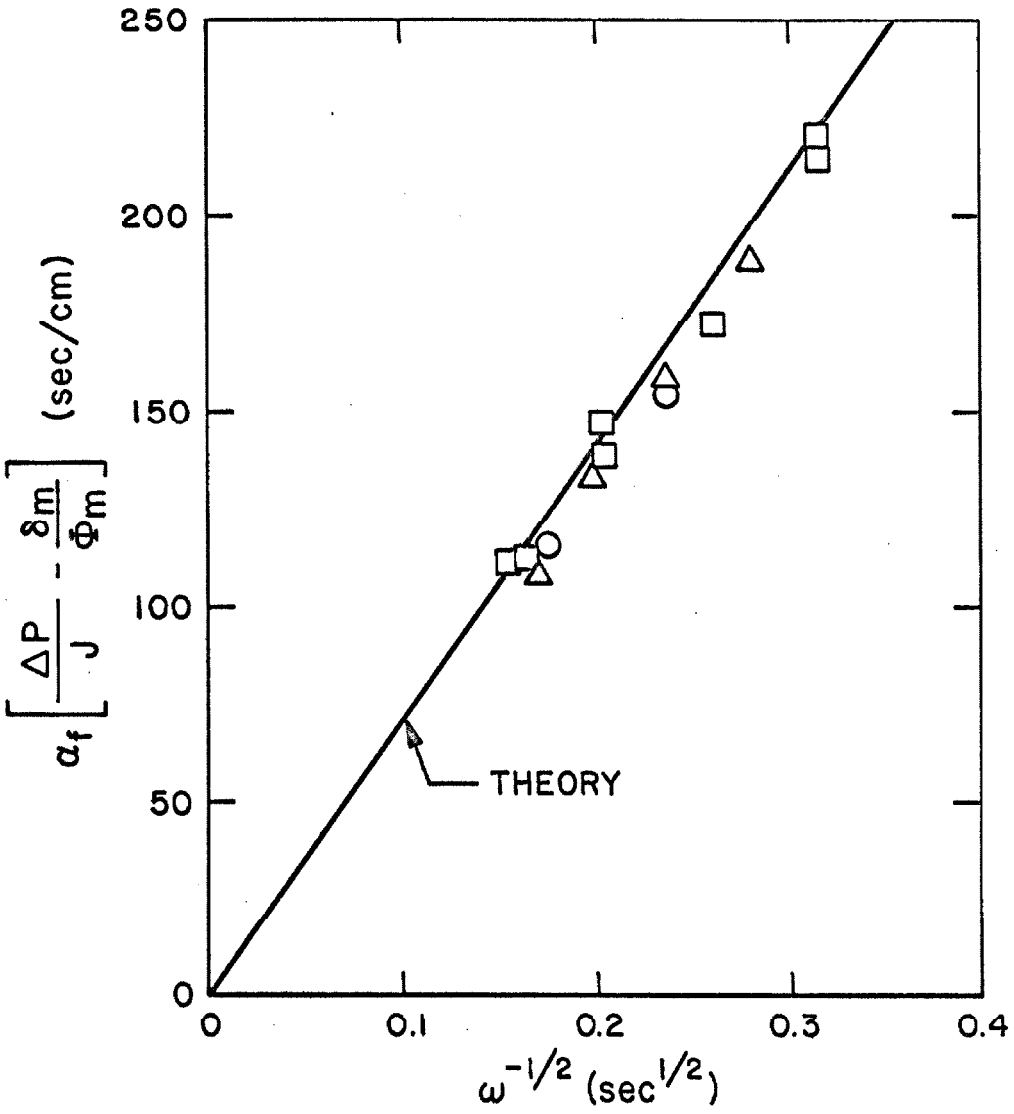

Figure III-4. A Comparison of the Experimental Data for Oxygen Desorption from Water with the Theoretical Curve. Different Symbols Correspond to Different Membranes, and Include Data Taken Before and After Use of the Membrane in an Experiment with Freshly Drawn Blood. The Values of $P_{O_2,\infty}$ Range from 100-500 mm Hg.

of the slope of the oxygenation curve, and small errors in the measurement of this curve, introduced large errors into the transfer rate data. A further limitation was that experiments could only be performed on blood nearly saturated with oxygen. Since the oxygen capacity of blood is so great in the unsaturated region ($P_{O_2} \ll 150$ mm Hg), and the volume of blood in the apparatus is so large, experiments with highly unsaturated blood would produce immeasurably small changes in oxygen tension. The few oxygenation experiments were carried out with nearly saturated blood ($f \sim 0.9$). The blood oxygenation curve was determined spectrophotometrically (41). The average of the measured transfer rates was slightly higher than the transfer rate for saturated blood, but the experimental error was too large to allow meaningful conclusions to be drawn.

The oxygen extraction technique was developed to allow accurate measurements to be made with unsaturated blood. These transfer rate measurements did not require any information about the oxygenation curve, since direct measurements were made of the quantity of oxygen gas removed from the blood. The transfer rates measured during the deoxygenation of several blood samples at various oxygen pressures are presented in Figure III-5. The data fall near the theoretical line for oxygen diffusion through blood in the absence of chemical reaction ("inert" transfer) only at high values

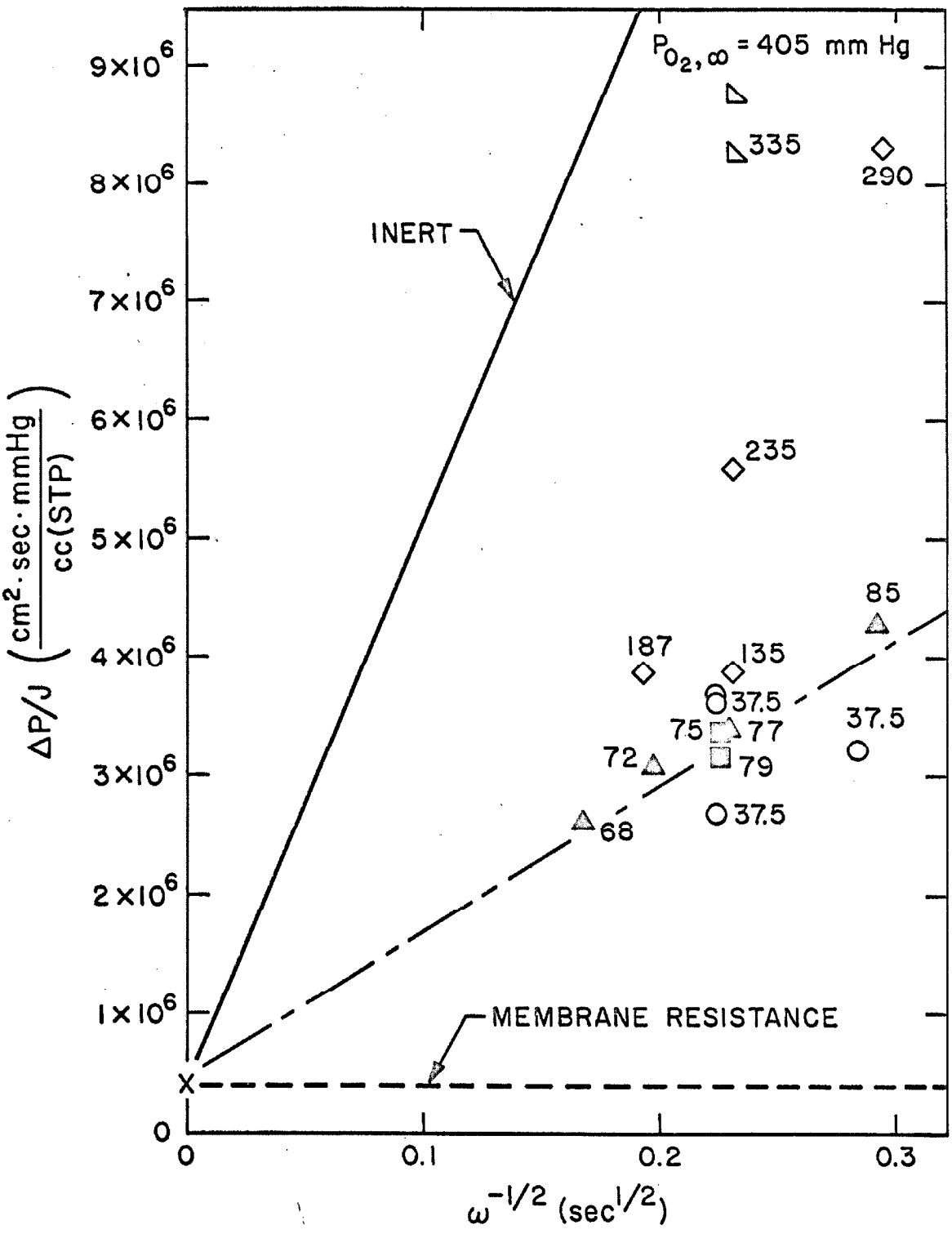

Figure III-5. A Comparison of the Experimental Data for the Deoxygenation of Citrated, Freshly Drawn Blood (P_{CO_2} = 25 - 59 mm Hg), with the Inert Theoretical Curve. Different Symbols Correspond to Different Blood Samples.

of $P_{O_2,\infty}$. At low oxygen pressures the measured transfer rates are more than three times the theoretical inert transfer rates for the same driving force.

Several effects can be noted in Figure III-5. The shaded data points represent data taken at similar values of $P_{O_2,\infty}$ in a pressure range just above the steep portion of the oxygenation curve. These two sets of experimental measurements show first that the transfer rate is reproducible from one experiment to another. They also show that the relationship between the flux and $\omega^{-1/2}$ is approximately linear for oxygen transfer in blood. This linear behavior indicates the absence of a net chemical reaction term in the conservation of species equation, as expected, but also suggests that local chemical equilibrium exists in the system. If local equilibrium did not exist, the fractional saturation of the blood would be unable to keep up with the changes in oxygen pressure through the boundary layer. The degree of chemical equilibrium would become a function of the residence time of the blood in the boundary layer, and since the fluid velocities, and therefore the residence times, depend on the rotational speed, the transfer rate would be expected to exhibit an abnormal dependence on ω , or in other words, a non-linear dependence on $\omega^{-1/2}$.

Even if local equilibrium does exist, it can be shown

that the linear relationship between transfer rate and $\omega^{-1/2}$ will hold only for a constant set of boundary conditions. Since the shaded data points correspond to approximately the same boundary conditions, the observed linear behavior suggests that local chemical equilibrium is approached within the boundary layer.

2. Comparison of the Experimental Results with Three Theoretical Models.

The deoxygenation rates measured in these experiments were compared with the transfer rates predicted by solutions to three forms of the general convective diffusion equation for blood. First, and simplest, is the "inert" model, which neglects the existence of any reversibly combined species. For this model the general equation becomes:

$$\frac{D}{Dt}(P_i) = \mathcal{D}_{i,B} \nabla^2 P_i \qquad (33)$$

or, for the rotating disk system:

$$v_y \frac{dP_i}{dy} = \mathcal{D}_{i,B} \frac{d^2P_i}{dy^2} \qquad (34)$$

This is the equation solved analytically by Levich, whose solution was presented earlier (equation (29)). The "inert"

model has already been shown to describe the convective diffusion of krypton in blood.

The second model not only recognizes the existence of reversibly combined species, but assumes that a state of local chemical equilibrium exists. The diffusivity, however, is assumed to be unfacilitated. For this "local equilibrium" model the general equation becomes:

$$\frac{D}{Dt}\left(\alpha_{i,\beta} P_i + N_i^*\right) = \alpha_{i,\beta} \mathcal{D}_{i,\beta} \nabla^2 P_i \qquad (35)$$

or, for the case of oxygen transfer in the rotating disk system:

$$v_y\left[\alpha_{o_2,\beta} + 1.34 C_{Hb}\left(\frac{df}{dP_{o_2}}\right)\right]\frac{dP_{o_2}}{dy} = \alpha_{o_2,\beta}\mathcal{D}_{o_2,\beta}\frac{d^2P_{o_2}}{dy^2} \qquad (36)$$

It can be seen from the form of equation (36) that the effect of the oxygen-oxyhemoglobin equilibrium is to increase the size of the convective term when the oxygen tension drops to values corresponding to the steep portion of the equilibrium curve, since the derivative term, $1.34\ C_{Hb}\left(df/dP_{o_2}\right)$, becomes large with respect to $\alpha_{o_2,\beta}$ there. Physically this can be interpreted as follows: At high partial pressures of oxygen most of the oxygen convected towards the surface of the rotating disk is present in the immobile form,

oxyhemoglobin. Only at low oxygen pressure is this enormous supply of oxygen released as the diffusible species, physically dissolved oxygen. When this release occurs, diffusion is no longer able to remove the additional oxygen rapidly enough to reduce the partial pressure at the same rate as before. Therefore, the partial pressure remains at a high value until the distance to the surface of the disk is so small that large partial pressure gradients are produced, enabling diffusion to remove the additional oxygen. This effect is shown in Figure III-6 where concentration profiles, obtained by numerically solving (see Appendix III-1) the equations for the inert model and local equilibrium model, are presented for the case of equal transfer rate. The $P_{O_2,\infty}$ required in the local equilibrium case is a fraction of that required in the inert case, and the compression of the boundary layer toward the surface of the disk ($y = 0$) is obvious. This effect tapers off at higher values of $P_{O_2,\infty}$ for two reasons. First, the fraction of the boundary layer in which the oxygen-oxyhemoglobin equilibrium is active becomes a smaller fraction of the total thickness. Second, the region where the convective term is enhanced by the chemical equilibrium draws closer and closer to the surface of the disk. Since the velocity v_y varies with the square of the distance from the disk, the decrease in velocity tends to offset the chemical enhancement. Concentration profiles at higher $P_{O_2,\infty}$

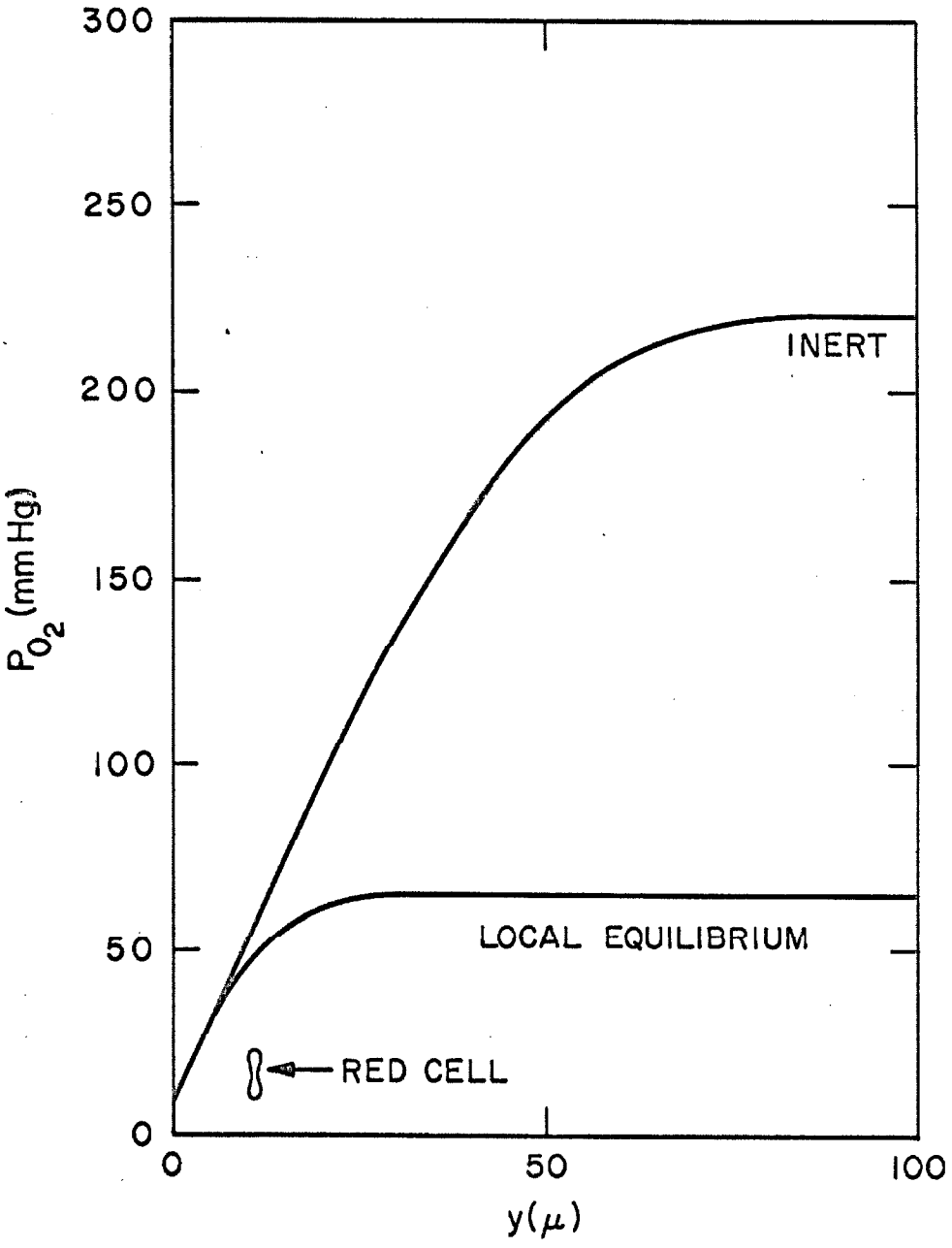

Figure III-6. Deoxygenation Concentration Profiles at Low P_{O_2} Predicted by the Inert and Local Equilibrium Models for the Same Transfer Rate.

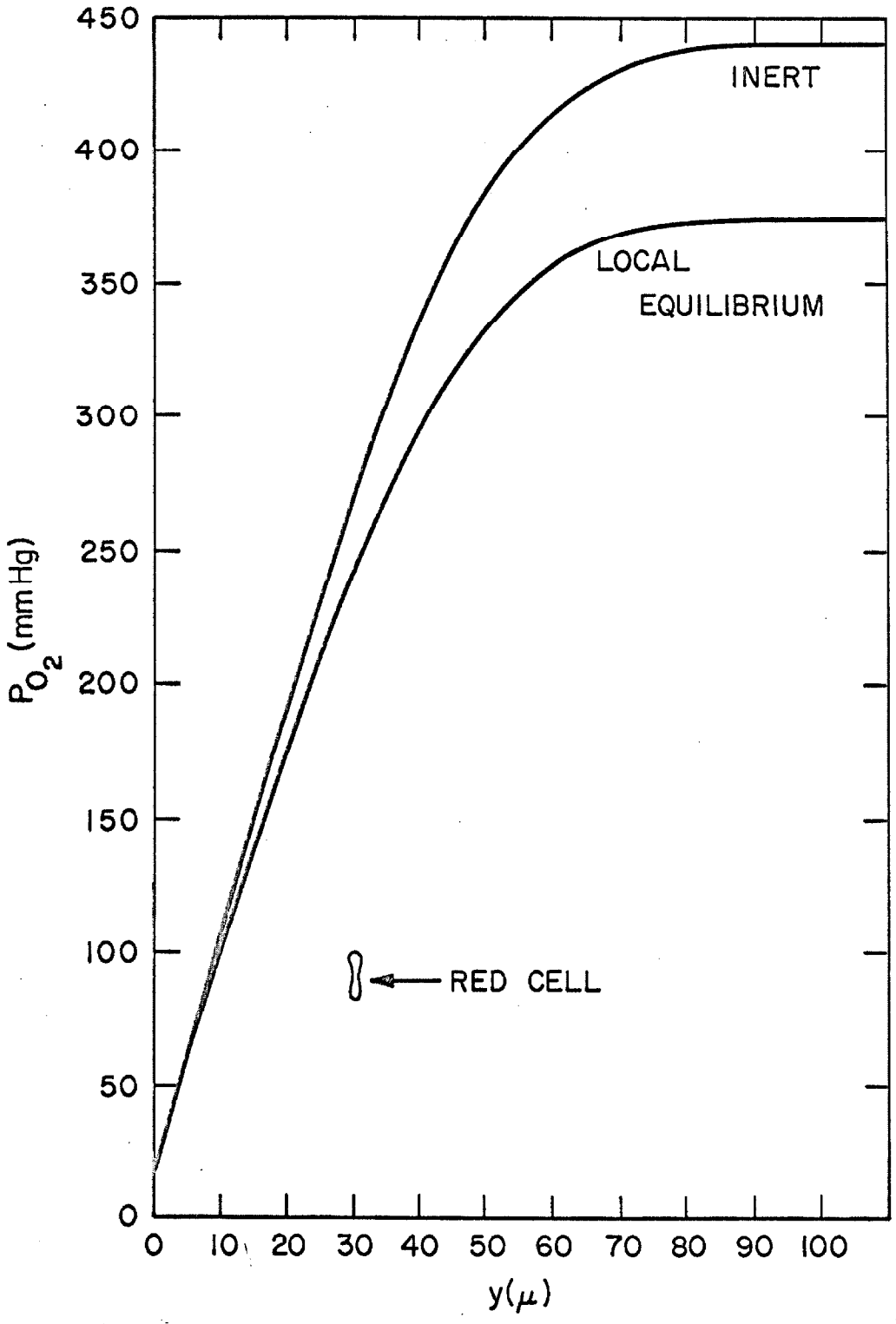

Figure III-7. Deoxygenation Concentration Profiles at High P_{O_2} Predicted by the Inert and Local Equilibrium Models for the Same Transfer Rate.

are shown in Figure III-7, and the difference between the equilibrium and inert cases is clearly reduced.

The third model applicable to convective diffusion in blood involves the same assumptions as the local equilibrium model, with the additional feature of completely facilitated diffusion. The general convective equation then becomes:

$$\frac{D}{Dt}\left(\alpha_{i,\beta} P_i + N_i^*\right) = \alpha_{i,\beta} \nabla \cdot \left(\mathcal{D}_{i,\beta}^* \nabla P_i\right) \qquad (37)$$

where $\mathcal{D}_{i,\beta}^*(P_i)$ is the facilitated diffusivity obtained from the heterogeneous media theory. For the case of oxygen transfer, this effective diffusivity is obtained using the facilitated diffusivity within the red cell:

$$\mathcal{D}_{O_2,RC}^* = \mathcal{D}_{O_2,Hb} + \mathcal{D}_{Hb}\left[\frac{1.34\, C_{Hb}}{\alpha_{O_2,RC}}\right]\left(\frac{df}{dP_{O_2}}\right) \qquad (38)$$

For oxygen transfer in the rotating disk system, equation (37) then becomes:

$$v_y\left[\alpha_{O_2,\beta} + 1.34\, C_{Hb}\left(\frac{df}{dP_{O_2}}\right)\right]\left(\frac{dP_{O_2}}{dy}\right) = \alpha_{O_2,\beta}\frac{d}{dy}\left(\mathcal{D}_{O_2,\beta}^*\frac{dP_{O_2}}{dy}\right) \qquad (39)$$

The facilitated effective diffusivity of oxygen in blood, calculated using equation (38), is shown in Figure III-8 as a function of oxygen tension.

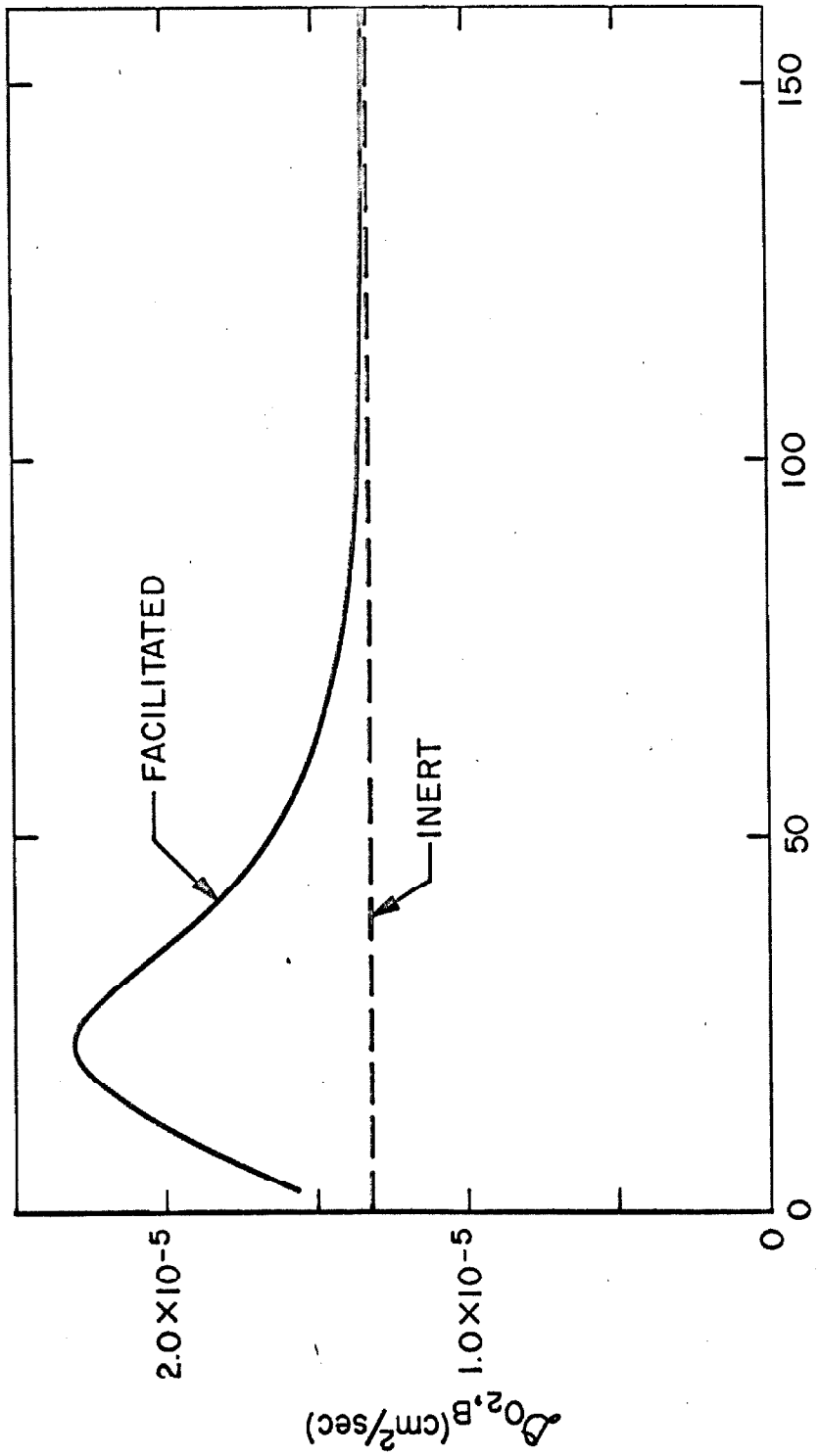

Figure III-8. The Effective Diffusivity of Oxygen in Standard Blood Calculated Using the Facilitated Local Equilibrium Model, With $\mathcal{D}'_{Hb,Rc}$ = 1.25×10^{-7} cm^2/sec, $\alpha_{O_2,Rc} = 2.2 \times 10^{-5}$ cc (STP)/cm^3 mm Hg, $\mathcal{D}_{O_2,Rc}$ = 1×10^{-5} cm^2/sec.

The measured deoxygenation rates of blood, adjusted to standard conditions, are compared with numerical solutions to these three models in Figure III-9. An additional comparison is made with the local equilibrium model calculated at pH = 7.8. The carbon dioxide gradients existing in the boundary layer can alter the pH of the blood, depending on the degree of chemical equilibrium, and this would in turn change the oxygenation curve, as discussed earlier. The oxygenation curve is also changed upon removal of carbon dioxide because of a steric effect on the affinity of hemoglobin for oxygen (60). The pH 7.8 curve is included in Figure III-9 to illustrate the possible effect of these phenomena on the oxygen transfer rate.

The experimental data lie slightly above the local equilibrium curve, but not as high as the facilitated local equilibrium model would predict, perhaps in part due to effects associated with the simultaneous CO_2 removal. Since the local equilibrium model is the closest fit, and is slightly conservative, it represents a good design theory for oxygen transfer to flowing blood. Thus, while all of the above mechanisms may be occurring simultaneously in the boundary layer, the net effect appears to be satisfactorily described by the simple local equilibrium model.

Table III-3. Data from the Deoxygenation Experiments with Citrated, Freshly Drawn Blood.

$P_{O_2,\infty}$ (mm Hg)	ω (sec^{-1})	J_{O_2} ($cc(STP)/cm^2 sec$)	$P_{O_2,m}$ (mm Hg)	$J_{adj.}$ †	J_{adj}/J_{inert}
79	.226	25.0×10^{-6}	9.0	25.0×10^{-6}	3.53
75	.226	22.3×10^{-6}	8.0	22.3×10^{-6}	3.32
85	.293	20.1×10^{-6}	7.2	20.1×10^{-6}	3.39
77	.228	22.9×10^{-6}	8.2	22.9×10^{-6}	3.31
72	.198	23.3×10^{-6}	8.4	23.3×10^{-6}	3.18
68	.168	25.9×10^{-6}	9.3	25.9×10^{-6}	3.19
290	.295	34.9×10^{-6}	12.5	31.4×10^{-6}	1.57
235	.232	42.0×10^{-6}	15.1	37.7×10^{-6}	1.84
187	.193	48.5×10^{-6}	17.5	43.2×10^{-6}	2.22
135	.230	35.0×10^{-6}	12.6	31.1×10^{-6}	2.61
405	.232	46.2×10^{-6}	16.6	44.9×10^{-6}	1.27
335	.232	40.6×10^{-6}	14.6	39.1×10^{-6}	1.34
37.5	.285	11.6×10^{-6}	4.2	12.2×10^{-6}	4.54
37.5	.224	13.9×10^{-6}	5.0	14.6×10^{-6}	4.31
37.5	.224	10.3×10^{-6}	3.7	10.8×10^{-6}	3.19
37.5	.224	9.9×10^{-6}	3.6	10.4×10^{-6}	3.07

† The data are adjusted to the "standard" conditions listed in Table II-2, using the results of a parametric study on the local equilibrium model.

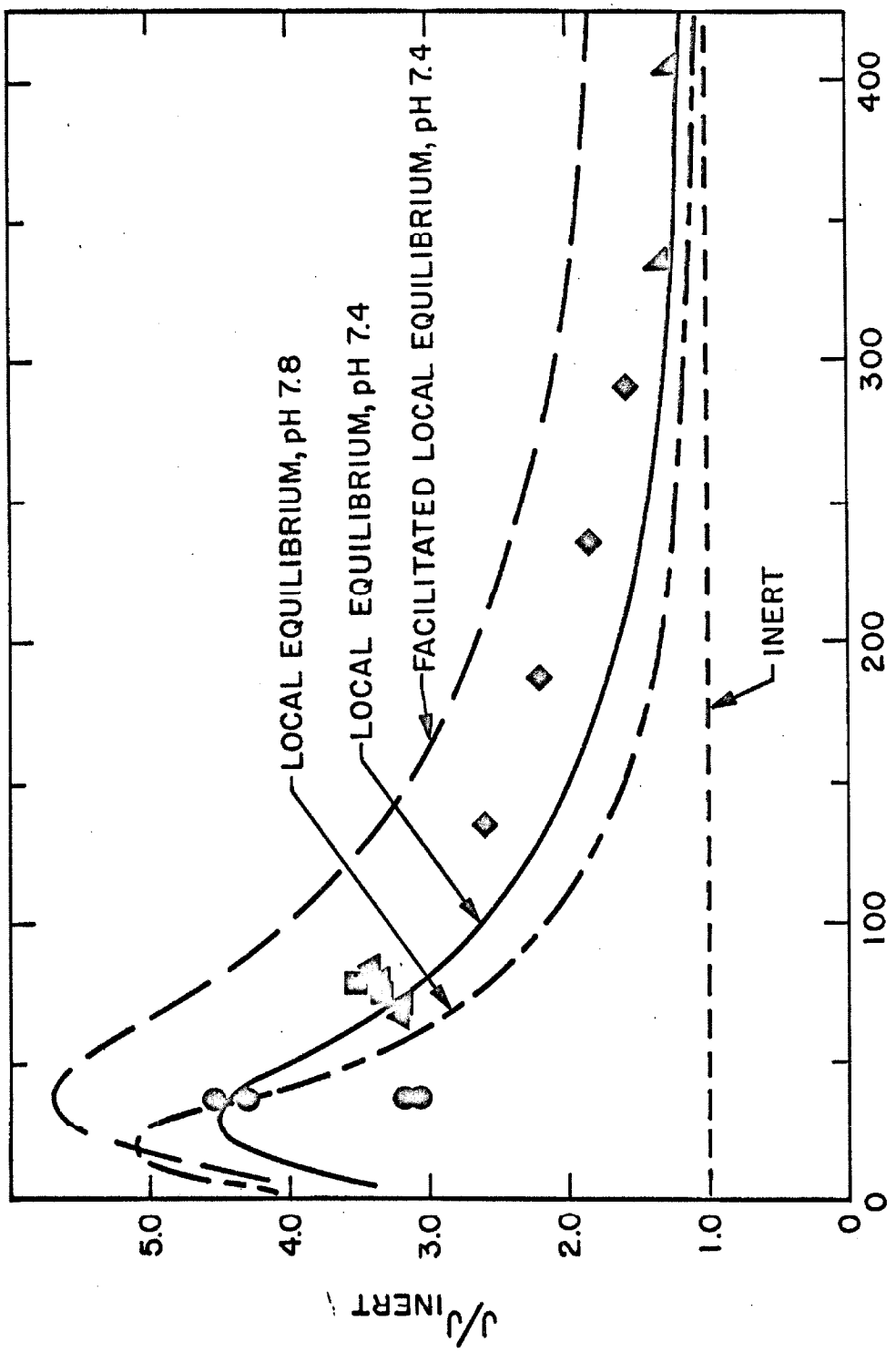

Figure III-9. A Comparison of the Measured Deoxygenation Transfer Rates in Freshly Drawn, Citrated Blood (Corrected to Standard Conditions) with the Three Mathematical Models.

3. Test of the Local Equilibrium Hypothesis.

Both the local equilibrium and facilitated local equilibrium models assume that a state of chemical equilibrium exists between the red cells and the surrounding plasma. The extent of equilibrium possible in an actual red cell-plasma system can be visualized by determining the distance a red cell would travel during the time required for re-equilibration, following a perturbation in the plasma tension. This "re-equilibration length" would vary throughout the boundary layer because of the variation of the velocity v_y. Since the equilibration rate of red cells with oxygen has been found to follow a first-order rate law, the characteristic time during which a specified fractional approach to equilibrium occurs, can be easily calculated. The product of this characteristic time and the velocity of the red cell then gives the "re-equilibration length."

Since v_y varies as y^2 near the surface of the disk, a conservative value of the residence time would be obtained using y_r, the total thickness of the region within the boundary layer where significant chemical reaction occurs (that is, the region corresponding to $P_{O_2} \leq 100$ mm Hg). When $P_{O_2,\infty} \leq 100$ mm Hg, y_r equals δ_c, the diffusion boundary layer thickness. For this situation a more reasonable value would be obtained using half the boundary layer

thickness, since the concentration gradient at the edge of the boundary layer is very small and lack of chemical equilibrium would not have as large an effect as it would nearer the surface of the rotating disk, where the concentration gradient is steep. Values of y_r obtained from the numerical solutions of the local equilibrium model are given in Figure III-10. The boundary layer thickness is a function of $P_{O_2,\infty}$ because of the compression effect the oxygen-oxyhemoglobin equilibrium has on the concentration profile. From Figure III-10, the maximum value is seen to be approximately 40μ for $\omega = 10.0$ sec^{-1}, 30μ for $\omega = 19.0$ sec^{-1}, and 25μ for $\omega = 30.0$ sec^{-1}. These values would be expected to lead to underestimates of the residence times, and as stated above one half these values would be more reasonable.

The time required for re-equilibration of a red cell in response to a sudden decrease in plasma oxygen tension can be estimated from the rate constant k_{RC} measured in red cell deoxygenation experiments using the Hartridge-Roughton rapid reaction apparatus. The average of the reported values at standard physiological conditions is 25 sec^{-1}. Using this value, the time, τ, required to attain 95% of chemical equilibrium in response to a perturbation is found to be about 0.1 second.

The re-equilibration lengths can now be calculated.

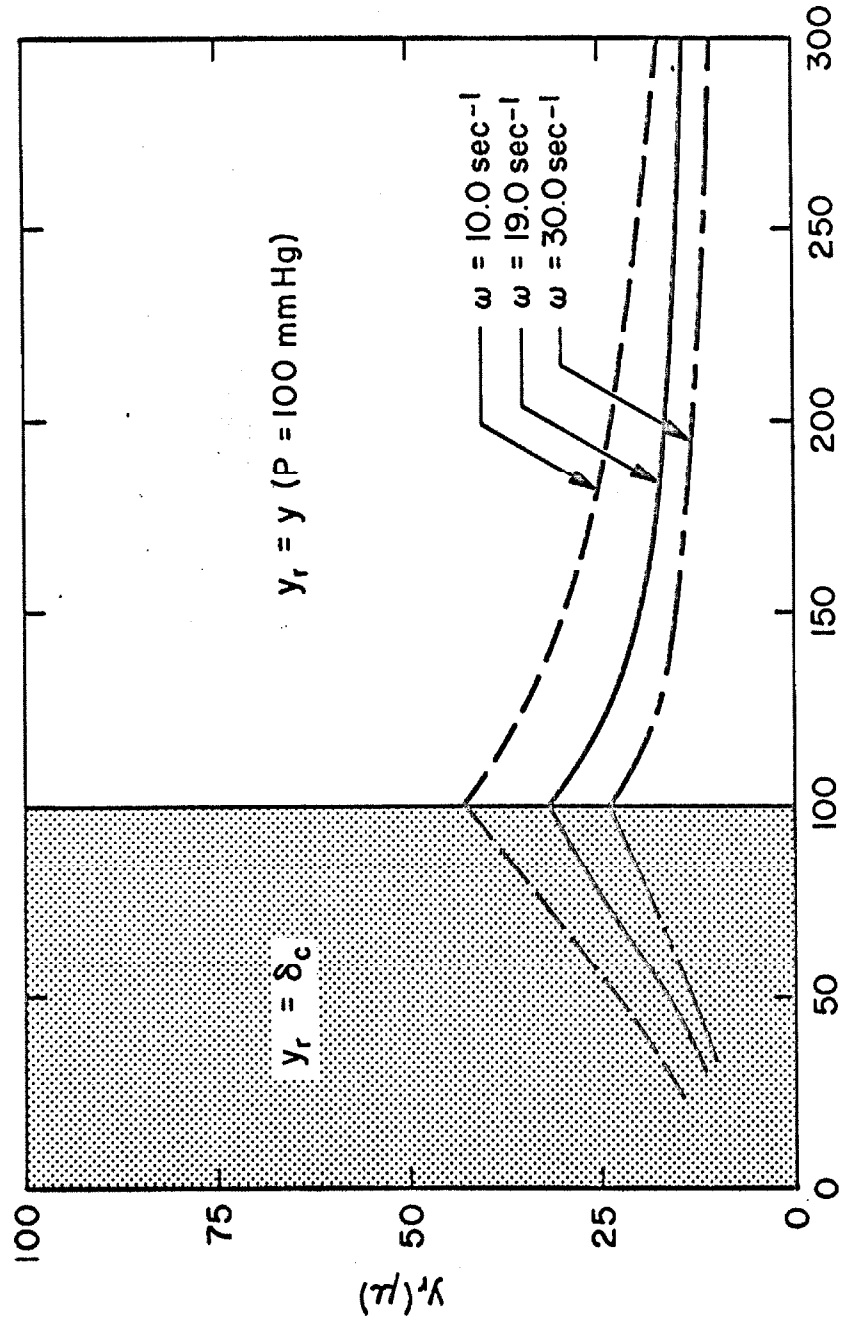

Figure III-10. The Location of the Edge of the Chemically Reactive Region in the Concentration Boundary Layer Formed During the Deoxygenation of Standard Blood.

Using the maximum values of y_r given above to obtain v_y, the re-equilibration lengths are found to be 1.8, 2.0, and 3.3 μ respectively, for ω = 10.0, 19.0, and 30.0 sec^{-1}. Using the more reasonable value of 0.5 y_r to obtain v_y, the re-equilibration lengths are found to be only a few tenths of a micron over this range of ω. Thus, a state of near equilibrium would be expected to exist within the reacting region of the concentration boundary layer, and the use of a local equilibrium analysis appears to be justified.

4. Results with Hemoglobin Solution.

Since the numerical solutions to the convective diffusion equation require values for diffusivities, solubilities, oxygen-oxyhemoglobin equilibrium curves, etc., and these values are generally obtained by correcting published values measured at a variety of experimental conditions, it is important to obtain an independent experimental check on the errors introduced by these corrections. This was done by measuring oxygen transfer rates in a free hemoglobin solution, since Keller and Friedlander (42) have shown that the facilitated local equilibrium model describes the behavior of this system. A hemoglobin solution was prepared from fresh blood, using their procedure, and deoxygenation transfer rate measurements were made with the rotating disk apparatus.

Table III-4. Measured and Calculated Properties Used to Describe the Deoxygenation Experiment with Hemoglobin Solution.

I. Measured Properties:

pH = 7.23

$P_{CO_2} \cong$ 0

ν = 0.015 (cm^2/sec)

C_{Hb} = 0.087 (gm/cm^3)

T = 37.5° C

II. Calculated Properties:

$\mathcal{D}_{O_2,Hb}$ = 2.0×10^{-5} (cm^2/sec) (30)

$\alpha_{O_2,Hb}$ = 2.7×10^{-5} ($cc(STP)/cm^3$ mm Hg) (4)

$\mathcal{F}_{pH}$ = 0.9 (60)

$\mathcal{D}_{Hb,Hb}$ = 6.7×10^{-7} (cm^2/sec) (43)

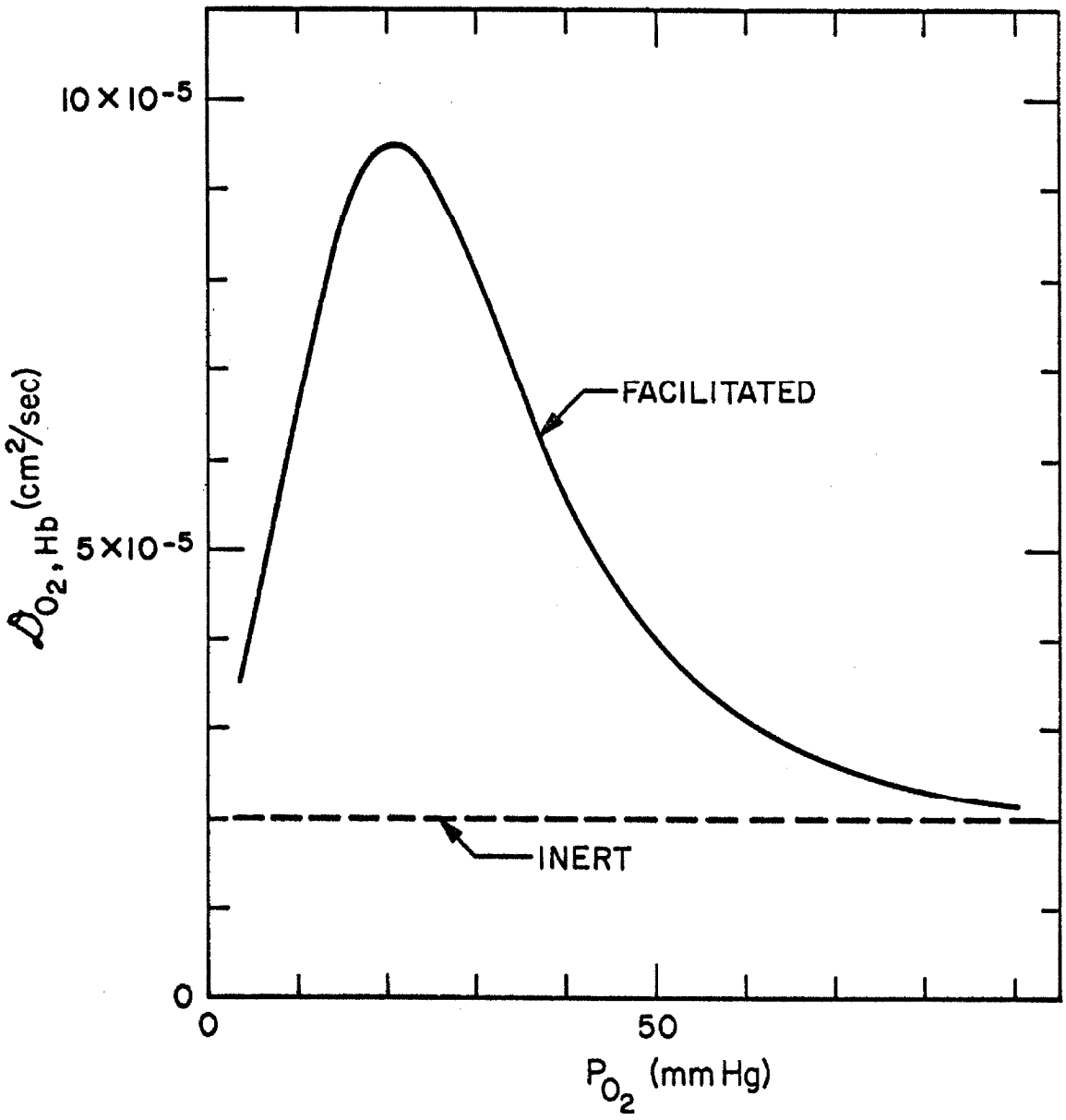

Figure III-11. The Effective Diffusivity of Oxygen in the Hemoglobin Solution Described in Table III-4.

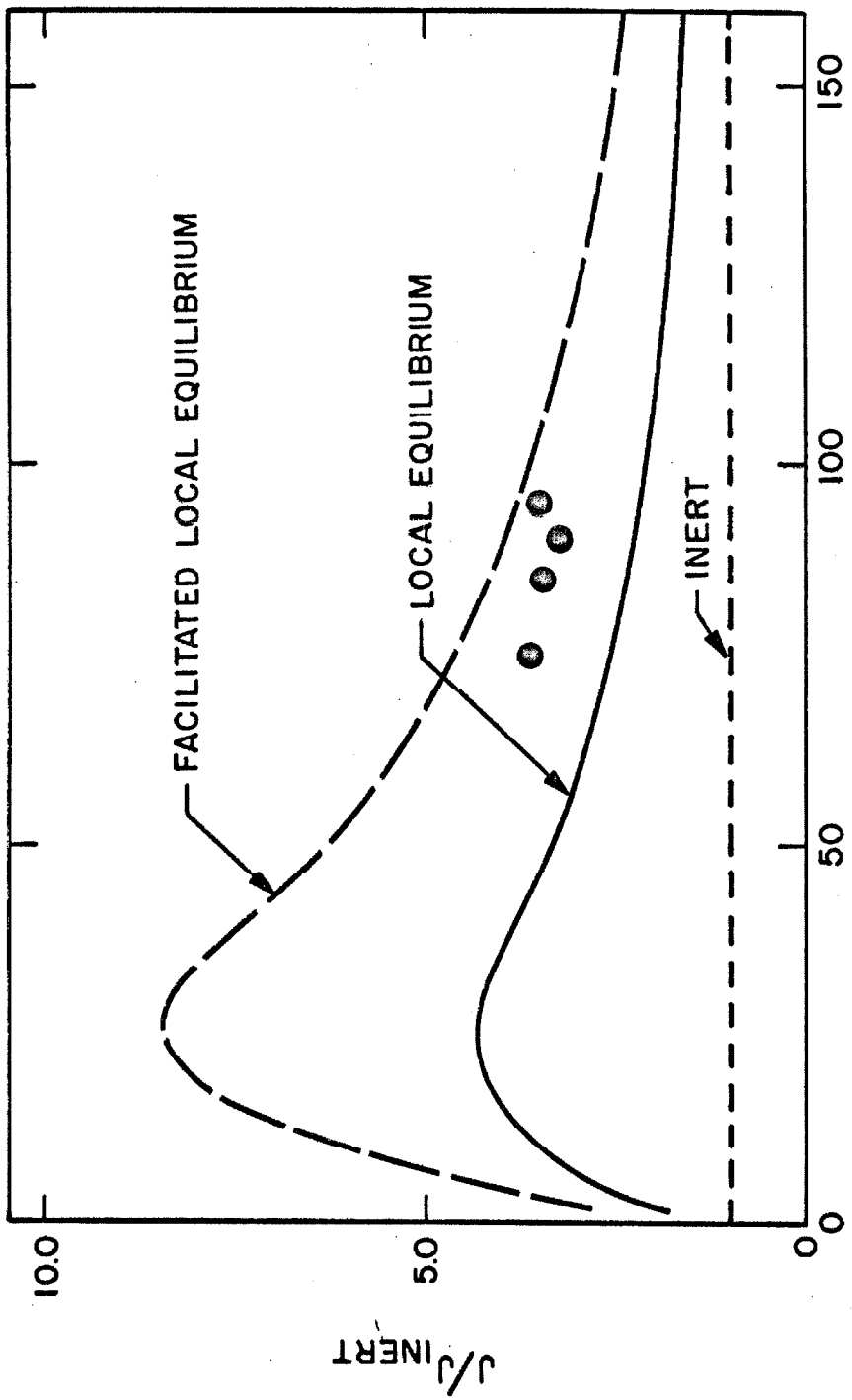

Figure III-12. A Comparison of the Measured Deoxygenation Transfer Rates in Free Hemoglobin Solution with the Three Mathematical Models.

The measured physical properties of the hemoglobin solution, and the published properties adjusted to the experimental conditions are given in Table III-4. The numerical solutions for both the facilitated local equilibrium model and the local equilibrium model are shown in Figure III-12, along with the experimental data. The data lie somewhat below the facilitated local equilibrium curve, indicating some error in the values used for the physical constants. The data are definitely not fitted by the simple local equilibrium curve, however, so the errors introduced during the calculation of the physical constants are not so large as to make the mechanism indistinguishable. It is interesting to note that the facilitation effect is larger for the free hemoglobin solution than for blood. Since the hemoglobin in whole blood is confined within the red cells, the facilitation effect does not occur throughout the fluid, and the overall effect is reduced.

D. Carbon Dioxide Experiments.

The results of the carbon dioxide extraction experiments with water are shown in Figure III-13. The data represent transfer rates measured before and after use of the membrane in a blood experiment. The theoretical line represents the case of inert transfer. It is reasonable to expect this model to hold since

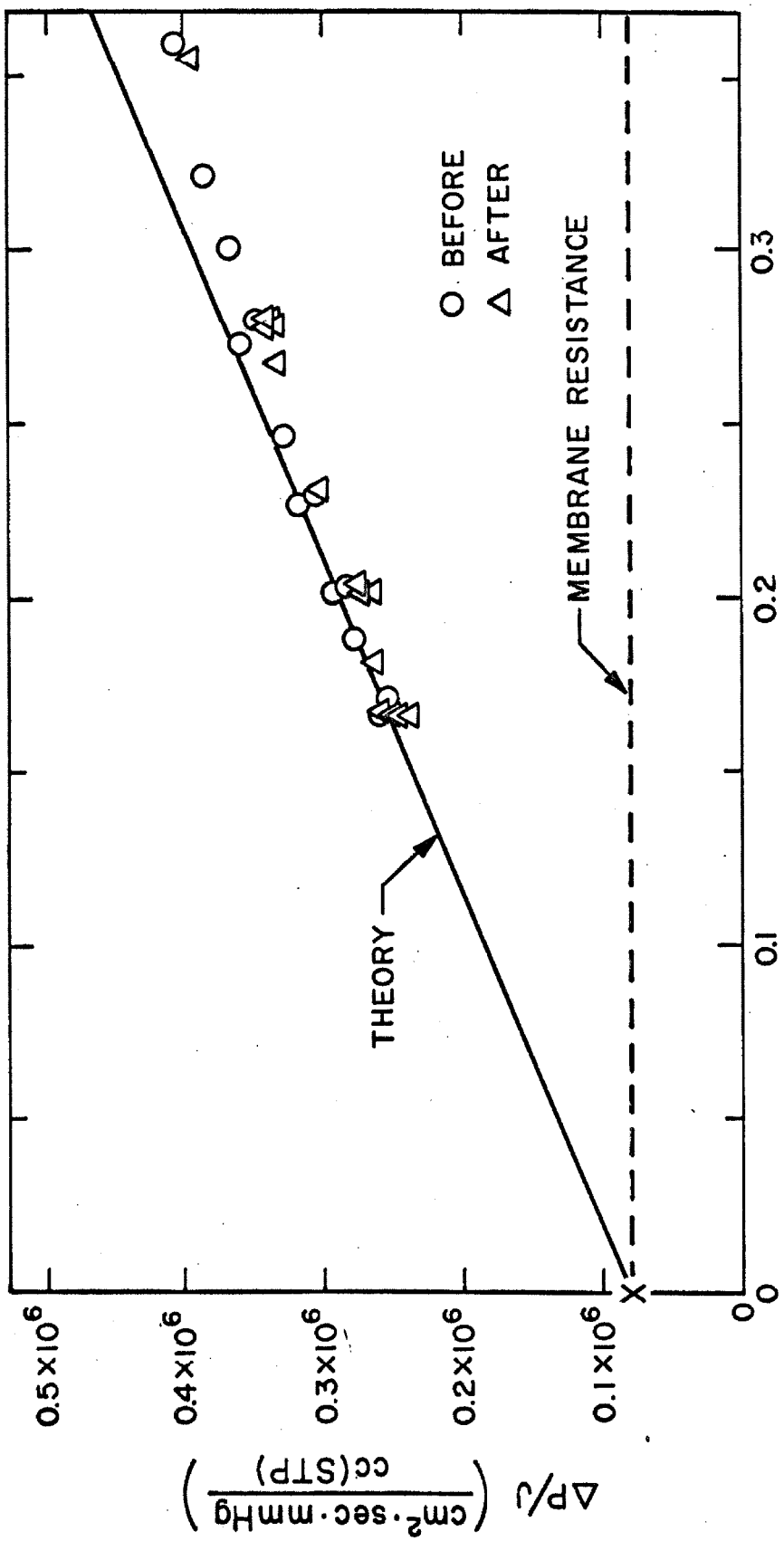

Figure III-13. A Comparison of the Transfer Rate Data for CO_2 Extraction from Water, Taken Before and After Exposure of the Membrane to Freshly Drawn, Citrated Blood, with the Inert Theoretical Curve ($T = 37.5^{\circ}$ C, $\mathcal{D}'_{CO_2,H_2O} = 2.82 \times 10^{-5}$ cm^2/sec, $\alpha_{CO_2,H_2O} = 7.37 \times 10^{-4}$ cc (STP)/cm^3·mm Hg).

the kinetics of the reaction between H_2CO_3 and CO_2 are known to be slow (75). The data, indeed, fall near this line, especially at high values of ω, when the residence times in the boundary layer are short. Clearly no change in membrane permeability occurred as a result of exposure of the membrane to blood.

The experimental results for carbon dioxide extraction from blood are presented in Figure III-14. The transfer rate calculated for the case of inert blood, using the physical properties presented earlier, is also shown. The measured transfer rates are much greater than the inert model would predict, as in the case of oxygen transfer at low oxygen tension. A linear relationship between the transfer rate and $\omega^{-1/2}$ is exhibited, again as in the case of oxygen transfer. As discussed above, this suggests either a complete absence of local equilibrium or a close approach to it. The existence of local chemical equilibrium can be tested by solving the local equilibrium model, since the carbon dioxide dissociation curve for blood is available in the literature (40,62). The dissociation curve representing the conditions of the blood used in this experiment was presented earlier in Figure I-3. The use of the local equilibrium theory for carbon dioxide transfer cannot be justified as convincingly as in the case of oxygen transfer, since few red cell equilibration-rate measurements are available. Only the carbon dioxide uptake rate is known to have been measured (14), and that was found to be about one-third the deoxygenation rate. Since the concentration

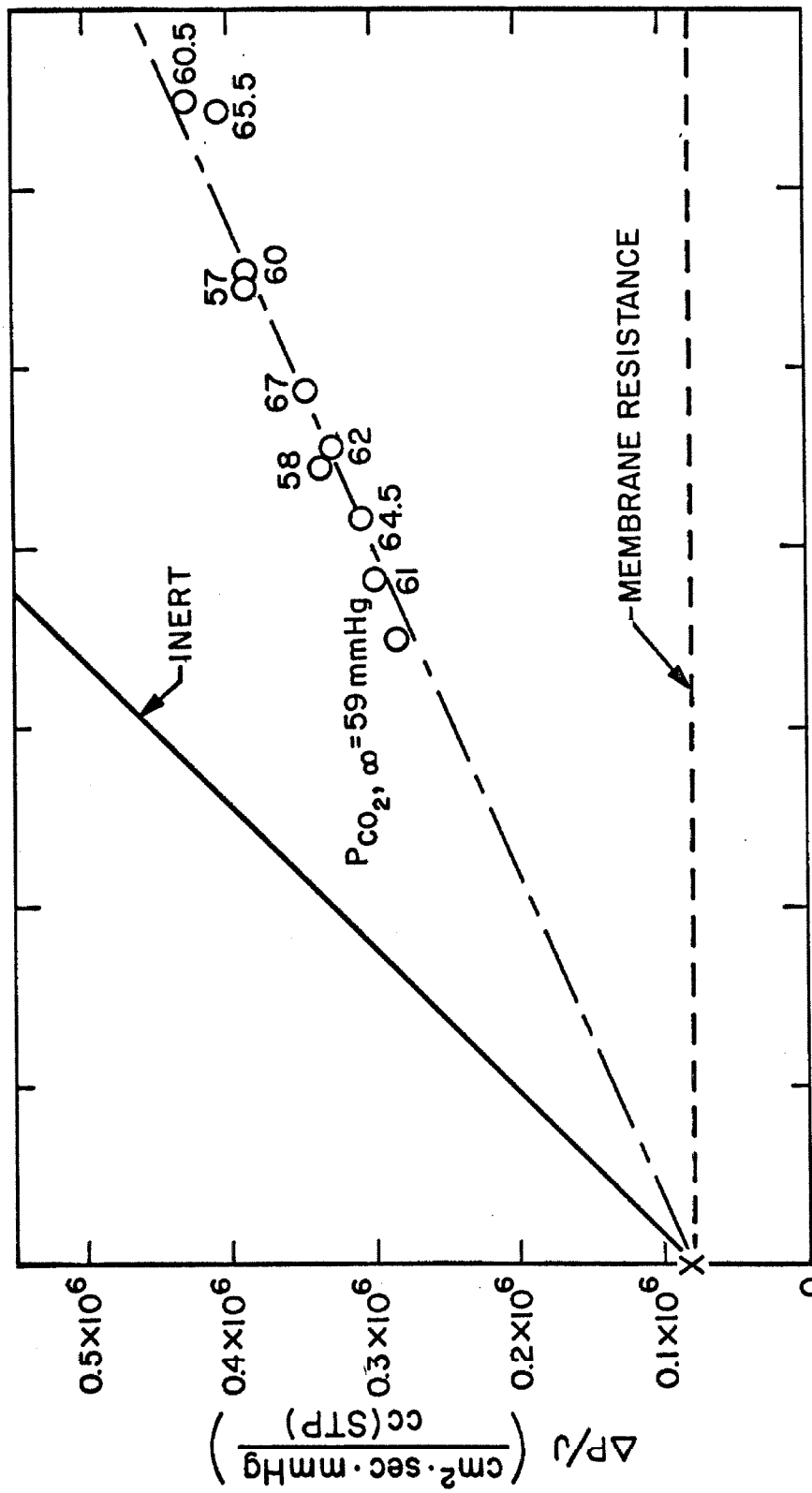

Figure III-14. A Comparison of the Transfer Rate Data for CO_2 Extraction from Freshly Drawn, Citrated Blood (P_{O_2} = 40 mm Hg, pH = 7.22, ν = 0.026 cm^2/sec) with the Inert Theoretical Curve (T = 37.5° C, $\delta_{\omega_2,\beta}$ = 1.3 x 10^{-5} cm^2/sec, $\alpha_{\omega_2,\beta}$ = 6.3 x 10^{-4} cc(STP)/cm^3 mmHg).

boundary layer thicknesses for carbon dioxide transfer are similar to those for oxygen transfer, the re-equilibration lengths calculated in section III-C-2 would have to be increased by a factor of three. This would not seriously affect the equilibrium assumption near the surface of the disk, but would result in significant departure from equilibrium near the outer edge of the concentration boundary layer. These re-equilibration lengths are for carbon dioxide uptake, however, and their use to describe carbon dioxide removal is not necessarily justified. It is important to determine whether the removal rates are even slower, as is the case for oxygen transfer. Only more detailed measurements of the carbon dioxide equilibration rates can resolve this question.

The differential equation representing the local equilibrium model for the case of carbon dioxide is:

$$v_y \left[\frac{d(n_T)_{CO_2}}{dP_{CO_2}} \right] \frac{dP_{CO_2}}{dy} = \alpha_{CO_2,B} \mathcal{D}_{CO_2,B} \frac{d^2 P_{CO_2}}{dy^2} \qquad (37)$$

The numerical solution to equation (37) is compared with the experimental data in Figure III-15, along with the solution to the inert model. The assumption of local equilibrium clearly does not account for all of the measured transfer rate. A possible explanation for the high transfer rate of carbon dioxide in blood is that the actual effective diffusivity is larger than

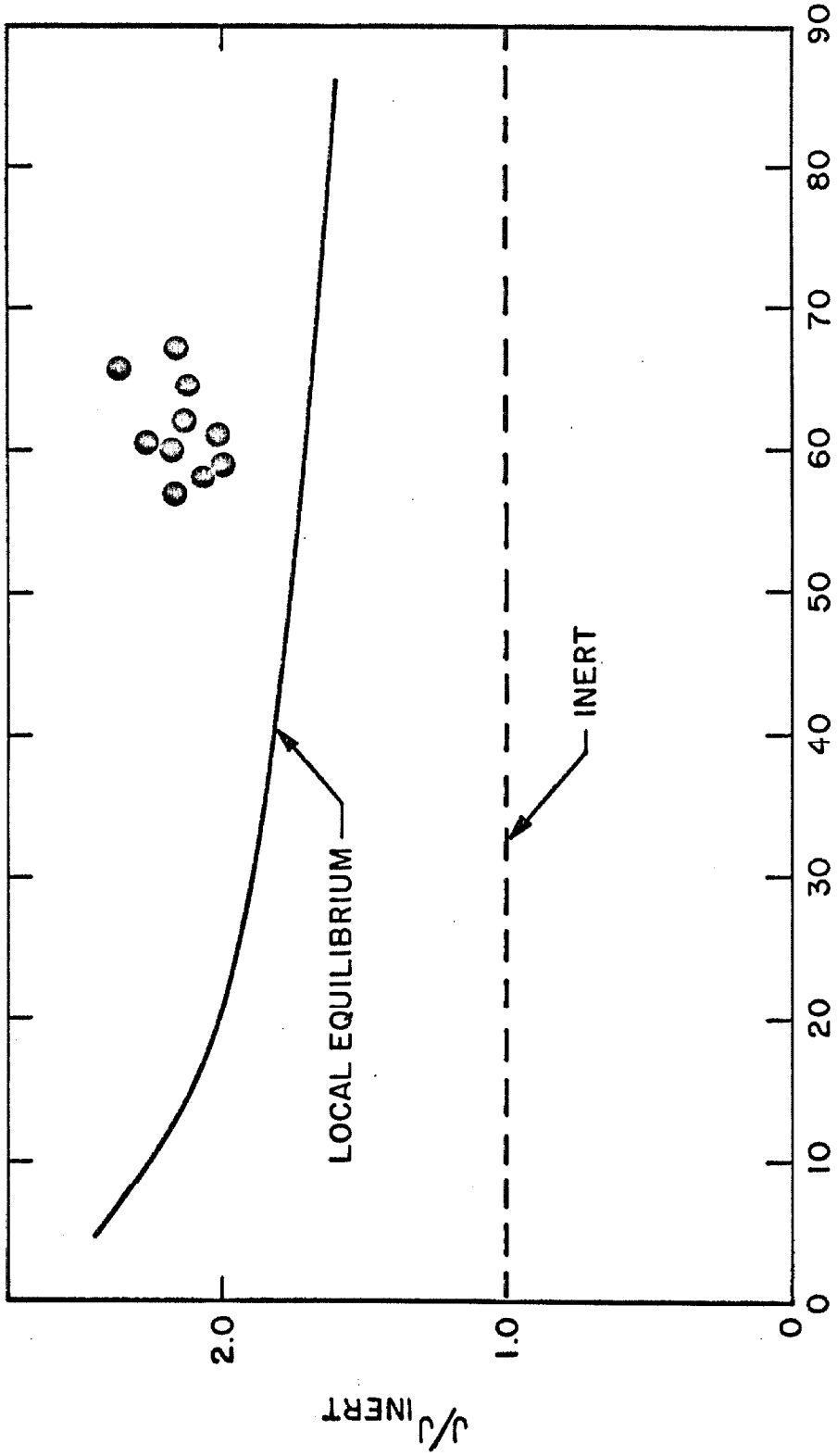

Figure III-15. A Comparison of the Measured Carbon Dioxide Removal Rate from Blood with the Transfer Rates Predicted by the Inert and Local Equilibrium Models.

the inert effective diffusivity obtained from the heterogeneous media theory. There could be a facilitation effect produced by the simultaneous diffusion of bicarbonate ion. Of the total amount of carbon dioxide removed from blood as a result of a gradient in P_{CO_2}, about 65% of it is originally in the form of bicarbonate. The bicarbonate diffuses to the red cell, where the catalyst carbonic anhydrase allows it to react to form carbon dioxide. Thus, along with a gradient in dissolved carbon dioxide, there will be a gradient in bicarbonate ion through the blood, and a facilitation effect similar to that occurring in the oxygen-oxyhemoglobin system could result from diffusion of the bicarbonate. If this indeed occurred, the inert diffusivity calculated from the heterogeneous media theory would be an underestimate, and calculations based on it would not be expected to account for all of the measured transfer rate. More detailed studies than this would be required to confirm such a mechanism.

The primary intent of the carbon dioxide study was to obtain a value for the transfer rate that would occur in a membrane oxygenator. From this value, the value for the transfer rate of oxygen, it can then be determined which of the two is the limiting process. This subject is discussed in the next chapter.

CHAPTER IV

APPLICATIONS TO ARTIFICIAL LUNG DESIGN

A. Local Equilibrium Oxygenation.

In the preceding chapter it was shown that the local equilibrium model leads to a satisfactory design theory for oxygen desorption from flowing blood. It therefore becomes reasonable to study the behavior of the rotating disk system for the case of oxygen uptake by numerically solving the local equilibrium model, providing that the assumption of local equilibrium is not violated in this new situation. The results of such a study on "standard blood" are presented in Figure IV-1. In this computer experiment, $P_{O_2,g}$ (the oxygen partial pressure of the gas flushing the membrane) was varied from 100 to 710 mm Hg, and the value of $P_{O_2,\infty}$ for a given flux was determined numerically. The boundary conditions $(P_{O_2,\infty} < P_{O_2,g})$ are the reverse of those in the deoxygenation experiments. The calculated boundary layer thicknesses were about the same as for deoxygenation, and since the red cell equilibration rate for the oxygenation process is known to be similar to the rate for the deoxygenation process (68,48), a state of near

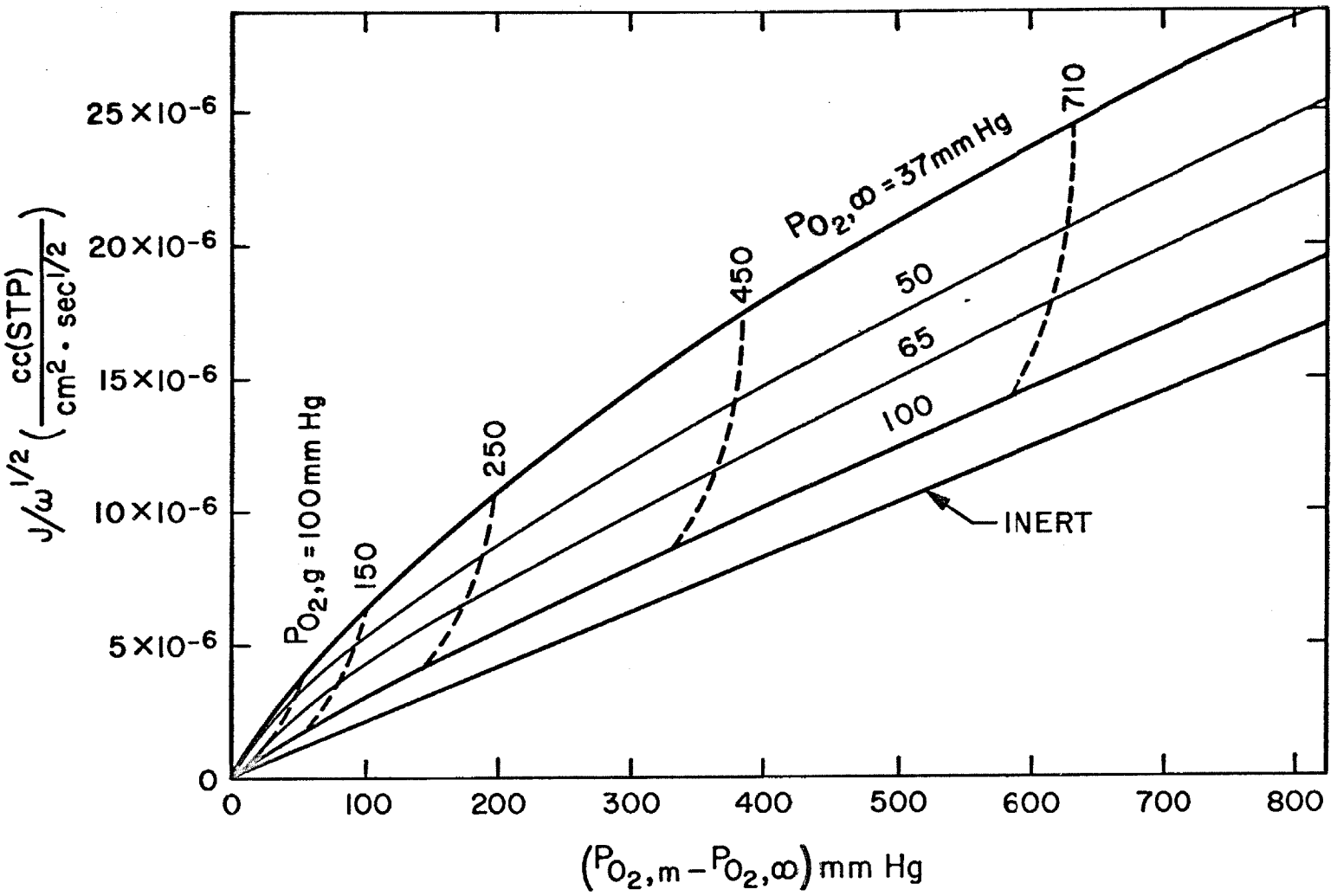

Figure IV-1. The Rate of Oxygen Uptake by Standard Blood in the Rotating Disk Apparatus, Calculated Using the Local Equilibrium Model.

chemical equilibrium should also be followed by blood being oxygenated in the boundary layer of a rotating disk apparatus.

Two effects are evident from the curves in Figure IV-1:

1. At high P_{O_2}, the local equilibrium oxygenation rate approaches that of inert blood more slowly than in the case of deoxygenation - that is, $\left[J/J_{inert}\right]_{oxy.} > \left[J/J_{inert}\right]_{deoxy.}$

2. The oxygenation rate is especially dependent upon the oxygen tension of the blood fed into the boundary layer, as evidenced by the steep slope of the dashed curves, compared to the slope of the inert curve.

The first of these effects results from the wide difference between the velocities in the unsaturated region of the boundary layer ($P_{O_2} << 150$ mm Hg) for the cases of oxygen uptake and removal. This effect is shown schematically in Figure IV-2. During the oxygenation of blood, the unsaturated region forms the outermost portion of the concentration boundary layer, where the velocity v_y is large. This increases the importance

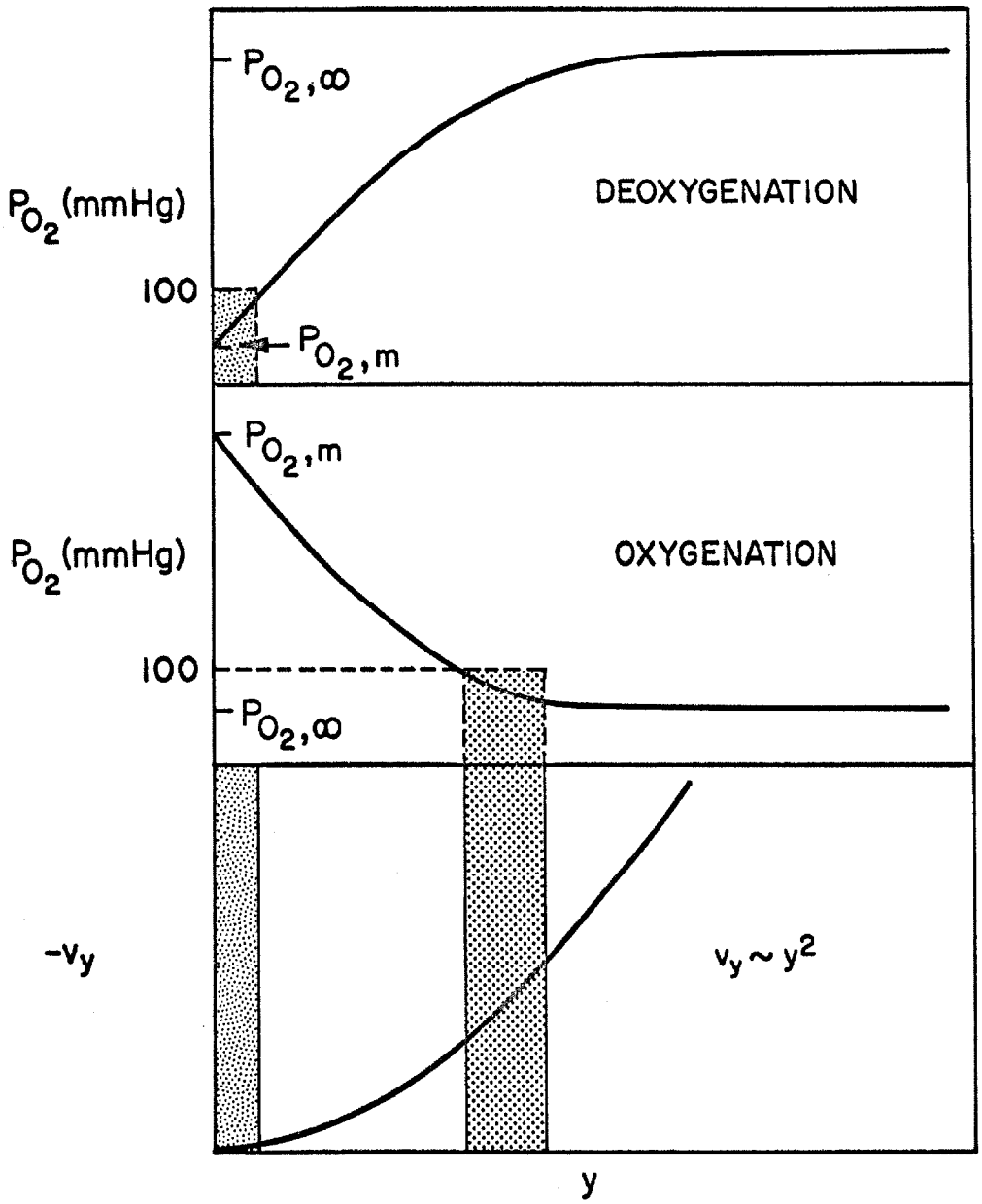

Figure IV-2. A Schematic Comparison of the Flow Velocities in the Chemically Reactive Region ($P_{O_2} < 100$ mm Hg) for Deoxygenation and Oxygenation of the Concentration Boundary Layer.

of the convective term in equation (6), and since the local equilibrium effect on the transfer rate depends on convection, the effect is magnified. During the deoxygenation of blood, the unsaturated region is next to the surface of the disk, where the velocity v_y is small, and therefore the convective effect is not as great.

The second effect noted in Figure IV-1 has great significance with respect to the design of artificial lungs. If pure oxygen gas is used to oxygenate blood in the rotating disk system, and the tension of the blood entering the boundary layer is raised just 13 mm Hg above venous conditions, the transfer due to the local equilibrium effect is reduced by more than 30%, reducing the total transfer rate by almost 15%. For the same change in conditions, the inert transfer rate is reduced by only 2%. If arterial blood is introduced into the boundary layer, the transfer due to the local equilibrium effect is reduced by 75%, and the total transfer rate reduced by almost 40%, while the inert transfer rate is decreased by only 10%. It is therefore especially advantageous to design an artificial lung which continuously introduces blood at low oxygen tension into the concentration boundary layer.

B. The Relative Transfer Rates of O_2 and CO_2.

The operation of an artificial lung must be considered from the point of view of CO_2 removal as well as O_2 uptake. Using the data presented above for O_2 uptake, and the data presented in Chapter III for CO_2 removal, the relative rates of these processes can now be determined. These relative rates were calculated for both the case of arterial blood and the case of venous blood entering the boundary layer, the blood being oxygenated by wet O_2 gas across a 1 mil silicone rubber membrane. If an artificial lung were to duplicate the function of the natural lung, it would have to remove enough carbon dioxide to lower the P_{co_2} of the blood from 46 mm Hg to 40 mm Hg, and simultaneously add enough oxygen to raise the P_{o_2} from 37 mm Hg to 100 mm Hg. To do this, the transfer rate of oxygen must be about twice that of carbon dioxide. The results of the above described calculations, summarized in Table IV-1, show that this condition is exceeded in a silicone rubber membrane oxygenator by a factor of 2.4 to 4.0 , depending on the efficiency of the oxygenation process. Thus, the use of the silicone rubber membrane at atmospheric pressure results in an excessive loss of CO_2 from the blood, and as in the case of non-membrane lungs, a back pressure of CO_2 would have to be introduced into the oxygen gas stream. A more

Table IV-1. The Relative Rates of Oxygen Uptake and Carbon Dioxide Removal in Standard Blood at 37.5°C, Exposed to Wet Oxygen Gas Across a 1 mil Silicone Rubber Membrane.

$$\left(J_{CO_2}\,\omega^{-1/2}\right) = 2.90 \times 10^{-5} \quad (cc(STP)/cm^2 sec^{1/2})$$

$$\left(J_{O_2}\,\omega^{-1/2}\right)_{\text{venous blood}} = 2.45 \times 10^{-5} \quad (cc(STP)/cm^2 sec^{1/2})$$

$$\left(J_{O_2}\,\omega^{-1/2}\right)_{\text{arterial blood}} = 1.43 \times 10^{-5} \quad (cc(STP)/cm^2 sec^{1/2})$$

Condition	$\frac{J_{CO_2}}{J_{O_2}}$	$\frac{J_{CO_2}}{J_{CO_2,\text{required}}}$
Venous Blood	1.2	2.4
Arterial Blood	2.0	4.0

fruitful way of reducing the relative CO_2 flux would be to operate the artificial lung hyperbarically. This would not change the CO_2 concentration difference across the boundary layer, since there is no CO_2 in the oxygen stream, but would increase the O_2 concentration difference, thereby selectively increasing the oxygen transfer rate. The total pressure of the system could be raised to the point where the oxygen flux became twice the carbon dioxide flux, and then any desired adjustment in the CO_2 tension of the blood leaving the artificial lung could be made by simply varying this total pressure. At these hyperbaric conditions, the lung would be operating at maximum efficiency, as opposed to the case of operation at atmospheric pressure, where the carbon dioxide transfer rate must be deliberately retarded. Of course, a hyperbaric lung would have to allow the highly oxygenated blood leaving the boundary layer to equilibrate with the reduced blood outside, so that the oxygen tension falls to a sub-atmospheric level before the blood is decompressed. Otherwise, gas bubbles would form during the decompression.

C. Artificial Lung Design.

On the basis of the analysis presented above, the following comments can be made concerning the improvement of the mass

transfer efficiency of a membrane lung:

1. The nature of the local equilibrium augmentation of oxygen transfer in blood makes it especially important to introduce highly reduced blood into the concentration boundary layer.

2. A silicone rubber membrane lung should be operated hyperbarically to correctly proportion the O_2 and CO_2 transfer rates at the condition of maximum oxygen transfer rate.

These suggestions are made solely from the point of view of improving mass transfer efficiency. The actual design of a membrane lung must be viewed on a much broader basis, however, taking into consideration medical, operational and eventually economic criteria as well.

The major objective in improving the mass transfer efficiency of an artificial lung is to reduce the surface area contacted by the blood, thereby reducing the protein denaturation and other interfacial trauma. It must be remembered, however, that the lung is only one of the devices in an extracorporeal

circuit. A reduction in lung surface area would become ineffective when the remainder of the extracorporeal circuit comprised most of the total surface area. An interesting possibility for reducing the total surface area in this case would be the multiple use of surfaces. Heat transfer and mass transfer could occur simultaneously across the same surface, and perhaps this surface could even be incorporated into the pumping mechanism.

Reduction in blood trauma can also be accomplished by developing more compatible surfaces. The long-term use of an artificial lung depends on this. Adequate mass transfer is a necessary condition for the use of a lung, but such a lung is useable only as long as no irreparable damage is done to the blood.

Correctly proportioned gas exchange capacity is necessary to prevent CO_2 retention (respiratory acidosis) or CO_2 depletion (respiratory alkalosis). A valuable feature in an artificial lung would be a means of varying the relative rates of O_2 and CO_2 transfer to allow correction of an imbalance. As stated above, hyperbaric operation would provide this without sacrificing the oxygen transfer rate.

A consideration of overriding importance in the design of an artificial lung is the reliability of the device, since it

will be used to support the life of the patient. The development of a lung with a low priming volume might be of great benefit in this respect, since such a lung could be replaced in an emergency without excessive loss of blood from the circuit. Another consideration is the overall size of the lung, since it must be located near the patient in the operating room without crowding the surgical team. The lung must also be easy to operate and control. Some of the current lung designs are so difficult to operate that widespread use is not possible (27).

Finally, the design of a membrane lung should lead to a commercially feasible unit. Complicated construction, the use of costly materials, difficult servicing (cleaning, sterilizing, etc.) can result in prohibitive costs. Perhaps a disposable lung is the ultimate goal in this respect.

CHAPTER V

SUMMARY AND CONCLUSIONS

A. Principal Results of This Research.

The convective diffusion of oxygen, carbon dioxide and krypton in blood was studied from the point of view of the general convective diffusion equation:

$$\frac{D}{Dt}(\alpha_i P_i + N_i^*) = -\nabla \cdot \vec{J}_i + \frac{D}{Dt}(N_i^* - N_i) \qquad (6)$$

Transfer rates of these gases in freshly drawn, citrated whole blood were measured using a rotating disk apparatus especially designed for this purpose. Analytical techniques were developed for use with this device, which do not require handling of the fluid being studied.

The apparatus utilizes a one mil silicone rubber membrane as the surface of the rotating disk. Since this membrane is highly permeable to the gases studied, most of the transfer resistance resulted from the boundary layer on the membrane surface. Experiments performed with oxygen and water confirm the well-defined behavior of this system.

The permeability of the silicone rubber membrane was unaffected by exposure to freshly drawn blood for periods of up to four hours. The membrane permeability was affected in one experiment made with blood obtained from a non-membrane oxygenator following several hours use in surgery. The blood corresponded to the priming volume and was a combination of the patient's blood and the original priming volume. After about two hours operation of the rotating disk apparatus, the resistance of the membrane increased more than four-fold over a period of about 30 minutes. This increase in resistance resulted from the deposition of an unknown material from the blood onto the surface of the membrane.

The results of the transfer rate studies using inert krypton gas are adequately described by equation (6), using the velocity field calculated from the Navier-Stokes Equations and assuming that the diffusive flux is given by:

$$\vec{J}_i = -\alpha_{i,s}\, \mathcal{D}_{i,s}\, \nabla P_i \qquad (38)$$

where $\mathcal{D}_{i,s}$ is evaluated using the theory for conduction in a stagnant heterogeneous media. These equations should hold for the transport of other inert materials as well.

The results for the convective diffusion of oxygen in blood, with simultaneous carbon dioxide transfer, fell slightly above

the values predicted by the simple "local equilibrium model":

$$\frac{D}{Dt}(\alpha_{O_2,\beta} P_{O_2} + N^*_{O_2}) = \alpha_{O_2,\beta} \mathcal{D}_{O_2,\beta} \nabla^2 P_{O_2} \tag{39}$$

The measured transfer rates were also compared with both the maximum value, given by the "facilitated local equilibrium model":

$$\frac{D}{Dt}(\alpha_{O_2,\beta} P_{O_2} + N^*_{O_2}) = \alpha_{O_2,\beta} \nabla \cdot (\mathcal{D}^*_{O_2,\beta} \nabla P_{O_2}) \tag{40}$$

where $\mathcal{D}^*_{O_2,\beta}$ includes the effect of oxyhemoglobin diffusion, and with the minimum value, given by the "inert model":

$$\frac{D}{Dt}(P_{O_2}) = \mathcal{D}_{O_2,\beta} \nabla^2 P_{O_2} \tag{41}$$

The transfer rate of carbon dioxide in blood was found to be greater than a simple local equilibrium model would predict. The simultaneous diffusion of HCO_3^- may explain this result. The complex nature of the reaction of carbon dioxide with blood prevents quantitative development of this theory here.

B. Application of the Results.

The variation in the transport properties of the blood samples used in this study was not large enough to significantly affect the design criteria for an artificial lung, so the results presented here should be generally applicable to the design of these devices. On the basis of oxygen transfer rates calculated for a one mil silicone rubber membrane lung, the transfer rate of carbon dioxide was shown to be several times greater than that necessary to restore venous blood to arterial conditions. Therefore, the operating conditions would have to be adjusted to bring the oxygenation and carbon dioxide removal rates into balance. It is recommended that the oxygenation rate be increased by operating the lung hyperbarically, since the efficiency of the device would then be at its maximum value. It is also recommended, on the basis of the nature of the local equilibrium effect occurring during the oxygenation of blood, that the membrane lung incorporate a mechanism for introducing blood at low tension into the concentration boundary layer.

C. Further Studies.

In order to apply the results of this work to the design of membrane lungs suitable for long-term use, it will be necessary

to study the deposition of material onto the membrane surface in greater detail. The drastic decrease in membrane resistance observed during the isolated experiment described above, and its rapid occurrence, would severely limit the useful life of a membrane oxygenator.

Since hypothermia is often used in conjunction with extracorporeal circulation, studies on gas transfer rates in flowing blood at lower temperatures should be performed. The increased viscosity of the blood at these conditions could affect the conclusions presented here.

It would be of value to determine the transport properties of oxygen and carbon dioxide in whole blood at various hematocrits and temperatures, to test the use of conductivity theory to evaluate $\mathcal{D}_{i,B}$. It would also be of interest to measure $\mathcal{D}_{O_2,RC}$ to determine the extent to which facilitated diffusion takes place within the red cell. This could be done using packed red cell layers in the O_2 electrode device described by Keller and Friedlander (42). The determination of $\mathcal{D}_{O_2,RC}$ would be of great significance in the case of physiological gas transport. The mechanism of carbon dioxide transport in blood should also be evaluated, since this too would contain important physiological implications. Such a study would involve red cell equilibration rate measurements, as well as detailed transfer measurements.

The state of knowledge concerning convective diffusion of gases in blood has now reached the point where it is possible to compare various convective systems theoretically. It is suggested that such a theoretical study be performed to compare stagnation flows against parallel flows, pulsatile flows against steady flows, etc., within the framework of the design criteria for artificial lungs, to determine the most fruitful areas for future study. This would represent a break with the empirical trial and error method used in the past, and hopefully would result in an acceleration of the design process.

APPENDICES

APPENDIX II-1

THE γ COUNTING TECHNIQUE USED TO MEASURE KRYPTON UPTAKE RATES

A. Introduction.

The rate of uptake of radioactive Kr-85 was determined by monitoring the γ activity of the rotating disk apparatus. A Harshaw NaI (Tl) Integral Line Scintillation Detector (Type 125/QGX) was mounted against the side of the disk apparatus and shielded by two inch lead bricks. The entire experiment was placed in a ventilated hood, and is shown in Figure II-1-1. The scintillation detector was connected in series to a Baird Atomic Model 250 single-channel analyzer and Baird Atomic Model 132 scaler. A Nuclear Chicago Model 1620 B Analytical Count Rate-meter was used to monitor counting rates. The analyzer was tuned with a Cs-137 reference source so that the 0.66 Mev peak was positioned as shown in Figure II-1-2. The equipment apparently reached thermal equilibrium with the laboratory after about one day's operation, after which the tuning remained quite stable. The tuning was checked after each experiment, and the Cs-137 peak was always found to be stationary to within $\pm$ 2% of the analyzer scale. The window used in counting the Kr-85

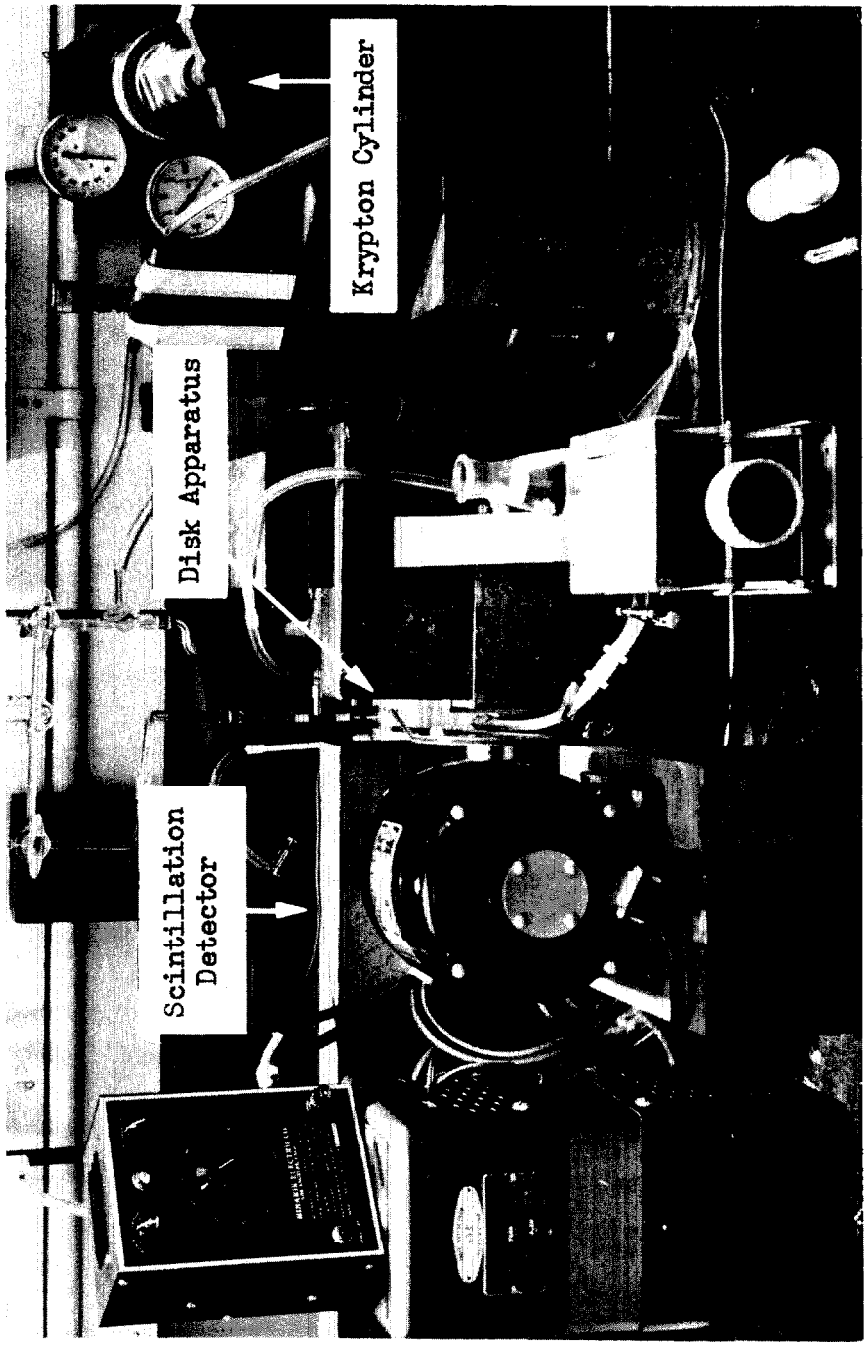

Figure II-1-1. The Rotating Disk System as Used During the Krypton Experiments

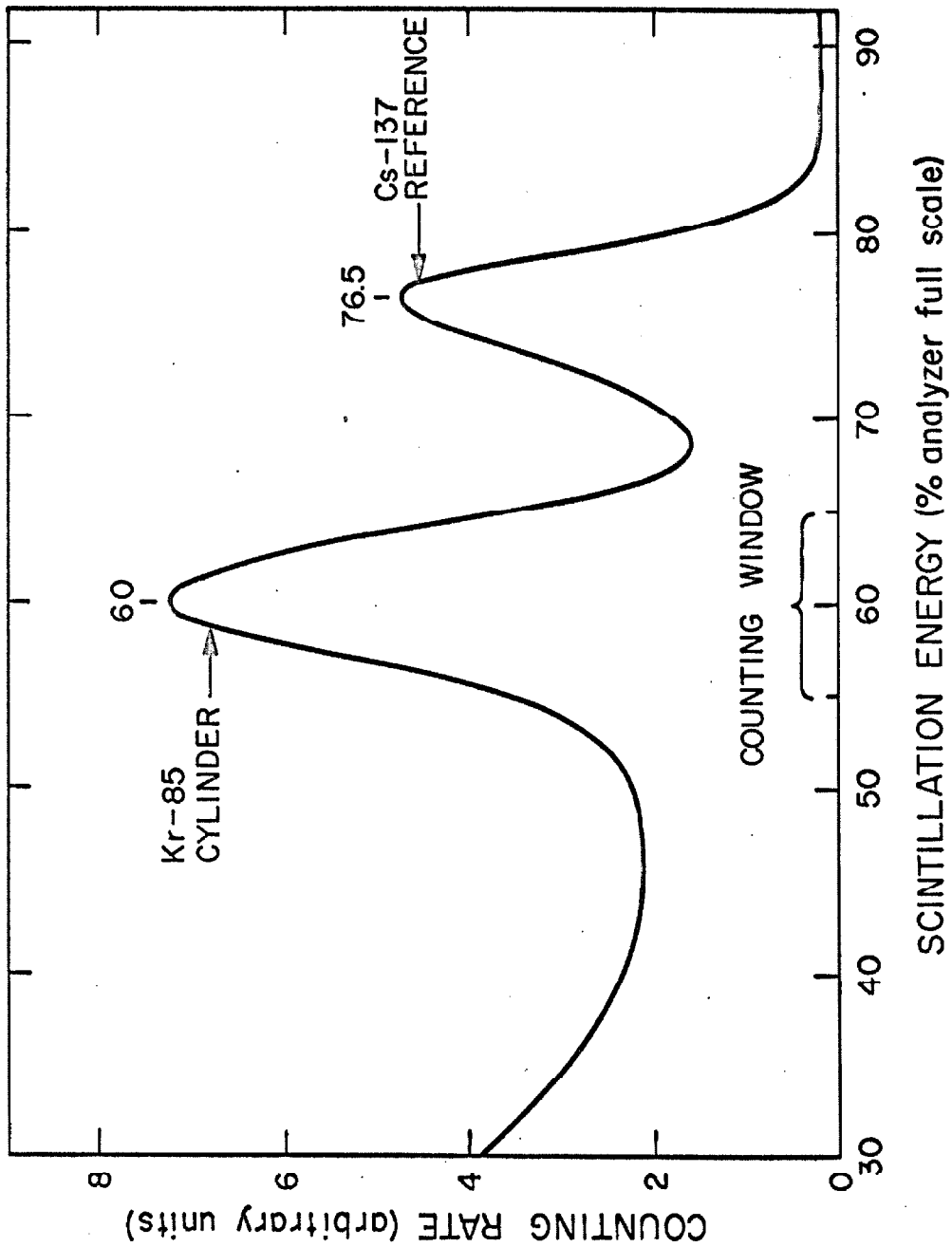

Figure II-1-2. The Experimental γ Spectrum Used to Tune the Counting Equipment.

was centered on a portion of the photopeak where slight drifting would not significantly affect the count rate.

B. Experimental Procedure.

A portion of the ratemeter output during a typical uptake experiment is shown in Figure II-1-3. The experimental procedure was as follows:

1. The apparatus was filled with the fluid to be studied, as described in Chapter II.

2. The background count rate was measured without Kr gas in the core of the disk.

3. The stationary disk was flushed with Kr gas for about 30 seconds, the gas flow was stopped, and then the total background count rate was measured.

4. At $t \equiv 0$ the disk rotation and gas flow were begun simultaneously.

5. After the desired Δt, the disk rotation and Kr gas flow were stopped, and the fluid stirred for about 60 seconds.

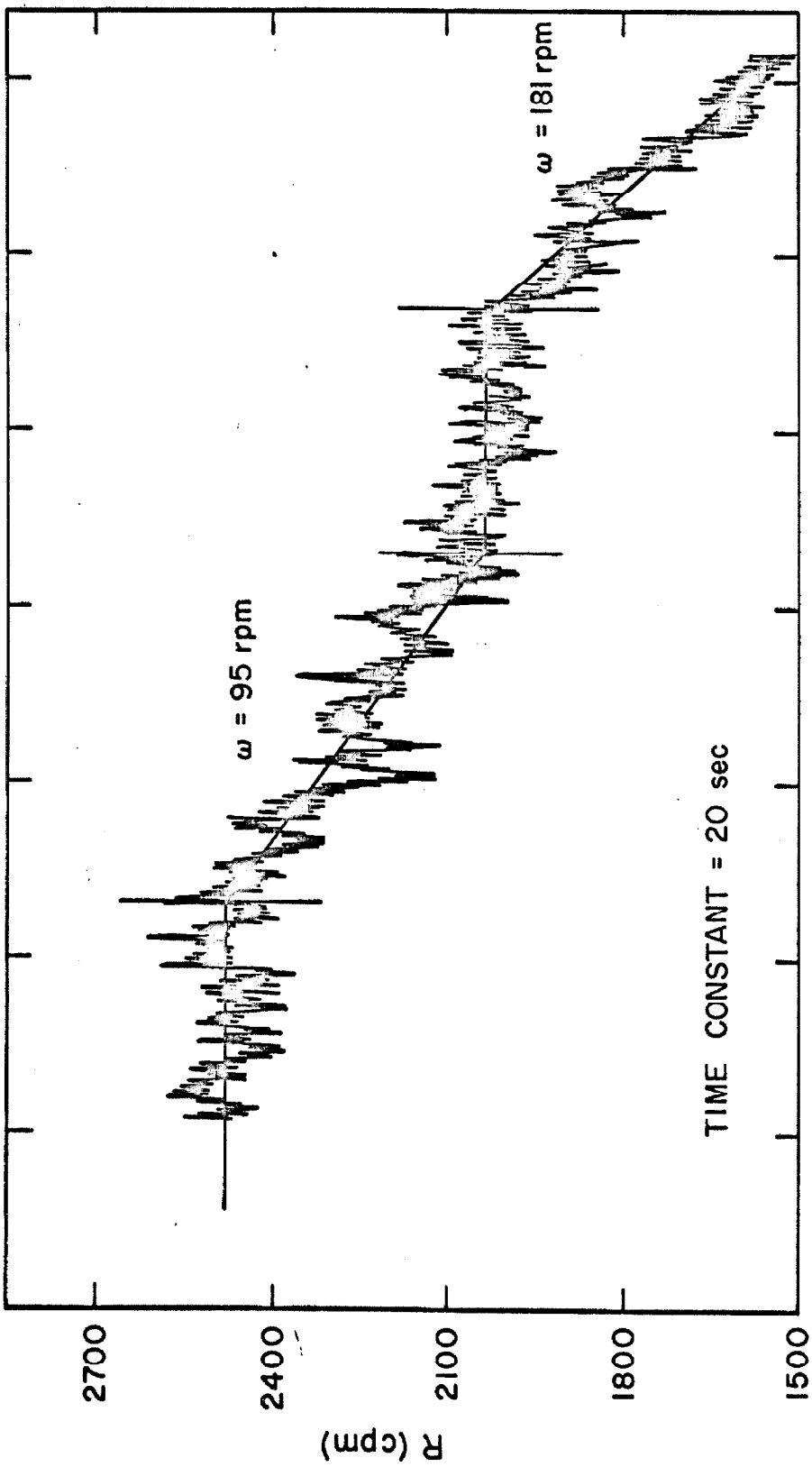

Figure II-1-3. A Typical Count-Rate History Obtained During a Krypton Experiment.

6. After obtaining a statistically significant plateau reading (5 - 10 minutes), the setting for the rotational speed was changed and steps 4 through 6 repeated to obtain a new measurement.

C. Discussion.

Theoretically the instantaneous transfer rate is given by the slope of the count rate versus time tracing shown in Figure II-1-3. In practice, it was found more accurate to measure the initial and final count rates and divide their difference by Δt. The increase in count rate during each run was usually about 500 cpm. The data were used to calculate the total transfer resistance of the membrane and boundary layer, using the equation:

$$\frac{\Delta P}{J} = \left[\frac{(A)(\Delta P)_{lm}(\Delta t)}{(R_{\Delta t} - R_o)/C_R} \right] \qquad (42)$$

where C_R is the geometrical factor relating the dissolved gas concentration to the measured count rate R, and $(\Delta P)_{lm}$ is the log mean value of the pressure difference across the membrane and boundary layer:

$$\Delta P = P_g - \frac{(R/C_n)}{(\alpha_{Kr})(V)} \qquad (43)$$

The geometrical factor was determined by comparing the activity of a saturated water solution with the activity of a sample taken from the apparatus. The variation of this factor with the activity of the Kr gas is shown in Figure II-1-4.

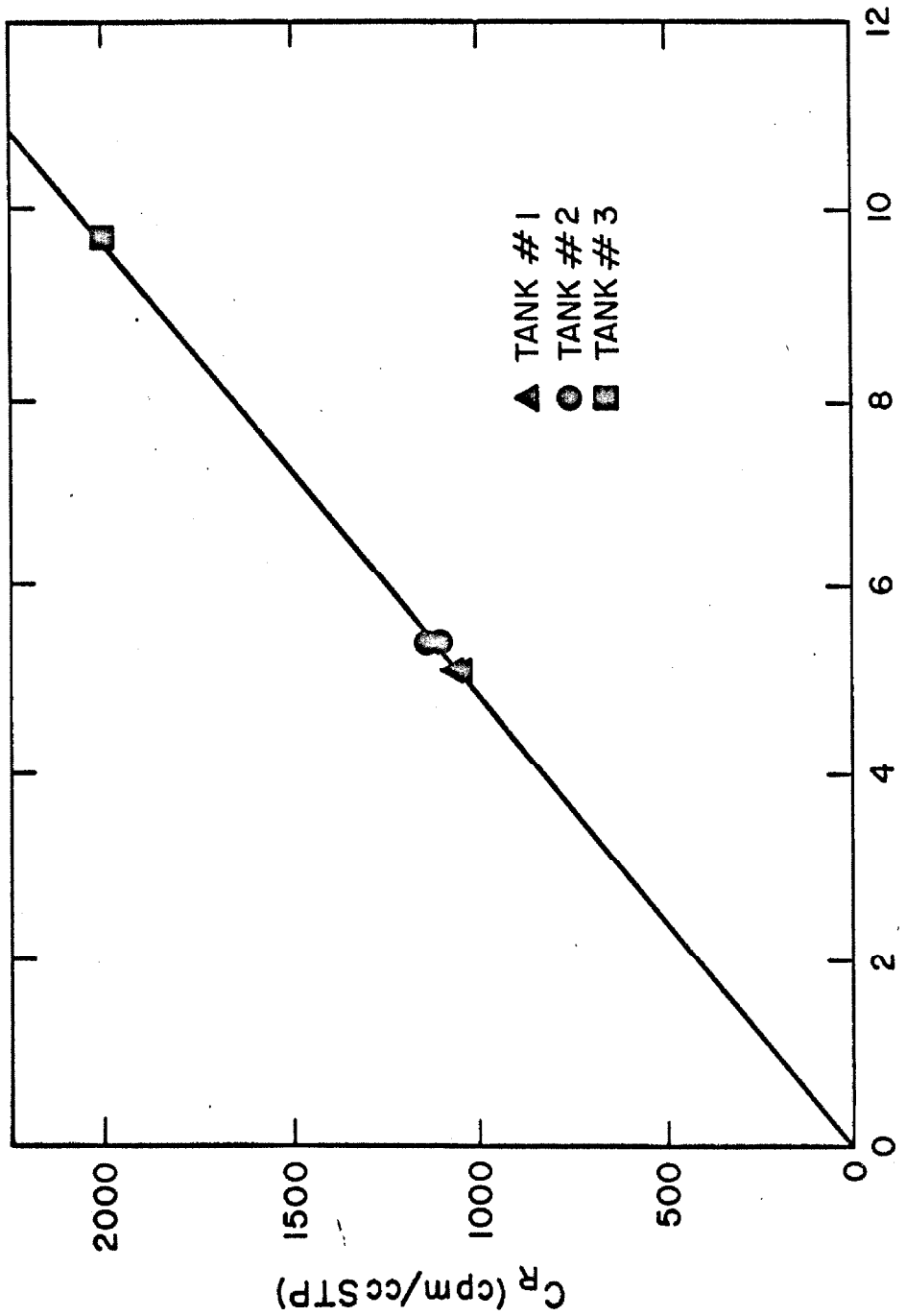

Figure II-1-4. The Geometrical Factor Relating the Change in Dissolved Gas Concentration in the Apparatus to the Change in Count-Rate, for Different Gas Activities.

APPENDIX II-2

A MANGANESE OXIDATION METHOD USED TO MEASURE DEOXYGENATION TRANSFER RATES

A. Introduction.

Morgan and Stumm (59) have shown that the oxidation of Mn (II) by dissolved oxygen at 25° C proceeds heterogeneously and autocatalytically, with a reaction rate dependent on the second power of the hydroxide ion concentration. Thus, the reaction can be controlled by varying the pH of the solution - at high pH (> 10) the reaction proceeds rapidly, and at low pH (< 7) the reaction is effectively frozen. The amount of oxidized manganese formed is directly proportional to the oxygen concentration, and is reproducible at a given pH and temperature. The oxidized manganese can be measured spectrophotometrically, following reaction with o-tolidine.

B. Experimental Method.

This chemical reaction was adapted for use with the rotating disk system to measure deoxygenation transfer rates. The N_2 gas stream leaving the core of the disk during a deoxygenation experiment contains only a trace amount of O_2 (about 100 PPM). In order

to collect a measurable quantity of oxygen, this gas stream was made to displace an oxygen-free 10^{-2} M $MnSO_4$ solution in a specially constructed collection flask, as shown schematically in Figure II-2-1. Sufficient gas was collected to displace all but 36 ml. of the $MnSO_4$ solution. The volume of the flask (250-500 ml) determined the time period of collection, since the N_2 gas flow rate was held constant. The pressure within the core of the rotating disk was maintained at its normal value by setting the flow rate of the $MnSO_4$ solution leaving the flask equal to the flow rate of the gas leaving the apparatus. Blanks were obtained in this same way by shunting the N_2 gas past the disk apparatus.

The samples collected in this manner were then treated as follows:

1. 4.0 ml. of oxygen-free 1M NaOH were carefully added to each flask through the syringe stopper.

2. The flasks were shaken overnight to allow all of the oxygen to diffuse into the liquid phase and react.

3. The reaction was quenched by adding 5.0 ml. of oxygen-free 60% perchloric acid, and the solution

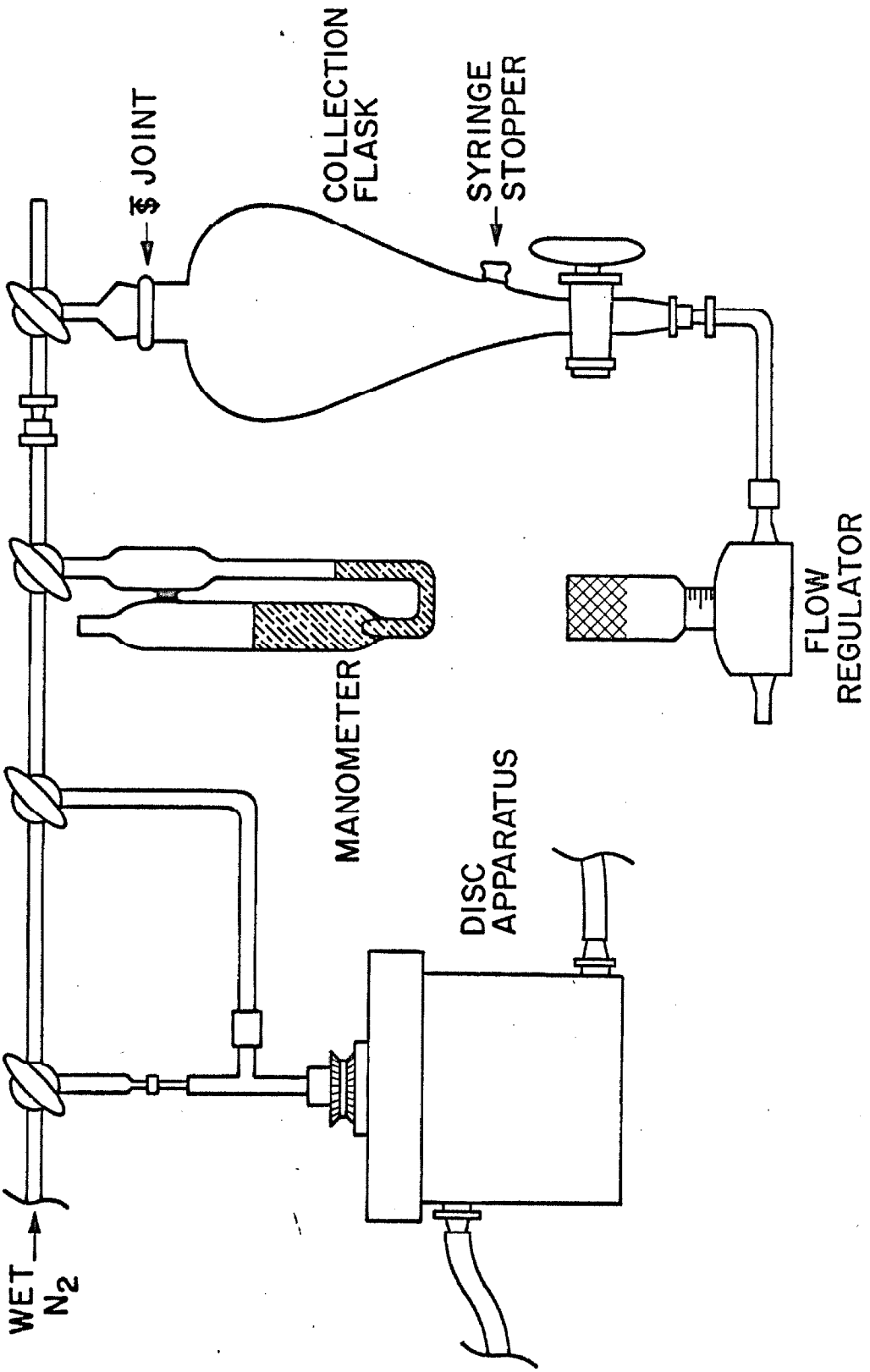

Figure II-2-1. A Schematic Diagram of the Gas Collection System Used During the Deoxygenation Experiments.

developed by adding 5.0 ml. of 0.1% o-tolidine.

4. The resulting yellow solution was diluted quantitatively to 100 ml., using a solution containing 8% IM NaOH and 10% concentrated perchloric acid. The absorbance of this diluted solution was measured at 440 mμ against distilled water, in a 1 mm cell. This measurement was made between 15 and 30 minutes after the time of development.

A standard curve, obtained by adding various amounts of distilled water at known oxygen tension to a series of nitrogen blanks, is shown in Figure II-2-2. The method is seen to be quite accurate over the desired range of oxygen concentrations (1-3 μmoles). The absorbance of a typical nitrogen blank was 0.03 ± 0.01. The development time for the o-tolidine reaction was determined by following the absorbance of a single sample with time, as shown in Figure II-2-3.

C. Discussion.

The only difficulty encountered during this analysis resulted from the use of greased standard taper joints in the collection flasks. The grease was taken up by the solution

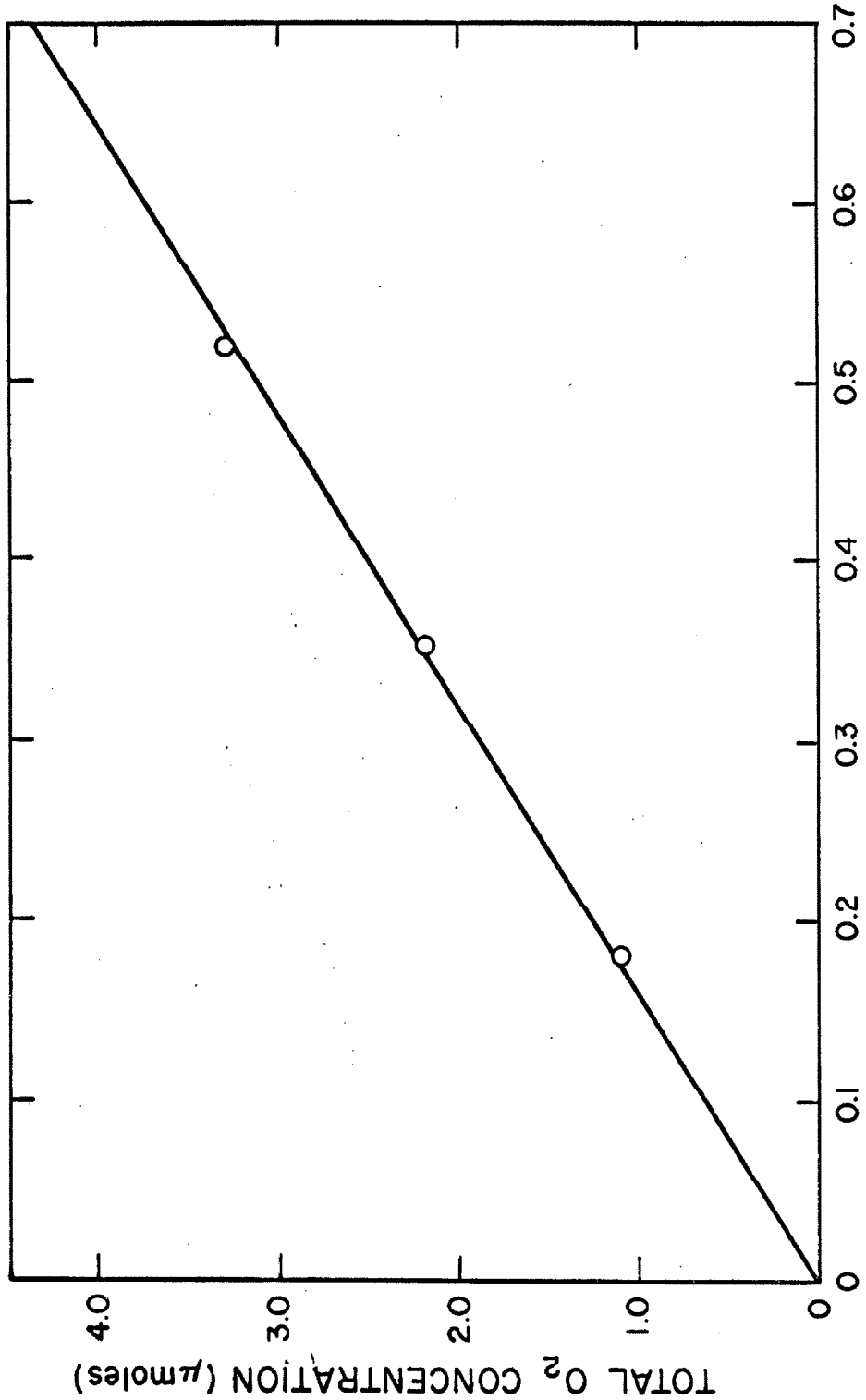

Figure II-2-2. The o-Tolidine Standard Curve Obtained Using Aliquots of a Calibrated Dissolved Oxygen Solution.

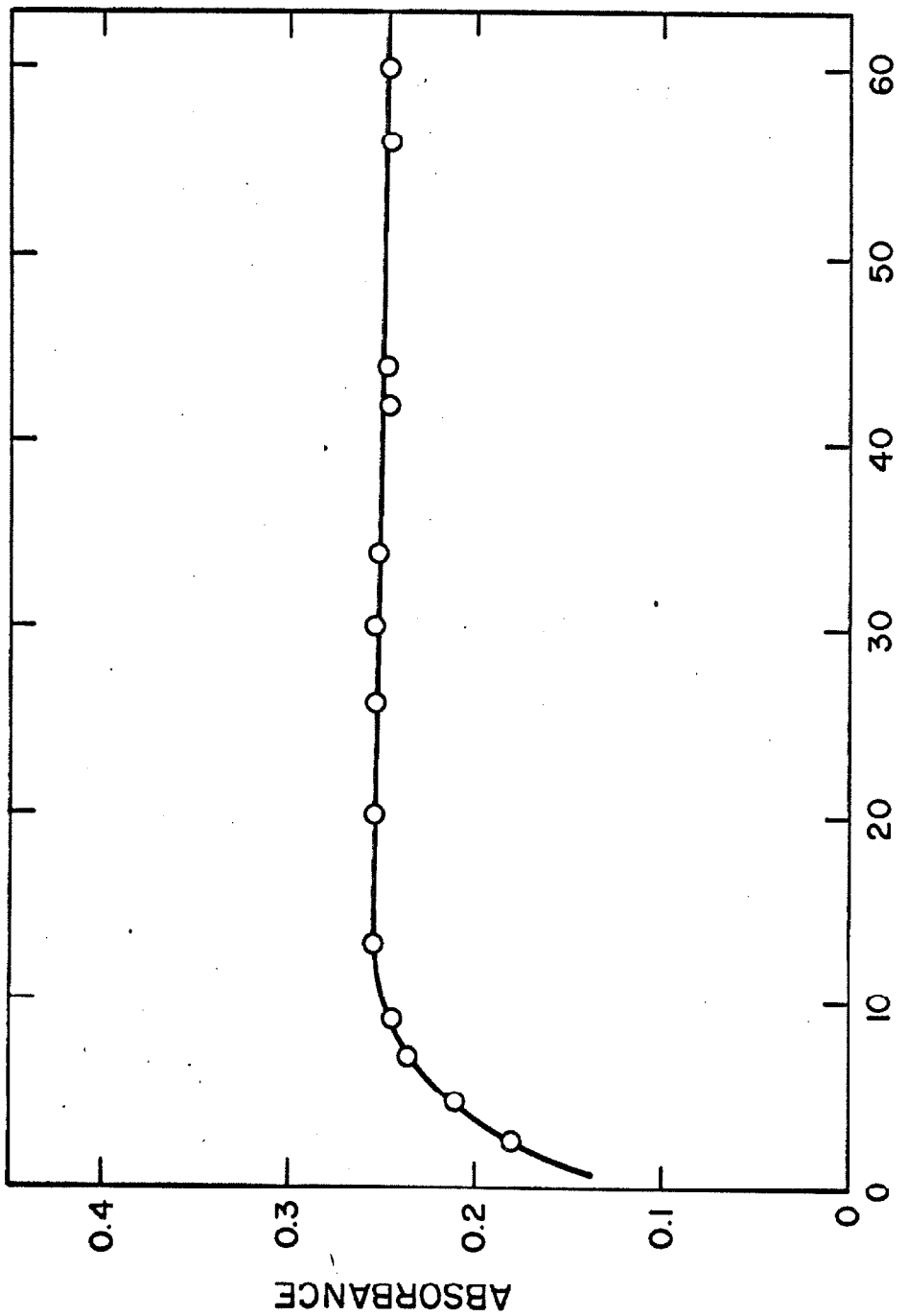

Figure II-2-3. The Development Time of the o-Tolidine Reaction in the Perchloric Acid - NaOH Environment (pH = 1.3).

during the shaking procedure and subsequently coated the silica cells during the absorbance measurements. Apiezon grease was found to reduce this problem, but the use of plastic joints would eliminate it completely.

APPENDIX II-3

BLOOD ANALYSIS PROCEDURES

A. Introduction.

In order to characterize the blood used in the experiments described in Chapter III, the following series of chemical and physical measurements were made.

B. Hemoglobin.

The total blood hemoglobin was measured spectrophotometrically by converting all the hemoglobin to cyanmethemoglobin (31). The concentration of methemoglobin originally present in the blood was determined in a separate spectrophotometric analysis (32), and the total ferro-hemoglobin was obtained from the difference between the two analyses. The methemoglobin concentrations were always less than two percent of the total hemoglobin concentration. The total plasma hemoglobin was also measured using the cyanmethemoglobin method.

The cyanmethemoglobin method was standardized using the whole-blood iron method of Connerty and Briggs (13). Since about 99.5% of the total iron in blood is contained in the hemoglobin molecules, a determination of the total iron provides an

accurate measure of the hemoglobin concentration. The results of the iron analyses for the hemoglobin standard solution are shown in Figure II-3-1. This calibrated hemoglobin solution was then used to prepare a series of cyanmethemoglobin solutions, giving the standard curve shown in Figure II-3-2. These cyanmethemoglobin standards were stored in a refrigerator, and their absorbance was observed to remain constant during the period in which the hemoglobin analyses were made.

C. Hematocrit.

The hematocrits of the blood samples were obtained in two ways - by centrifugation in 1 mm diameter capillary tubes with subsequent visual measurement of the relative volume fraction of the packed red cells, and by Coulter counter measurement of the actual number of cells (5). The Coulter counter measurements always gave a somewhat smaller relative volume (about -0.02), when multiplied by the normal red cell volume ($85\,\mu^3$). The average of the two numbers was used in the calculations. A typical red cell size distribution is given in Figure II-3-3.

D. Viscosity.

The viscosity of the blood samples was measured using two Cannon-Fenske glass capillary viscometers. The standard procedure

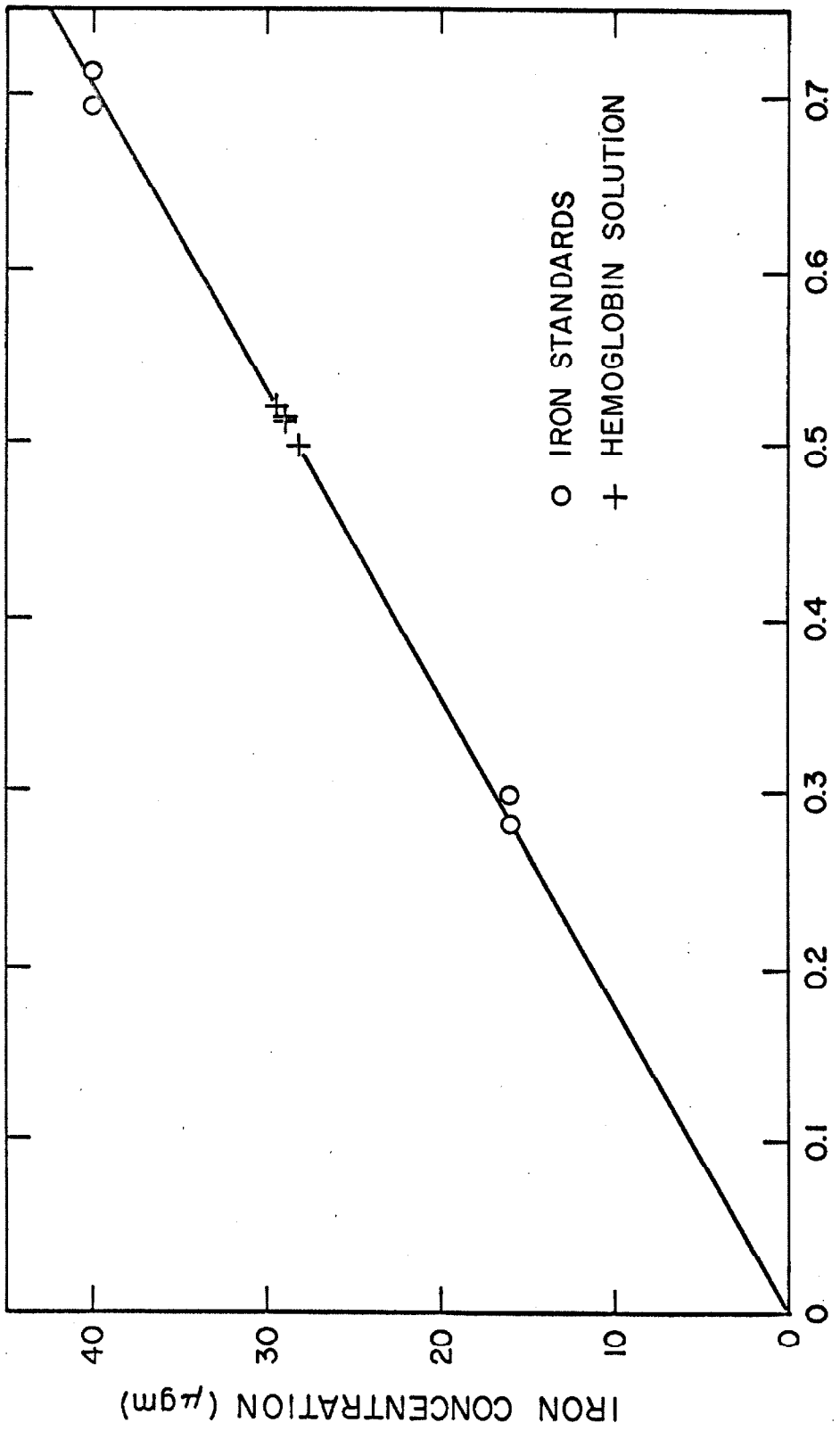

Figure II-3-1. The Calibration of the Hemoglobin Standard Solution Using the Connerty-Briggs Method for Total Iron.

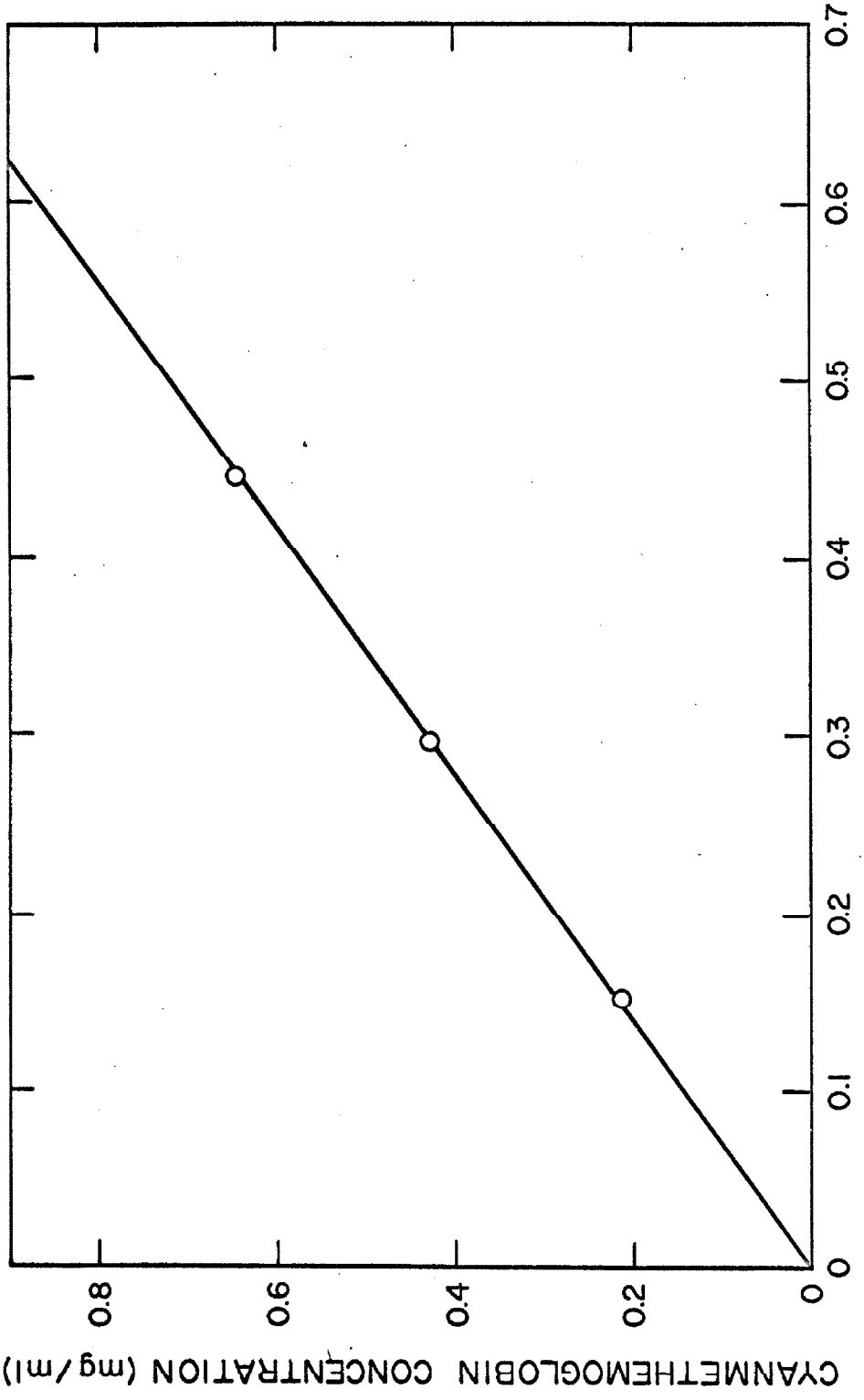

Figure II-3-2. The Cyanmethemoglobin Standard Curve Used in the Total Hemoglobin Determinations.

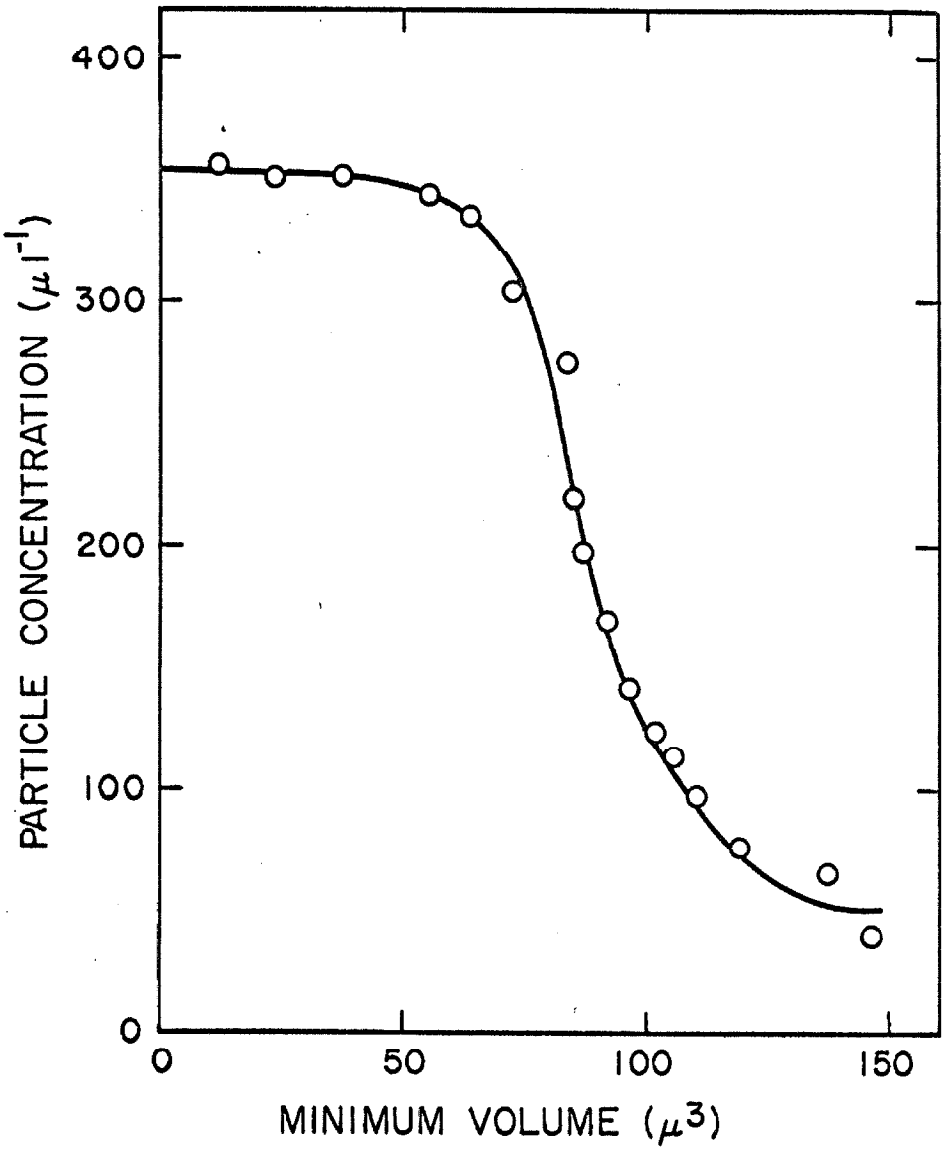

Figure II-3-3. The Red Cell Size Distribution of a Typical Blood Sample, Adjusted to Normal Red Cell Volume.

described in ASTM D 445 - 65 was followed as closely as possible, using standard laboratory equipment. The viscometers were cleaned with chromic acid "cleaning solution" between experiments, and rinsed with reagent grade acetone before drying. The viscometers were suspended vertically in a constant temperature water bath set at 37.5° C. The calibration constant for each viscometer was determined using two National Bureau of Standards calibrating liquids bracketing the viscosity of the blood samples. The calibration constants were found to be $1.73 \pm 0.03 \times 10^{-4}$ $(cm/sec)^2$ and $1.11 \pm 0.02 \times 10^{-4}$ $(cm/sec)^2$ for viscometers #100 and #200 respectively. Two viscometers were used to insure that the Newtonian viscosity (high shear) was measured. The wall shear rates in the viscometers were estimated to be 1000 and 500 sec^{-1} respectively, using the relation:

$$\dot{\gamma}_w = \frac{(a)(\Delta\pi)}{2\mu L} \qquad (44)$$

Both these values are in the range of near Newtonian behavior for blood flow in capillary tubes (58), and indeed the two measured values for the viscosity of blood always agreed within experimental error.

E. pH and Gas Tensions.

The pH, P_{O_2}, and P_{CO_2} were measured using the Radiometer Gas Monitor pHA 927 with thermostatted microelectrodes E5021

5036, and 5046. The oxygen and carbon dioxide electrodes were calibrated using dissolved gas solutions obtained by bubbling calibrated gas mixtures through distilled water in a device maintained at the electrode temperature (37.5° C).

APPENDIX III-1

NUMERICAL SOLUTION OF THE CONVECTIVE DIFFUSION EQUATION

A. Introduction.

In order to analyze the experimental results described above, it was necessary to solve the convective diffusion equation for several theoretical "models." The general form of the differential equation is:

$$\frac{d^2P_i}{dy^2} = A\left(y, \frac{df}{dP_i}\right)\frac{dP_i}{dy} \qquad (45)$$

where A includes the velocity profile and the non-linear terms describing each model. This equation was solved numerically using the IBM 7094 digital computer.

B. Method and Results.

Equation (45) was solved by expressing it as a system of linear first-order differential equations:

$$\frac{dY_1}{dy} = Y_2 \quad ; \quad \frac{dY_2}{dy} = \bar{A}(y)\,Y_2 \qquad (46)$$

$\bar{A}$ is the function A calculated at each numerical interval, assuming (df/dP_i) to be constant over the interval. The boundary conditions $Y_1(0)$ and $Y_2(0)$ are used to start the integration at $y = 0$, and the integration is carried out until the computed value of Y_2 (ie. dP_i/dy) approaches zero. The value of Y_1 at these conditions is then the value of $P_{i,\infty}$ corresponding to the specified boundary conditions.

The numerical procedure used to solve this system of first order equations (63) employs a variable interval size with automatic error control. The method of Runge-Kutta-Gill is used to start the integration, and is used to restart the process whenever the interval size is changed. During the period of fixed interval size, the more efficient Adams-Moulton predictor-corrector formulas continue the integration. Both the Runge-Kutta-Gill method and the Adams-Moulton method incorporate double precision calculations to control round-off error. An upper bound on the truncation error in the Adams-Moulton method is input to the program. This is equivalent to specifying the number of significant figures which are to be preserved locally throughout the integration. These values were chosen so that the total error for the integration of the "inert model" was less than $\pm 0.5\%$, and so that the precision of solutions for the "local equilibrium model" over the experimental range of ω was $\pm 2\%$.

NOMENCLATURE

a	=	radius (cm)
A	=	area (cm^2), or absorbance
C_{Hb}	=	hemoglobin concentration (gm/ml)
C_R	=	count-rate geometric factor (cpm/cc(STP))
d	=	diameter (cm)
$\mathcal{D}_{i,f}$	=	diffusivity of i in fluid f (cm^2/sec)
f	=	fractional saturation of hemoglobin
$\mathcal{F}_{pH}$	=	Sveringhaus pH factor
H	=	hematocrit
J	=	transfer rate (cc(STP)/cm^2 sec)
$\vec{J}_i$	=	diffusional flux of i (cc(STP)/cm^2 sec)
J_j	=	chemical reaction rate with species (cc(STP)/cm^3 sec)
k_{RC}	=	red cell equilibration rate constant
L	=	length (cm)
n	=	concentration of dissolved material (cc(STP)/cm^3)
N	=	total concentration of reversibly bound material (cc(STP)/cm^3)
P	=	partial pressure (mm Hg)
ΔP	=	total pressure difference = $P_{i,g} - P_{i,\infty}$ (mm Hg)
R	=	count rate (cpm)
t	=	time (sec)
T	=	temperature (°C)

v = velocity (cm/sec)

V = volume of the rotating disk apparatus (cm^3)

y = normal distance from the disk surface (cm)

y_r = location of the edge of the reactive region within δ_c

α = solubility coefficient ($cc(STP)/cm^3$ mm Hg)

$\dot{\gamma}$ = shear rate (sec^{-1})

ξ = stoichiometric factor

δ_c = concentration boundary layer thickness

δ_f = hydrodynamic boundary layer thickness

δ_m = membrane thickness

ω = angular velocity (sec^{-1})

μ = viscosity (gm/cm sec), or symbol for micron

π = total pressure (mm Hg)

ν = kinematic viscosity (cm^2/sec)

Φ = permeability

τ = characteristic re-equilibration time (sec)

Superscripts:

$*$ = equilibrium value

Subscripts:

i = species i

j = reaction with species j

B = blood

RC = red cell

S = serum

P = plasma

T = total

g = gas phase

m = membrane, or at membrane surface

∞ = outside concentration boundary layer

w = wall value

y = in y - direction

BIBLIOGRAPHY

1. Adair, G. S., "The Hemoglobin System," J. Biol. Chem., 63, 529 (1925).
2. Altman, P. L., Dittmer, D. S., ed., Blood and Other Body Fluids, Fed. of Amer. Soc. for Exp. Biol., Washington, D. C. (1961).
3. Bird, R. B., Stewart, W. E., Lightfoot, E. N., Transport Phenomena, John Wiley & Sons, New York (1960).
4. Bohr, C., Skand. Arch. Physiol., 17, 104 (1905).
5. Brecher, G., Jakobek, E. F., Schneiderman, M. A., Williams, G. Z., Schmidt, P. J., "Size Distribution of Erythrocytes," Ann. N. Y. Acad. Sci., 99, 242 (1962).
6. Buckles, R. G., "An Analysis of Gas Exchange in a Membrane Oxygenator," Ph.D. Thesis, M.I.T. (1966).
7. Carslaw, H. S., Jaeger, J. C., Conduction of Heat in Solids, Oxford University Press (1959).
8. Charm, S. E., Kurland, G. S., Brown, S. L., "The Flow Characteristics of Blood Suspensions," Biomedical Fluid Mechanics Symposium, Denver (1966).
9. Cochran, W. G., Proc. Cambridge Phil. Soc., 30, 365 (1934).
10. Cokelet, G. R., "The Rheology of Human Blood," Sc.D. Thesis, M.I.T., Cambridge, Mass. (1963).
11. Cokelet, G. R., Biorheology (in press).

12. Collins, R. E., "Transport of Gases Through Hemoglobin Solution," Bull. Math. Biophys., 28, 223 (1961).

13. Connerty, H. V., Briggs, A. R., "New Method for the Determination of Whole Blood and Hemoglobin," Clin. Chem., 8, 151 (1962).

14. Constantine, H. P., Craw, M. R., Morello, J. A., Forster, R. E., "The Rate of Reaction of CO_2 with Dilute Human Red Cell Suspensions," Physiologist, 5, 120 (1962).

15. Cook, G. A., ed., Argon, Helium and the Rare Gases, Interscience Publishers, New York (1961).

16. Copley, A. L., "Apparent Viscosity and Wall Adherence of Blood Systems," in Flow Properties of Blood, Symposium Publications Division, Permagon Press, New York (1960).

17. De Groot, S. R., Mazur, P., Non-Equilibrium Thermodynamics, North-Holland Publishing Company, Amsterdam (1962).

18. Dirken, M. N. J., Mook, H. W., "The Rate of Gas Exchange Between Blood Cells and Serum," J. Physiol., London, 73, 349 (1931).

19. Dobell, A. R. C., Mitri, M., Galva, R., Sarkozy, E., Murphy, D. R., "Biologic Evaluation of Blood after Prolonged Recirculation through Film and Membrane Oxygenators," Ann. Surg., 161, 617 (1965).

20. Fasciolo, J. C., Chiodi, H., "Arterial Oxygen Pressure During Pure O_2 Breathing," Am. J. Physiol., 147, 54 (1946).

21. Fatt, I., La Force, R. C., "Dispersion Conductivity Theory Applied to Oxygen Diffusion in Blood," Jour. Phys. Chem., 67, 2260 (1963).

22. Forster, R. E., Roughton, F. J. W., Kreuzer, F., Briscoe, W. A., "Photocolorimetric Determination of Rate of Uptake of CO and O_2 by Reduced Human Red Cell Suspensions at 37°C," J. Appl. Physiol., 11, 260 (1957).

23. Fricke, H., "A Mathematical Treatment of the Electric Conductivity and Capacity of Disperse Systems," Physical Rev., 24, 575 (1924).

24. Friedlander, S. K., Keller, K. H., "Mass Transfer in Reacting Systems Near Equilibrium," Chem. Eng. Sci., 20, 121 (1965).

25. Galily, I., Friedlander, S. K., "Kink Poisons and the Reduction of Dissolution Rate at Crystal-Liquid Interfaces," J. Chem. Phys., 42, 1503 (1965).

26. Galletti, P. M., Brecher, G. A., Heart-Lung Bypass - Principles and Techniques of Extracorporeal Circulation, Grune and Stratton, New York (1962).

27. Gentsch, T. O., Bopp, R. K., Siegel, J. H., Cev, M., Glenn, W. W. L., "Experimental and Clinical Use of a Membrane Oxygenator," Surgery, 47, 301 (1960).

28. Glauser, S., "Effect of pH Change on the Oxyhemoglobin Dissociation at High Partial Pressures of Oxygen, Fed. Proc., 22, 516 (1963).

29. Goldstein, S., Modern Developments in Fluid Dynamics, Dover Publications, Inc., New York (1965).

30. Goldstick, T. K., "Diffusion of Oxygen in Protein Solutions," Ph.D. Thesis, Univ. of Calif., Berkeley (1966).

31. Hainline, A. Jr., "Hemoglobin," in Standard Methods of Clinical Chemistry, Vol. 2, Academic Press, New York (1958).

32. Hainline, A. Jr., "Methemoglobin," in Standard Methods of Clinical Chemistry, Vol. 5, Academic Press, New York (1965).

33. Handbook of Chemistry and Physics, Chemical Rubber Publishing Co., Cleveland, Ohio.

34. Hardewig, A., Rochester, D. F., Briscoe, W. A., "Measurement of the Solubility Coefficients of Krypton in Water, Plasma, and Human Blood, Using Radioactive Kr-85," J. Appl. Physiol., 15, 723 (1960).

35. Harris, J. W., The Red Cell, p. 199, Harvard Univ. Press, Cambridge (1963).

36. Hartridge, H., Roughton, F. J. W., "A Method of Measuring the Velocity of Very Fast Chemical Reactions," Proc. Roy. Soc. A, 104, 376 (1923).

37. Hedley-Whyte, J., Laver, M. B., "O_2 Solubility in Blood and Temperature Correction Factors for P_{O_2}," J. Appl. Physiol., 19, 901 (1964).

38. Hemmingsen, E., Scholander, P. F., "Specific Transport of O_2 through Hemoglobin Solutions," Science, 132, 1979 (1960).

39. Hirschfelder, J. O., Curtiss, C. F., Bird, R. B., Molecular Theory of Gases and Liquids, John Wiley & Sons, New York (1954).

40. Joffe, J., Poulton, E. P., "The Partition of CO_2 Between Plasma and Corpuscles in Oxygenated and Reduced Blood," J. Physiol., LIV, 129 (1920).

41. Johnston, G. W., "Oxygen Saturation of Blood," Standard Methods of Clinical Chemistry, Vol. 4, Academic Press, New York (1963).

42. Keller, K. H., Friedlander, S. K., "The Steady-State Transport of Oxygen through Hemoglobin Solutions," Jour. Gen. Physiol., 49, 663 (1966).

43. Keller, K. H., Friedlander, S. K., "Diffusivity Measurements of Human Methemoglobin," J. Gen. Physiol., 49, 681 (1966).

44. Kreuzer, F., Yahr, W. Z., "Influence of Red Cell Membrane on Diffusion of Oxygen," J. Appl. Physiol. 15 (6), 1117 (1960).

45. La Force, R. C., Fatt, I., "Steady-State Diffusion of Oxygen through Whole Blood," Trans. Far. Soc., 58, 1451 (1962).

46. Landau, L. D., Lifshitz, E. M., Fluid Mechanics, Permagon Press, London (1959).

47. Landino, E., McCreary, J. G., Thompson, W. A., Powers, J. E. "Mass Transfer in a Horizontal Rotating Cylinder with Applications to the Oxygenation of Blood," A.I.Ch.E. Jour., 12, 117 (1966).

48. Lawson, W. H. Jr., Holland, R. A. B., Forster, R. E., "Effect of Temperature on Deoxygenation Rate of Human Red Cells," J. Appl. Physiol., 20, 912 (1965).

49. Lawson, W. H. Jr., "Interrelation of pH, Temperature, and Oxygen on Deoxygenation Rate of Red Cells," J. Appl. Physiol., 21, 905 (1966).

50. Lee, W. H. Jr., Krumhaar, D., Fonkalsrud, E. W., Schjeide, O. A., Maloney, J. V. Jr., "Denaturation of Plasma Proteins as a Cause of Morbidity and Death after Intracardiac Operations," Surgery, 50, 29 (1961).

51. Lee, W. H. Jr., Krumhaar, D., Derry, G., Sachs, D., Lawrence, S. H., Clowes, G. H. A., Maloney J. V. Jr., "Comparison of the Effects of Membrane and Non-Membrane Oxygenators on the Biochemical and Biophysical Characteristics of Blood," Surg. Forum, 12, 200 (1961).

52. Levich, V. G., Physicochemical Hydrodynamics, Prentice-Hall, Inc., Englewood Cliffs, New Jersey (1962).

53. Litt, M., Serad, G., "Chemical Reactions on a Rotating Disk," Chem. Eng. Sci., 19, 867 (1964).

54. Longmiur, I., Colman, C., "Effect of pH Change on the Shape of the Oxyhemoglobin Dissociation Curve," Fed. Proc., 22, 516 (1963).

55. Marks, P. A., Johnson, A. B., Hirschberg, E., Banks, J., "Studies on the Mechanism of Aging of Human Red Blood Cells," Ann. N. Y. Acad. Sci., 75, 95 (1958).

56. Marx, T. I. Snyder, W. E., St. John, A. D., Moeller, C. E., "Diffusion of Oxygen into a Film of Whole Blood," J. Appl. Physiol., 15, 1123 (1960).

57. Merrill, E. W., Gilliland, E. R., Cokelet, G., Shin, H., Britten, A., Wells, R. E., "Rheology of Human Blood Near and at Zero Flow," Biophysical Journal, 3, 199 (1963).

58. Merrill, E. W., Benis, A. M., Gilliland, E. R., Sherwood, T. K., Salzman, E. W., "Pressure-Flow Relations of Human Blood in Hollow Fibers at Low Flow Rates," J. Appl. Physiol., 20, 954 (1965).

59. Morgan, J. J., Stumm, W., "Analytical Chemistry of Manganese," J. Am. Water Works Assn., 57, 107 (1965).

60. Naeraa, N., Petersen, E. S., Boye, E., "The Influence of Simultaneous Independent Changes of pH and Carbon Dioxide Tension on the In-vitro Oxygen Tension-Saturation Relationship of Human Blood," Scan. J. Clin. Lab. Invest., 15, 141 (1963).

61. Nakamura, T., Staub, N. C., "Synergism in the Kinetic Reactions of O_2 and CO_2 with Human Red Blood Cells," J. Physiol., 173, 161 (1964).

62. Parsons, T. R., "The Reaction and Carbon Dioxide Carrying Power of Blood - a Mathematical Treatment," J. Physiol., LIII, 42 (1919).

63. Redner, K. H., "DEQ - Differential Equation Solver," CIT Programmer's Manual, 128 (1964).

64. Riddiford, A. C., "The Rotating Disk System," in Advances in Electrochemistry and Electrochemical Engineering, Vol. 4, Interscience Publishers, New York (1966).

65. Robb, W. L., "Thin Silicone Membranes - Their Permeation Properties and Some Applications," Report No. 65-C-031, General Electric Co., October (1965).

66. Rodbard, S., Alonza, C. J., "Deposition of Flowborne Materials on Vessel Walls," Circulation Research, XI, 664 (1962).

67. Roughton, F. J. W., "The Oxygen Equilibrium of Mammalian Hemoglobin," in Oxygen, Proceedings of a Symposium Sponsored by the New York Heart Assoc., Little-Brown & Co., Boston (1965).

68. Roughton, F. J. W., "Kinetics of Gas Transport in Blood," Brit. Med. Bull., 19, 80 (1963).

69. Roughton, F. J. W., Rupp, J. C., "Problems Concerning the Kinetics of the Reactions of Oxygen, Carbon Monoxide, and Carbon Dioxide in the Intact Red Cell," Ann. N.Y. Acad. Sci., 75, 156 (1958).

70. Schlichting, H., Boundary Layer Theory, Fourth Edition, McGraw-Hill, New York (1960).

71. Scholander, P. F., "O_2 Transport through Hemoglobin Solutions," Science, 131, 585 (1960).

72. Sendroy, J. Jr., Dillon, R. T., Van Slyke, D. D., "The Solubility and Physical State of Uncombined Oxygen in Blood," J. Biol. Chem. 105, 597 (1935).

73. Sharp, Excell, Salzman, Thorup, "The Haematology of Extracorporeal Circulation with and without Hypothermia," in Thrombosis and Anticoagulant Therapy, Livingstone, London (1960).

74. Sherwood, T. K., Reid, R. C., The Properties of Gases and Liquids, McGraw-Hill Pub. Co., New York (1958).

75. Sienko, J. J., Plane, R. A., Physical Inorganic Chemistry, W. A. Benjamin, Inc., New York (1963).

76. Sirs, J. A., Roughton, F. J. W., "Stopped Flow Measurements of CO and O_2 Uptake by Hemoglobin in Sheep Erythrocytes," J. Appl. Physiol., 18, 158 (1963).

77. Snell, F. M., "Facilitated Transport of Oxygen through Solutions of Hemoglobin," J. Theoret. Biol., 8, 469 (1965).

78. Sveringhaus, J. W., "Blood Gas Concentrations" in Handbook of Physiology - Respiration II, Am. Physiol. Soc., Washington, D. C. (1964).

79. Texeira, J., "A Study of Major Causes of Death Following Cardiac Surgery with Extracorporeal Circulation," J. Card. Surg., 5, 386 (1964).

80. Tosteson, D. C., "A Flow Tube for Measuring the Rapid Transport of Halides in Red Cell Suspensions," Intern. Congr. Physiol. Sci., 20th Congr., 892 (1956).

81. Von Karman, Th., Z. Angew. Math. Mech., 1, 244 (1921).

82. Whittam, R., Transport and Diffusion in Red Blood Cells, Williams and Wilkins, Baltimore (1964).

83. Wittenberg, J. B., "The Molecular Mechanism of Hemoglobin - Facilitated Oxygen Diffusion," J. Biol. Chem., 241, 104 (1966).

84. Wyman, J., "Facilitated Diffusion and the Possible Role of Myoglobin as a Transport Mechanism," J. Biol. Chem., 241, 115 (1966).

85. Yoshida, F., Oshima, N., "Diffusivity of Oxygen in Blood Serum," J. Appl. Physiol., 21, 915 (1966).